Zoological Journal of the Linnean Society, 2024, **202**, zlae150
https://doi.org/10.1093/zoolinnean/zlae150
Advance access publication 18 December 2024
Original Article

OXFORD

Original Article

Osteology, relationship, and feeding ecology of the theropod dinosaur *Noasaurus leali* Bonaparte and Powell, 1980, from the Late Cretaceous of North-Western Argentina

Christophe Hendrickx[1,2,*], Mauricio A. Cerroni[3], Federico L. Agnolín[3,4], Santiago Catalano[2,5], Cátia F. Ribeiro[6], Rafael Delcourt[7,8]

[1]Dinosauria Lab, Fundación Miguel Lillo, Miguel Lillo 251, San Miguel de Tucumán 4000, Tucumán, Argentina
[2]Unidad Ejecutora Lillo, CONICET-Fundación Miguel Lillo, Miguel Lillo 251, San Miguel de Tucumán 4000, Tucumán, Argentina
[3]CONICET-Laboratorio de Anatomía Comparada y Evolución de los Vertebrados, Museo Argentino de Ciencias Naturales 'Bernardino Rivadavia', Av. Ángel Gallardo 470, C1405DJR Buenos Aires, Argentina
[4]Fundación de Historia Natural 'Félix de Azara', Universidad Maimónides. Hidalgo 775 (CP C1405BDB), Buenos Aires, Argentina
[5]Facultad de Ciencias Naturales, Universidad Nacional de Tucumán, Miguel Lillo 205, 4000 San Miguel de Tucumán, Argentina
[6]Museu da Lourinhã, 95 Rua João Luis de Moura, 2530-158, Lourinhã, Portugal
[7]Laboratório de Paleontologia, Faculdade de Filosofia, Ciências e Letras de Ribeirão Preto, Universidade de São Paulo, Av. Bandeirantes, 3900, 14040-901, RibeirãoPreto, SP, Brazil
[8]SNSB, Bayerische Staatssammlung für Paläontologie und Geologie, Department of Earth and Environmental Sciences, GeoBioCenter, Ludwig-Maximilians-University, Richard-Wagner-Straße 10, D-80333 München, Germany

[*]Corresponding author. Dinosauria Lab, Fundación Miguel Lillo and Unidad Ejecutora Lillo, CONICET-Fundación Miguel Lillo, Miguel Lillo 251, San Miguel de Tucumán 4000, Tucumán, Argentina. E-mail: christophendrickx@gmail.com

ABSTRACT

Noasaurus leali is a small (~2 m) carnivorous theropod and the nominal genus of the clade Noasauridae, one of the two radiations of abelisauroid ceratosaurs predominantly present in the Southern Hemisphere during the Mesozoic. This eponymous theropod from the Maastrichtian Lecho Formation of Salta, Argentina, is known from an incomplete skeleton of which the strongly curved manual ungual is the most peculiar element. We here provide for the first time a comprehensive description of the holotypic specimens of *Noasaurus*, whose phylogenetic position was explored using three independent datamatrices on theropod relationships. This species is diagnosed by several apomorphies such as a dorsal ridge in the maxillary fossa, a strongly arched quadrate, a cervical neural arch with anterior epipophyseal prongs, and a manual ungual with a subtriangular flexor fossa delimited by a V-shaped ridge. Results of the phylogenetic analyses recovered *Noasaurus* closely related to *Velocisaurus*, *Masiakasaurus*, and *Laevisuchus*, which together form a Late Cretaceous radiation of small-bodied noasaurids restricted to the Southern Hemisphere. The peculiar morphology of the lateral dentition and manual unguals suggests that *Noasaurus* was an opportunistic carnivore feeding on small prey items and a possible piscivore gaffing fish with its specialized hand claws.

Keywords: Abelisauroidea; Ceratosauria; dinosaur ecology; dietary preference; Theropoda

INTRODUCTION

Report of the discovery of fragmentary and poorly preserved radioactive bones from the El Brete area of southern Salta Province, Argentina, by Celestino Danieli and colleagues in 1960 led to one of the most important dinosaur discoveries from the Southern Hemisphere 15 years later (Danieli *et al.* 1960, Bonaparte *et al.* 1977, Powell 2003). In April 1975, a team from the Fundación Miguel Lillo of San Miguel de Tucumán decided to explore the Southern region of Salta with the hope of finding additional fossil remains in the El Brete zone (Bonaparte *et al.* 1977; Apesteguía *et al.* 2022). The team led by Prof. José Bonaparte (14 June 1928–18 February 2020; Giacchino and Agnolín 2020) included Bonaparte's Ph.D. student Jaime Eduardo Powell, as well as participant Tomás H. Fasola and lab technicians Martín Vince and Juan Carlos Leal (Fig. 1A; Abdala *et al.* 2022; Supporting Information, S1.1, Fig. SA1). It was the latter who uncovered a rich fossiliferous zone on a site of the El Brete Estancia close to the top of a small hill (Bonaparte *et*

Received 5 December 2023; revised 14 September 2024; accepted 17 October 2024

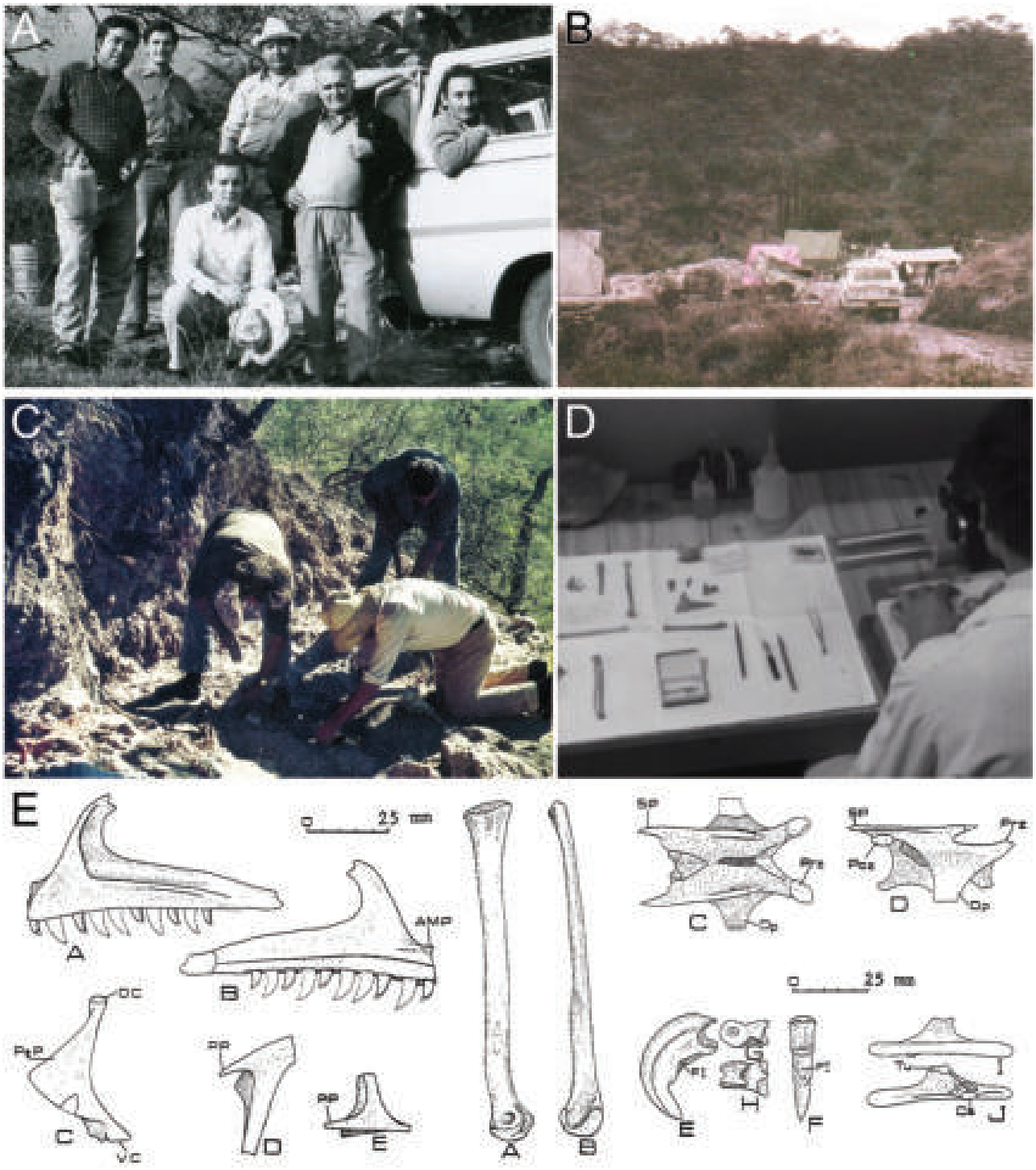

Figure 1. Historical research on *Noasaurus leali*. A, group picture of the fieldwork team on the 1975 expedition to the El Brete site from which the *Noasaurus* material was found. From left to right, lab technician Juan Carlos Leal, who discovered the fossil locality and to whom the species *Noasaurus leali* is dedicated, Ph.D. student Jaime Eduardo Powell, palaeontologist and leader of the team Prof. José Bonaparte, participant Tomás H. Fasola, an unknown man, and lab technician Martín Vince [from Abdala *et al.* (2022), modified; courtesy of Pablo Ortiz]; B, field camp at the base of the hill in 1975 and where the fossils were brought to the vehicles (Bonaparte 1996b); C, El Brete fossil site during the excavation of 1975 (Bonaparte 2007); D, *Noasaurus* material deposited and examined with a microscope at the palaeontological lab of the Museo Miguel Lillo around 1975–76 (*La Universidad Trabaja* 1976); E, plate and first illustration of the *Noasaurus* holotypic material (PVL 4061) by Bonaparte and Powell (1980) (modified). From the left half of the plate E: A, B, maxilla in lateral (A) and medial (B) views; C, quadrate in medial view; D, E, posterior cervical rib, originally misidentified as a squamosal, in lateral (D) and dorsal (E) views. From the right half of the plate E: A, B, second metatarsal in medial (A) and posterior (B) views; C, D, cervical vertebral arch in dorsal and lateral views; E, F, manual ungual, initially misinterpreted as a pedal ungual, in medial (E) and proximal (F) views. G, H, manual phalanx, initially misinterpreted as a pedal phalanx, in lateral (G) and ventral (H) views; I, J, mid-cervical rib in lateral (I) and medial (J) views.

al. 1977, Bonaparte and Powell 1980; Fig. 1B). Due to the inaccessibility of the site and the fragility of the bones, excavation only started at the end of May and extended to August 1975 (Bonaparte *et al.* 1977). The bonebed was so rich (i.e. a large number of disarticulated bones and isolated teeth belonging to several dinosaur taxa was present at the site) that fieldwork continued during the two following years (1976–77) resulting in the excavation of a large collection (>100) of dinosaurs bones from the El Brete site (Bonaparte and Powell 1980, Powell 2003; Fig. 1C; Supporting Information, S1.1, Fig. SA1). A footage from the Instituto Cinefotográfico Universidad Nacional de Tucumán and Canal 10 shows in great detail the excavation on the El Brete site, the transport of the bone, and their preparation around 1976 and 1977 (*La Universidad Trabaja* 1976; Supporting Information, S1.2, Movie SA1). The video reveals that the remote site was accessed via a small path 100 m away from the main camp down the hill (Fig. 1B) and that the plaster jackets containing the bones were moved to the camp in a wheelbarrow or a small-wheel moped before being transported, prepared, and studied at the Instituto Miguel Lillo of San Miguel de Tucumán by Prof. Bonaparte and Jaime Powell (Fig. 1D; Supporting Information, S1.1, S1.2 and Fig. SA2 Movie SA1).

The discovery and richness of the fossiliferous site was first reported in 1977 by Bonaparte and colleagues (1977) who detailed the geology and sedimentology of the El Brete locality. The authors mentioned the presence of sauropod remains belonging to five individuals, as well as a small coelurosaur theropod represented by a few cranial and postcranial bones, several isolated teeth assigned to a carnosaurian theropod, and many bones belonging to Cretaceous birds. A brief description of the tetrapod assemblage was presented in September 1978 and published two years later by Bonaparte and Powell (1980), who referred the sauropod and theropod material to new dinosaur taxa, namely the armoured titanosaurid *Saltasaurus loricatus* Bonaparte and Powell, 1980 and the small carnivorous noasaurid *Noasaurus leali* Bonaparte and Powell, 1980 (Fig. 1E). The osteology of *Saltasaurus* received a thorough account by Powell (1992, 2003), whereas Cerda and Powell (2010) explored the armour histology, and Zurriaguz and Powell (2015) expanded the information on the presacral anatomy of *Saltasaurus* a few years later. The avian material was first studied by Walker (1981) who erected, in a *Nature* paper, a new clade of Cretaceous fossil birds coined 'Enantiornithes' based on their peculiar morphology. A comprehensive description and phylogenetic review of the enantiornithines from El Brete were later given by Chiappe (1993), Walker *et al.* (2007), and Walker and Dyke (2009), who counted no less than five enantiornithine taxa (i.e. *Enantiornis*, *Lectavis*, *Soroavisaurus*, *Yungavolucris*, and *Martinavis*) in this assemblage.

Contrary to the sauropod and enantiornithes material, the non-avian theropod specimens from El Brete never received a proper description. Detailed description and illustrations of the isolated carnosaur teeth mentioned by Bonaparte and Powell (1980) is yet to appear in the literature. Likewise, the osteology of *Noasaurus* was only briefly described by Bonaparte and Powell (1980), Bonaparte (1991, 1996a, b, 2007), Carrano and Sampson (2008), and Novas (2009), where the bones were either illustrated in simplistic plates (e.g. Bonaparte and Powell 1980, Norman 1985, 1990, Bonaparte 1991, 1996a, b; Fig. 1E), in figures illustrating a single bone (e.g. Tykoski and Rowe 2004, Candeiro 2007, Powell and Ortiz 2014, Ezcurra and Novas 2016, Delcourt 2018), or in low-resolution photos showing only part of the material (Bonaparte 2007: 170; Supporting Information, S1.1, Fig. SA3; Novas 2009: fig. 6.16). The misidentification of the peculiar ungual phalanx of *Noasaurus*, interpreted as a pedal and possible raptorial claw by Bonaparte and Powell (1980), however, led Agnolín and Chiarelli (2010) to provide a thorough description of the manual phalanges of this theropod. Additionally, an almost complete cervical vertebra from the El Brete site originally described as belonging to a possible oviraptorosaur by Frankfurt and Chiappe (1999) was described in detail by Agnolín and Martinelli (2007) and referred to a noasaurid eventually representing *Noasaurus*.

The singularity of *Noasaurus*' anatomy convinced Bonaparte and Powell (1980) to erect the new family-based and monotypic clade of theropods Noasauridae (here defined as the most inclusive clade containing *Noasaurus leali* but not *Carnotaurus sastrei*; see Table 1). Initially thought to be related to the basally branching coelurosaurians Coeluridae or Compsognathidae by these authors, Noasauridae were later recognized to be closely related to abelisaurs by Paul (1988; who grouped Megalosaurinae, Abelisaurinae, and Noasaurinae into the clade Megalosauridae) and classified as the sister-taxon of Abelisauridae among abelisauroid ceratosaurs by Bonaparte (1991). If the phylogenetic placement of Noasauridae among Abelisauroidea remained essentially unchanged within the next two decades, the taxonomic diversity of Noasauridae, regarded as monotypic at the end of the 20th century (Bonaparte and Powell 1980, Bonaparte 1991), has considerably increased in the 21st century. According to some of the most recent phylogenetic analyses on ceratosaurs (i.e. Rauhut and Carrano 2016, Wang *et al.* 2017a), Noasauridae are a clade including more than 10 species-level taxa separated into two subclades: Noasaurinae and Elaphrosaurinae. The latter are, however, recovered as a more basal radiation of ceratosaurs outside Abelisauroidea by other authors such as Tortosa *et al.* (2014), Dal Sasso *et al.* (2018), and Agnolín *et al.* (2022), with Noasauridae, therefore, representing a more inclusive radiation of less than 10 taxa all from the Cretaceous of Gondwana. Pivotal discoveries of incomplete to nearly complete ceratosaurs in Madagascar (Sampson *et al.* 2001, Carrano *et al.* 2002), India (Mohabey *et al.* 2024), China (Xu *et al.* 2009), and Brazil (Langer *et al.* 2019, de Souza *et al.* 2021) additionaly revealed that some noasaurids, such as *Masiakasaurus* and a closely related form from India, were specialized carnivores with strongly procumbent mesial teeth (Carrano *et al.* 2002, 2011, Mohabey *et al.* 2024), whereas other possible noasaurids, such as *Berthasaura* (de Souza *et al.* 2021) and the elaphrosaurine *Limusaurus*, had toothless jaws covered by a rhamphotheca, suggesting an omnivorous to strictly herbivorous feeding ecology (Xu *et al.* 2009, Wang *et al.* 2017a, b). Despite the important diversity in skull morphologies and dietary preferences, noasaurid theropods (*sensu* Rauhut and Carrano 2016, Wang *et al.* 2017a, Langer *et al.* 2019, de Souza *et al.* 2021) were small- to medium-bodied theropods (i.e. body length ranging from 1.5 to 7 m) with slender proportion, characterized by a small head, long neck, reduced and gracile forelimbs, as well as long and slender

Table 1. Phylogenetic definitions of ceratosaur clades used in this study.

Taxon	First definitional author	First phylogenetic definition	Definition type	Definition	Definitional author
Abelisauridae (Bonaparte and Novas 1985)	Novas 1997	*Abelisaurus comahuensis*, *Carnotaurus sastrei*, *Xenotarsosaurus bonapartei*, *Indosaurus matleyi*, *Indosuchus raptorius*, *Majungasaurus crenatissimus* and all descendants of their common ancestor	Stem-based	The most inclusive clade containing *Carnotaurus sastrei* but not *Noasaurus leali* and *Ceratosaurus nasicornis*	Modified from Rauhut and Pol 2021
Abelisaurinae (Bonaparte and Novas 1985)	Sereno 1998	All theropods closer to *Abelisaurus* than to *Carnotaurus*	Stem-based	The most inclusive clade containing *Abelisaurus comahuensis* but not *Carnotaurus sastrei*	Sereno 1998
Abelisauroidea (Bonaparte and Novas 1985) = Abelisauria *sensu* (Tykoski and Rowe 2004)	Holtz 1994	Abelisaurids and those members of the *Ceratosaurus*-Abelisauridae clade which shared a more recent common ancestry than with the North American genus [*Ceratosaurus*]	Node-based	The least inclusive clade containing *Carnotaurus sastrei* and *Noasaurus leali*	Sereno 2005
Berthasauridae clade nov.		/	Stem-based	The most inclusive clade containing *Berthasaura leopoldinae* but not *Noasaurus leali*, *Elaphrosaurus bambergi* or *Ceratosaurus sastrei*	This paper
Brachyrostra (Canale *et al.* 2009)	Canale *et al.* 2009	All the abelisaurids more closely related to *Carnotaurus sastrei* than to *Majungasaurus crenatissimus*	Node-based	The most inclusive clade containing *Carnotaurus sastrei* but not *Majungasaurus crenatissimus*	Modified from Canale *et al.* 2009
Carnotaurinae (Sereno 1998)	Sereno 1998	All theropods closer to *Carnotaurus* than to *Abelisaurus*	Stem-based	The most inclusive clade containing *Carnotaurus sastrei* but not *Abelisaurus comahuensis*	Sereno 1998
Ceratosauria (Marsh 1884)	Rowe and Gauthier 1990	The group including *Ceratosaurus nasicornis*, *Dilophosaurus wetherilli*, *Liliensternus liliensterni*, *Coelophysis bauri*, *Syntarsus rhodesiensis*, *Syntarsus kayentakatae*, *Segisaurus halli*, *Sarcosaurus woodi*, and all other taxa stemming from their most recent common ancestor	Stem-based	The most inclusive clade containing *Ceratosaurus nasicornis* but not *Passer domesticus*	Sereno 2005 *sensu* Holtz and Padian 1995
Ceratosauridae (Marsh 1884)	Rauhut 2004	All ceratosaurs that are more closely related to *Ceratosaurus* than to abelisaurids	Stem-based	The most inclusive clade containing *Ceratosaurus nasicornis* but not *Carnotaurus sastrei* and *Noasaurus leali*	Hendrickx *et al.* 2015b
Elaphrosaurinae (Rauhut and Carrano 2016)	Rauhut and Carrano 2016	All noasaurids that are more closely related to *Elaphrosaurus* than to *Noasaurus*, *Abelisaurus*, *Ceratosaurus*, or *Allosaurus*	Stem-based	The most inclusive clade containing *Elaphrosaurus bambergi* but not *Noasaurus leali* or *Ceratosaurus sastrei*	Modified from Rauhut and Carrano 2016
Etrigansauria (Delcourt 2018)	Delcourt 2018	The most inclusive clade containing *Carnotaurus sastrei* and *Ceratosaurus nasicornis* but not *Noasaurus leali*	Stem-based	The most inclusive clade containing *Ceratosaurus nasicornis* and *Carnotaurus sastrei* but not *Noasaurus leali*	Delcourt 2018

Table 1. Continued

Taxon	First definitional author	First phylogenetic definition	Definition type	Definition	Definitional author
Furileusauria (Filippi *et al.* 2016)	Filippi *et al.* 2016	The most inclusive clade containing to *Carnotaurus sastrei* but not *Ilokelesia aguadagrandensis*, *Skorpiovenator bustingorryi* or *Majungasaurus crenatissimus*	Stem-based	The most inclusive clade containing *Carnotaurus sastrei* but not *Ilokelesia aguadagrandensis*, *Skorpiovenator bustingorryi* or *Majungasaurus crenatissimus*	Filippi *et al.* 2016
Majungasaurinae (Tortosa *et al.* 2014)	Tortosa *et al.* 2014	All the abelisaurids more closely related to *Majungasaurus crenatissimus* than to *Carnotaurus sastrei*	Stem-based	The most inclusive clade containing *Majungasaurus crenatissimus* but not *Carnotaurus sastrei*	Tortosa *et al.* 2014
Neoceratosauria (Novas 1992)	Holtz 1994	The most recent common ancestor of *Ceratosaurus* and Abelisauridae and all of its descendants	Node-based	The least inclusive clade containing *Ceratosaurus nasicornis* and *Carnotaurus sastrei*	Hendrickx *et al.* 2015b
Noasauridae (Bonaparte and Powell 1980)	Wilson *et al.* 2003	The most inclusive clade containing *Noasaurus leali* but not *Carnotaurus sastrei*	Stem-based	The most inclusive clade containing *Noasaurus leali* but not *Carnotaurus sastrei* and *Ceratosaurus nasicornis*	Modified from Rauhut and Pol (2021)
Noasaurinae (Bonaparte and Powell 1980)	Rauhut and Carrano 2016	All noasaurids that are more closely related to *Noasaurus* than to *Elaphrosaurus*, *Abelisaurus*, *Ceratosaurus*, or *Allosaurus*	Stem-based	The most inclusive clade containing *Noasaurus leali* but not *Elaphrosaurus bambergi* or *Ceratosaurus sastrei*	Modified from Rauhut and Carrano 2016 and Wang *et al.* 2017a

hindlimbs suggesting strong cursorial capabilities (Carrano *et al.* 2011, Rauhut and Carrano 2016, Delcourt 2018, Baiano *et al.* 2020, Smyth *et al.* 2020, de Souza *et al.* 2020). They have extensive palaeogeographic and stratigraphic distributions, with remains found in South America (Argentina and Brazil), Africa (Morocco, Niger, Tanzania, and Madagascar), Asia (China and India), Oceania (Australia), and possibly in North America (Colorado), from rocks dating from the Late Jurassic to the Upper Cretaceous (e.g. Galton 1982, Carrano *et al.* 2002, Evans *et al.* 2015, Brissón Egli *et al.* 2016, Rauhut and Carrano 2016, Cerroni *et al.* 2019, Langer *et al.* 2019, Brougham *et al.* 2020).

This contribution aims to: (i) provide a comprehensive osteological description and detailed illustrations of the holotype material of *Noasaurus leali*; (ii) examine its phylogenetic placement using the most updated datasets focused on ceratosaurs; (iii) explore its feeding ecology based on indirect information provided by the available remains; and (iv) discuss the classification, size evolution, and palaeogeographic history of noasaurid theropods based on the results of the phylogenetic analyses.

List of institutional abbreviations

ANSP: Academy of Natural Sciences, Philadelphia, Pennsylvania, USA; BHI: Black Hills Institute, Hill City, South Dakota, USA; BP: Evolutionary Studies Institute, University of the Witwatersrand, Johannesburg, South Africa; BSPG: Bayerische Staatssammlung für Paläontologie und Historische Geologie, München, Germany; BYU-VP: Brigham Young University Museum of Vertebrate Paleontology, Provo, USA; CAMZN: Sedgwick Museum, University of Cambridge, Cambridge, UK; DMNH: Perot Museum of Nature and Science, Dallas, Texas, USA; JME: Jura Museum Eichstätt, Eichstätt, Germany; FMNH: Field Museum of Natural History, Chicago, USA; IVPP: Institute for Vertebrate Paleontology and Paleoanthropology, Beijing, China; IWCMS: Dinosaur Isle Visitor Centre, Isle of Wight County Museums Service, Sandown, UK; MACN: Museo Argentino de Ciencias Naturales 'Bernardino Rivadavia', Buenos Aires, Argentina; MB: Museum für Naturkunde der Humboldt Universität, Berlin, Germany; MCF PVPF: Museo Municipal 'Carmen Fuñes', Plaza Huincul, Argentina; ML: Museu da Lourinhã, Lourinhã, Portugal; MLP: Museo de La Plata, La Plata, Argentina; MN: Museu Nacional, Universidade Federal do Rio de Janeiro, Rio de Janeiro, Brazil; MNN: Musée National du Niger, Niamey, Niger; MNHN: Muséum national d'Histoire naturelle, Paris, France; MPC-D: Institute of Paleontology and Geology, Mongolian Academy of Sciences (formerly IGM), Ulaanbaatar, Mongolia; MPCN PV: Museo Patagónico de Ciencias Naturales, General Roca, Río Negro, Argentina; MPCO.V: Museu de Paleontologia de Cruzeiro do Oeste, Cruzeiro do Oeste, Brazil; MPEF PV: Museo Paleontológico 'Egidio Feruglio', Trelew, Argentina;

MPM: Museo Padre Manuel Molina, Río Gallegos, Santa Cruz, Argentina; MWC: Museum of Western Colorado, Fruita, Colorado, USA; MZSP: Museu de Zoologia da Universidade de São Paulo, São Paulo, Brazil; NHMUK: Natural History Museum, London, UK; NMV: Museums Victoria (National Museum of Victoria), Melbourne, Victoria, Australia; PIN: Paleontological Institute, Russian Academy of Sciences, Moscow, Russia; PVL: Fundación 'Miguel Lillo', San Miguel de Tucumán, Argentina; SMA: Sauriermuseum Aathal, Aathal, Switzerland; TPII: Thanksgiving Point Institute, Inc., North American Museum of Ancient Life, Lehi, Utah, USA; UA: Université d'Antananarivo, Antananarivo, Madagascar; UC: University of Chicago Paleontological Collection, Chicago, USA; UCMP: University of California Museum of Paleontology, Berkeley, USA; UMNH VP: Natural History Museum of Utah, University of Utah, Salt Lake City, USA; USNM: United States National Museum Vertebrate Paleontology, National Museum of Natural History, Washington, District of Columbia, USA; YPM: Yale Peabody Museum of Natural History, Yale, Connecticut, USA.

MATERIALS AND METHODS

Geographical, stratigraphical, and palaeoenvironmental settings

The holotypic specimens of *Noasaurus leali*, which consist of relatively well-preserved (i.e. undistorted, non-abraded, and slightly fractured) skeletal elements, were unearthed in the El Brete fossil site. The latter is situated in the southern tip of Salta Province, north-western Argentina (Fig. 2A), 2.6 km south of the El Brete Estancia in the Department of Candelaria, around 11 km west of the locality of El Tala, and 3 km north of the limit between the Salta and Tucumán provinces (Fig. 2A, B; Bonaparte and Powell 1980, Powell 2003). The El Brete fossiliferous site is precisely located at an altitude of 500 m, 140 m to the east of the arroyo Gonzalez, 1.55 km east of the Clavizán river and 2.48 km north of the National Route 6 (S26°02′22″ W65°20′06″; Fig. 2B), on the western slope and close to the top of a small hill dominated by a dry subtropical vegetation, around 500 m east of a disused limestone quarry (Bonaparte *et al.* 1977, Powell 2003).

Stratigraphically, the *Noasaurus* material comes from the middle part of the Lecho Formation, 22 m above the base of the stratigraphic unit (Bonaparte *et al.* 1977, Powell 2003; Fig. 2C). It was found among an accumulation of disarticulated elements mainly belonging to the titanosaurid *Saltasaurus*, in a small quarry about 36 m² in surface (8 × 4.5 m; Bonaparte *et al.* 1977, Walker *et al.* 2007; Supporting Information, S1.2, Movie SA1). Information on the exact location of the holotypic specimens of *Noasaurus* within the quarry, as well as their association and distribution among the other dinosaur bones, is, to our knowledge, missing, as the only available map of the El Brete site illustrating the distribution of the fossils (i.e. Bonaparte *et al.* 1977: fig. 2) only shows much larger bones all belonging to the sauropod *Saltasaurus*. The Lecho Formation and the overlying Yacoraite Formation belong to the Balbuena Subgroup

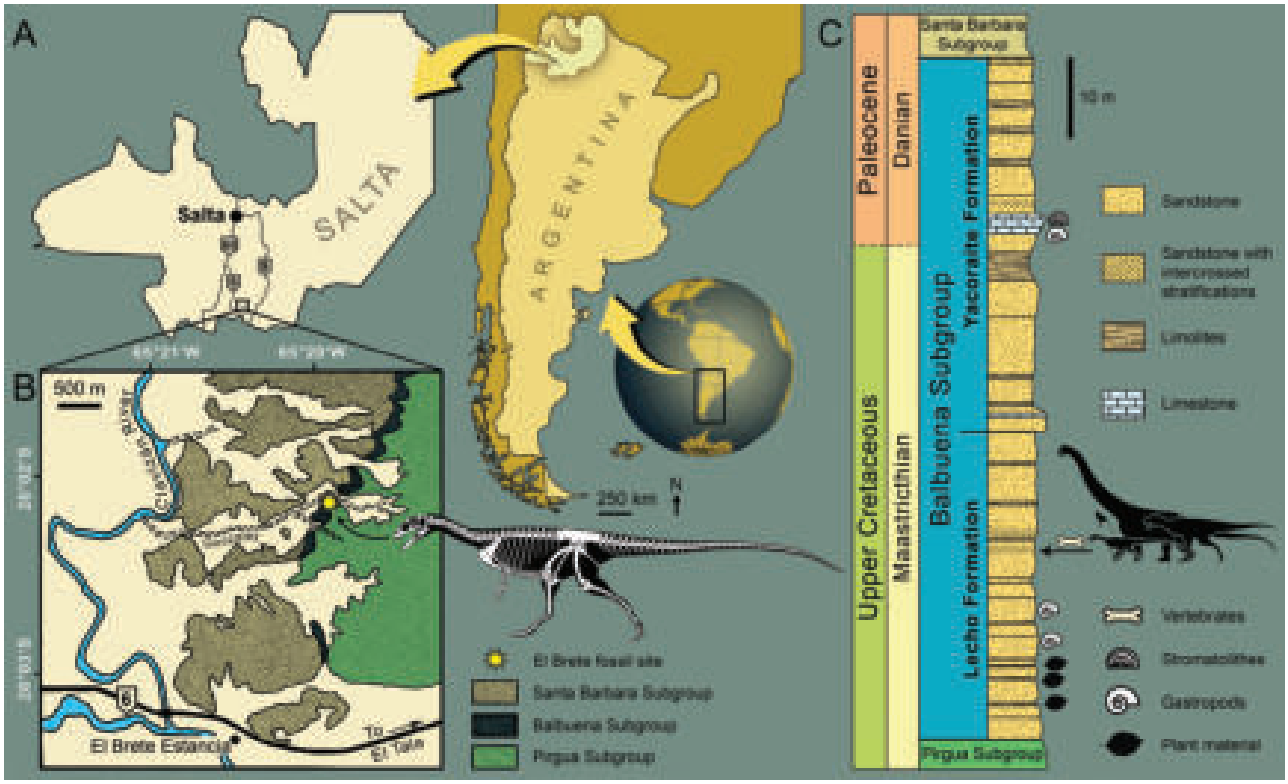

Figure 2. Geographical and stratigraphical distributions of *Noasaurus leali*. A, Salta Province in Northern Argentina (map of Argentina courtesy of Stephanie Abramowicz, Dinosaur Institute, Natural History Museum of Los Angeles County; modified); B, location of the El Brete fossil site 2.6 km north to the El Brete Estancia and 1.55 km west to the Clavizán River (from Chiappe 1993; modified); C, sedimentological log illustrating the stratigraphic occurrence of *Noasaurus* and other plant, invertebrate and dinosaur fossils within the Maastrichtian Lecho Formation and Maastrichtian–Danian Yacoraite Formation of the Balbuena Subgroup, Salta Group (log from Bonaparte *et al.* 1977; modified).

of the Salta Group, which is delimited at the base by the Los Blanquitos Formation of the Pirgua Subgroup and, on the top, by the Santa Bárbara Subgroup (Fig. 2C). The Lecho Formation is typically regarded as belonging to the latest stages of the Cretaceous, either as (?Upper) Campanian–Maastrichtian (Bonaparte and Powell 1980, Powell 2003, Zurriaguz and Powell 2015, Ezcurra and Novas 2016) or strictly Maastrichtian (Bonaparte *et al.* 1977, Chiappe 1993, Agnolín and Martinelli 2007, Fernández *et al.* 2008, Agnolín and Chiarelli 2010). The latest literature on the Lecho Formation (e.g. Kortyna *et al.* 2019, Deschamps *et al.* 2020, Villafañe *et al.* 2021), however, considers it to be Maastrichtian in age. Marquillas *et al.* (2005) place this lithostratigraphic unit in the latest stage of the Cretaceous based on the presence of the Palmar Largo volcanic rocks, intercalated between the top of the Los Blanquitos Formation and the base of the Balbuena Subgroup and dated to 70 ± 5 Mya (K/Ar) (Gómez Omil *et al.* 1989). The onset of sedimentation of the overlying Yacoraite Formation was additionally estimated by Montano *et al.* (2022) at 68.1 ± 0.9 Mya and 67.9 ± 1.7 Mya via zircon and carbonate geochronology, respectively, while the oldest date obtained by Rohais *et al.* (2019) for the base of the Yacoraite Formation was 69.1 ± 0.7 Mya from a reworked tuff/ash layer, indicating a slightly older age for the base of this unit. The results of these studies, therefore, suggest that the Lecho Formation probably deposited in the beginning or middle of the Maastrichtian, around 71 to 69 Mya.

In El Brete, the Lecho Formation is a 37-m thick layer consisting of mainly reddish, yellowish, or greyish, fine to medium, and occasionally coarse, sandstones with some micaceous levels deposited during an overall transgressive trend (Bonaparte *et al.* 1977, Powell 2003, Deschamps *et al.* 2020; Fig. 2C). Bonaparte and Powell (1980: 26) noted that the sedimentary sequence indicates 'a fluvial-lacustrine coastal plane made up of sandy sediments, plus surrounding ponds and lagoons where vegetation favored the reducing environment in which the sediments were deposited'. The dinosaur material was uncovered in fine greenish-grey sandstones with coarse and irregular stratification, as well as discontinued dolomitic cementation partially replaced by idiotopic hematite and dolomite (Bonaparte *et al.* 1977). The presence of bones with no attrition marks and articulated vertebrae suggests an accumulation in a low-energy river. Bonaparte *et al.* (1977) estimated that the direction of the current was NW–SE, with the river flowing towards the north-east, based on the orientation of 30 bones.

Although crocodiles, turtles, lizards, and fish must have been part of this ecosystem, the fauna from the Lecho Formation is currently restricted to dinosaurs and consists of the large herbivorous titanosaurid *Saltasaurus*, the small-bodied carnivore *Noasaurus*, one, possibly more, large apex theropods represented by isolated (abelisaurid?) teeth, as well as several species of primitive enantiornithes birds (see Introduction). All dinosaur specimens are represented by skeletal elements, and no ichnofossils or fossils of non-dinosaur vertebrate, insects, and plant material have been reported from the El Brete fossil site. The faunal assemblage from El Brete lived in a warm and humid environment close to the Tropic of Capricorn (PBDB palaeocoordinates: S28.6° W52.0°) with tropical to subtropical forests that may have developed in the coastal regions (Marquillas *et al.* 2005, Quattrocchio *et al.* 2005, Narváez and Volkheimer 2011). The floral assemblage from the Lecho Formation in the Quebrada de Vilches area, which is situated only a few kilometers away from El Brete, includes typical Mesozoic plants such as the conifers *Classopollis* (Cheirolepidiaceae) and *Callialasporites* (Podocarpaceae), the ferns *Azolla* (Salviniaceae) and *Todisporites* (Osmundaceae), the gnetophyte *Ephedripites* (Ephedraceae), as well as the angiosperms *Bombacacidites* (Bombacoideae), *Retitrescolpites* (Magnoliophyta), and *Rhoipites* (Rutaceae) (Quattrocchio *et al.* 2005).

Comparative anatomy, terminology, and classification

The holotype of *Noasaurus leali* (Figs 1E, 3A, B) is deposited at the palaeontological collections of the Fundación Miguel Lillo of San Miguel de Tucumán under the collection number PVL 4061. The material was examined first hand by four of us (C.H., M.A.C., F.L.A., and R.D.) with the help of digital cameras and a portable microscope AM411T-Dino-Lite Pro. The material could not be CT-scanned as holotypes are not allowed to be taken outside the palaeontological collections of the Fundación Miguel Lillo (P. Ortiz, pers. comm. 2022). Measurements were taken on the specimens with a digital calliper (Tables 2, 3; Supporting Information, S2.1). For comparisons, we thoroughly examined the material of more than 100 species-level theropods (Supporting Information, S1.3), among which eight taxa (i.e. *Huinculsaurus*, *Ligabueino*, *Limusaurus*, *Masiakasaurus*, *Noasaurus*, *Velocisaurus*, *Vespersaurus*, and ML 2050) classified as noasaurids by some authors (e.g. Rauhut and Carrano 2016, Wang *et al.* 2017a) and belonging to institutions from Argentina, Brazil, China, Portugal, and the USA.

The non-standardized traditional Owenian/Romerian directional and anatomical terms (Harris 2004, Wilson 2006) were favoured over the terminology of the Nomina Anatomica Veterinaria (Waibl *et al.* 2012) to describe the cranial and postcranial material of *Noasaurus*, so that anterior and posterior are used as directional terms rather than the alternatives cranial and caudal, respectively. Likewise, the dental anatomy of *Noasaurus* was described using the terminology, modus operandi, and annotations proposed by Hendrickx *et al.* (2015d). The latter is based on the recommendations of Smith and Dodson (2003) for positional and directional terms with mesial, distal, labial, and lingual being favoured over anterior, posterior, external/buccal, and internal, respectively. The terminologies provided by Hendrickx and Mateus (2014b) and Hendrickx *et al.* (2015a) were followed to describe the maxilla and quadrate of *Noasaurus*, respectively, whereas Wilson (1999) and Wilson *et al.*'s (2011) nomenclatures and abbreviations were used to describe the axial skeleton. We finally followed the phylogenetic definitions compiled in Table 1 for each ceratosaur clade, which is mainly based on the work of Wilson *et al.* (2003), Hendrickx *et al.* (2015b), Rauhut and Carrano (2016), and Rauhut and Pol (2021).

Phylogenetic analysis

The phylogenetic placement of *Noasaurus leali* was explored using three independently-developed datamatrices, namely Agnolín *et al.* (2022), Baiano *et al.* (2023), and Rauhut and Pol (2021) (Supporting Information, S3, S5). The scoring of

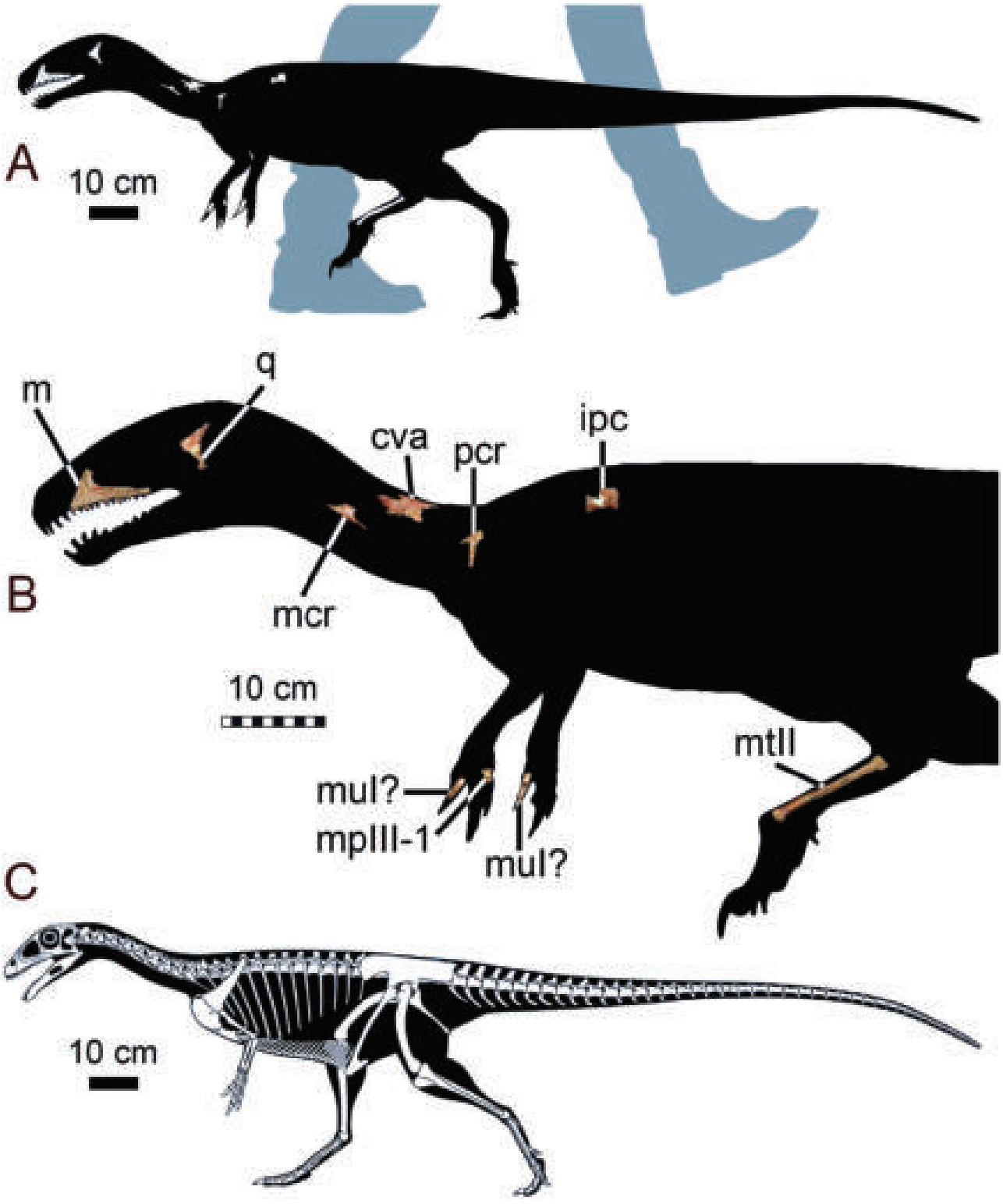

Figure 3. Preserved material and tentative reconstruction of *Noasaurus leali*. A, B, size estimation and position of the holotypic cranial and postcranial elements of *Noasaurus leali* (black silhouette with preserved material in white from Jaime A. Headden; used with permission; modified); C, skeletal reconstruction of *Noasaurus leali* in lateral view based on a reconstruction of *Masiakasaurus knopfleri* from Scott Hartman (used with permission; modified). Abbreviations: cva, cervical vertebral arch; ipc, indeterminate postcervical centrum; q, quadrate; m, maxilla; mcr, mid cervical rib; mpIII.1, first manual phalanx of digit III; mtII, metatarsal of digit II; muI?, manual ungual possibly from digit I; pcr, posterior cervical rib.

Table 2. Selected measurements on the cranial and postcranial material of *Noasaurus leali* (PVL 4061). Additional measurements are provided in the Supporting Information, S2.1.

	Measurements (in mm)
Maxilla	
Total length	74.86
Total height	33.48
Tooth row, length	66.71
Maxillary fossa, height	9.07
Anteromedial process, preserved length	7.59
Quadrate	
Maximum length (distance from the anterior margin of the pterygoid flange to the quadrate ridge)	20.34
Maximum height	43.18
Maximum width (at the mandibular articulation)	13.78
Mandibular articulation, preserved length	10.46
Cervical vertebral arch	
Maximum length	55.78
Maximum height	19.34
Maximum width	27.33
Mid cervical rib	
Maximum length (along the buttressed ridge)	46.99
Maximum height (distance from the capitulum to the tuberculum)	17.9
Maximum width (distance from the capitulum to the buttressed ridge)	15.26
Posterior cervical rib	
Maximum length (along the preserved buttressed ridge)	24.47
Maximum height (distance from the capitulum to the posterodorsal point on the buttressed ridge)	37.46
Maximum width (distance from the tuberculum to the buttressed ridge)	19.44
Indeterminate postcervical vertebra	
Maximum length	32.48
Maximum height (along the posterior articular surface)	20.64
Maximum width (along the posterior articular surface)	14.73
Width at midlength	6.38
Non-ungual manual phalanx	
Maximum length	15.9
Maximum height	8.22
Maximum width	11.49
Manual ungual I? (left?; incomplete)	
Maximum preserved length	25.75
Maximum height	13.17
Maximum width	7.94
Manual ungual I? (right?; complete)	
Maximum length (from the distal tip to the proximodorsal extremity)	36.66
Maximum height (along the proximal articular surface)	13.27
Maximum width	7.98
Flexor fossa, length	17.13
Metatarsal II	
Maximum height (from the proximal to the distal extremities)	115.56
Maximum length along the proximal articular surface	14.92
Maximum height along the proximal articular surface	6.23
Maximum length along the distal articular surface	15.07
Maximum width along the distal articular surface	12.08
Length at mid-height	8.98
Width at mid-height	4.4

Noasaurus was fully revised in each of these datasets based on our detailed examination of the holotypic specimens. The first two datamatrixes focus on the relationships of ceratosaurs, whereas Rauhut and Pol's (2021) dataset explores the non-avian theropod phylogeny more widely, with a good representation of ceratosaur taxa. Agnolín *et al.* (2022), Baiano *et al.* (2023), and Rauhut and Pol's (2021) datamatrices are based on the datasets initially assembled by Tortosa *et al.* (2014), Rauhut and Carrano (2016), and Wang *et al.* (2017a), respectively [NB—all these datasets, however, go back to the work of Carrano and Sampson (2008) and Canale *et al.* (2009)]. The type specimen of *Spinostropheus gautieri* MNHN 1961-28 was removed from the three datasets following Rauhut and Carrano's (2016) view that this taxon is most likely a non-ceratosaur theropod, possibly a basal tetanuran. Specimen MNN TIG6, referred to *Spinostropheus gautieri* by Sereno *et al.* (2004) but probably representing a different taxon of ceratosaur (Rauhut and Carrano 2016), was nevertheless included in all three datasets. The scoring of this specimen in Agnolín *et al.* (2022) and Rauhut and Pol's (2021) datasets is a revised version of the scoring of *Spinostropheus*, where all non-axial characters were considered as unknown. Likewise, *Camarillasaurus*, thought to be a ceratosaur by Sánchez-Hernández and Benton (2014) and reclassified as a spinosaurid by Samathi *et al.* (2021), was excluded from Agnolín *et al.* (2022) and Baiano *et al.*'s (2023) datamatrices.

Agnolín *et al.*'s (2022) include the modifications in the character list, character scoring, and operational terminal units (OTUs) provided by Filippi *et al.* (2016), Zaher *et al.* (2020), Gianechini *et al.* (2021), and Aranciaga Rolando *et al.* (2021). The putative noasaurids *Afromimus*, *Berthasaura*, *Huinculsaurus*, and *Vespersaurus* were added to this datamatrix based on the literature, photos shared by colleagues, and/or personal examination of the material by three of us (R.D., M.A.C., and F.L.A.). A few characters from *Austrocheirus*, *Masiakasaurus*, *Pycnonemosaurus*, *Viavenator*, and *Llukalkan* were also rescored

Table 3. Measurements and ratio variables in the maxillary dentition of *Noasaurus leali* (PVL 4061). Data partly taken from Hendrickx *et al.* (2015c). Abbreviations: CBL, crown base length; CBR, crown base ratio; CBW, crown base width; CH, crown height; CHR, crown height ratio; DC, distocentral denticle density; de/5 mm, denticles per 5 mm; MC, mesiocentral denticle density; MCR, mid-crown ratio.

First maxillary crown	
CH	>2.67 mm
CBL	3.19 mm
CBW	2.07 mm
CBR	0.6489
DC	21.25 de/5 mm
Third maxillary crown	
CH	>3.12 mm
CBL	3.54 mm
CBW	1.98 mm
CBR	0.5593
DC	22.5 de/5 mm
MC	32.5 de/5 mm
Sixth maxillary crown	
CH	3.54 mm
CBL	3.11 mm
CBW	1.84 mm
CHR	1.07
CBR	0.5916
DC	20/5 mm
Eighth maxillary crown	
CH	4.98 mm
CBL	3.04 mm
CBW	1.81 mm
CHR	1.6381
CBR	0.5954
MCR	0.589
DC	25 de/5 mm
MC	32.5 de/5 mm
Tenth maxillary crown	
CBL	2.83 mm
CBW	1.53 mm
CBR	0.5406

in Agnolín *et al.*'s (2022) datamatrix, whose revised version includes 431 characters (among which 64 are ordered) scored in 49 theropod taxa (1.21% of new and modified scorings; 70.79% of missing data; Supporting Information, S3.1, S5).

Baiano *et al.*'s (2023) updated dataset incorporates the abelisauroids *Afromimus*, *Arcovenator*, *Berthasaura*, *Huinculsaurus*, *Kiyacursor*, *Kurupi*, *Pycnonemosaurus*, *Spectrovenator*, *Thanos*, *Vespersaurus* (holotype and composite), and *Viavenator*, as well as the abelisaurid and elaphrosaurine specimens MPM 99 and NMV P25204, respectively, using the scorings of Langer *et al.* (2019), Poropat *et al.* (2020), Zaher *et al.* (2020), Baiano *et al.* (2021, 2023), Ibiricu *et al.* (2021), Iori *et al.* (2021), de Souza *et al.* (2021), and Averianov *et al.* (2024) [NB—scorings of *Aucasaurus* and *Kurupi* were taken from Baiano *et al.* (2023)]. We added to this combined datamatrix the noasaurid *Ligabueino* and the putative abelisauroid *Austrocheirus* [NB—the latter is considered as an indeterminate theropod by Rauhut (2012)]. We also coded the missing scorings for *Berthasaura*, *Deltadromeus*, MNN TIG6, and USNM 8415, as well as the holotype and composite specimen of *Vespersaurus*, and revised some scorings of *Deltadromeus*. Our updated version of Baiano *et al.*'s (2023) datamatrix encompasses 246 discrete characters (among which 14 are ordered) scored in 54 taxa (5.13% of new and modified scorings; 77.09% of missing data; Supporting Information, S3.2, S5).

We finally added to Rauhut and Pol's (2021) extensive datamatrix the noasaurids *Afromimus*, *Berthasaura*, *Huinculsaurus*, and *Vespersaurus*, and changed a few scorings in *Masiakasaurus*, *Dilophosaurus wetherilli*, and *Monolophosaurus*. Character 30 on the presence of a pneumatic structure in the anterior portion of the maxillary antorbital fossa was additionally revised to take into account the presence of a sharply rimmed maxillary fossa/fenestra in the maxilla of some theropods. The resulting dataset is comprised of 746 discrete characters (among which 106 are ordered) scored in 206 non-avian theropods (1.71% of new and modified scorings; 72.38% of missing data; Supporting Information, S3.3, S5).

The datamatrices were managed with MESQUITE 3.5 (Maddison and Maddison 2017) and analysed with the computer program TNT 1.5 and 1.6 (Goloboff and Catalano 2016, Goloboff and Morales 2023) using parsimony equal weight as an optimality criterion, as well as additivity following the original matrices. As a search strategy, we used the 'New technologies' option with 50 hits to the minimum length. We employed tree-fusing and tree-drifting algorithms in all three datamatrices and sectorial searches for Rauhut and Pol's (2021) dataset, in all cases with default options. The trees obtained were then subjected to a final round of TBR branch-swapping, keeping up to 3000 optimal trees. The resolution of the strict consensuses was improve using the 'prunnelsen' TNT function.

Both palaeogeographic history and size evolution of ceratosaurs were explored using the tree topologies obtained in the three phylogenetic analyses after pruning the most unstable taxa (see Table 4) and information on the continent of origin and body length of each taxon (Supporting Information, S2.2, S5). Data on geographic and stratigraphic distribution in theropods was taken from the primary literature, whereas data on estimated body length are either published values or personal estimations based on the body proportion of the most complete non-avian theropods, and correlation between the total body length and skull and long bone's (e.g. femur, tibia, and humerus) length (Supporting Information, S2.2, S5).

Feeding ecology analyses

No direct evidence of *Noasaurus*' diet is currently available and we, therefore, relied on its dental and appendicular anatomy to speculate about the possible feeding ecology of this small-bodied theropod. The morphology of teeth is the most conspicuous indicator of diet and we, therefore, explored the feeding habits of *Noasaurus* using a dentition-based datamatrix on theropods as comparative purposes. A cladistic analysis was performed on a revised version of the dentition-based datamatrix

Table 4. Information on the datamatrices used in the phylogenetic analyses and list of wildcard taxa pruned in each datamatrix. Abbreviations: CI, consistency index; char., characters; inf., informative; Nb, number; RI, retention index. *Wildcard taxa kept in the analyses whose results are illustrated in Figs 15–17.

Datamatrix	Nb of char.	Nb of inf. char.	Nb of taxa	Missing data	Nb of trees	Node consensus	Pruned taxa	CI	RI
Agnolín *et al.* (2022)	431	406	49	70.78%	>3000	19	*Deltadromeus, Guemesia, Huinculsaurus, Laevisuchus**, *Niebla, Pycnonemosaurus, Quilmesaurus, Tarascosaurus*, and *Velocisaurus**	0.491	0.653
Baiano *et al.* (2023)	246	246	54	77.09%	>3000	4	*Afromimus**, *Austrocheirus, Dahalokely, Deltadromeus**, *Elemgasem**, *Genusaurus, Huinculsaurus, Kryptops, Kurupi**, *Laevisuchus**, *Masiakasaurus**, MPCN PV 69, MNN TIG6, MPM 99*, *Pycnonemosaurus**, *Quilmesaurus, Thanos*, USNM 8415*, *Vespersaurus* (holotype)* and *Xenotarsosaurus*	0.452	0.708
Rauhut and Pol (2021)	746	736	206	72.38%	>3000	87	*Afromimus, Archaeornithomimus, Arcovenator, Austroraptor, Berberosaurus, Buitreraptor, Coelurus, Deltadromeus, Genusaurus, Gigantoraptor, Hesperonychus, Huinculsaurus, Ilokelesia, Irritator, Kelmayisaurus, Kileskus*, Lourinhã Fm ceratosaur, MB r 3621, Moenave coelophysoid, MPEF PV 10889, MPEF PV 6533, *Sarcosaurus woodi, Segisaurus, Shenzhousaurus, Sinotyrannus, Skorpiovenator, Troodon, Xenotarsosaurus*	0.194	0.631
Hendrickx *et al.* (2023) (dentition-based datamatrix)	148	143	125	32.35%	>10 000	42	*Aorun, Australovenator, Austroraptor, Caudipteryx**, *Compsognathus**, *Jaculinykus, Juravenator, Halszkaraptor, Haplocheirus, Megaraptor, Natovenator, Orkoraptor, Saltriovenator, Scipionyx**, *Sciurumimus*	0.224	0.592

implemented by Hendrickx and Mateus (2014a) and last updated by Hendrickx *et al.* (2023) without constraining a topological tree. Twenty non-avian saurischians (i.e. *Acheroraptor, Alxasaurus, Austroraptor, Beipiaosaurus, Berthasaura,* BP/1/5278, *Dracoraptor, Fukuivenator, Gnathovorax, Harpymimus, Jaculinykus, Natovenator, Notatesseraeraptor, Oxalaia, Saltriovenator, Spectrovenator, Vespersaurus, Wiehenvenator, Yi,* and *Ypupiara*) were added to Hendrickx *et al.*'s (2023) datamatrix. The unenlagiine dromaeosaurid *Ypupiara* was included using Brum *et al.*'s (2021) published scoring of this taxon, whereas the other taxa were scored based on personal observation of the material, photos shared by colleagues, and the literature (Supporting Information, S1.5). The scorings of many taxa were revised, especially those of *Bambiraptor, Daemonosaurus, Falcarius, Halszkaraptor, Saurornitholestes,* and *Velociraptor*. We finally added several new dental character states (i.e. state 5 of character 2; state 3 of character 13, and state 6 of character 45) to take into account variations in the dentition that were not considered before. This includes the number of tooth, the presence of an open alveolar groove, and the position of the tooth row in the premaxilla, as well as the cross-section outline of mesialmost teeth. The resulting dentition-based datamatrix includes 148 dentition-based characters scored in 125 theropod taxa (Supporting Information, S1.5). All cladistic analyses were performed using TNT 1.5 following the protocol detailed by Hendrickx *et al.* (2020b, 2023) and keeping up to 10 000 trees.

Although not intrinsically linked to the diet of an animal, the morphology of manual unguals has been used to hypothesize functionality and possible feeding habits in non-avian theropods (e.g. Lautenschlager 2014, Chinzorig *et al.* 2018, Qin *et al.* 2023, Kubota *et al.* 2024). We, therefore, compared the curvature and elongation of the manual ungual of *Noasaurus*, tentatively referred to the first digit (see below) and whose morphology is peculiar, to that of other non-avian theropods. Because this is a functional analysis, we here consider that the claw from the first finger of all non-avian theropods is manual ungual I [unlike a few authors such as Xu *et al.* (2009, 2015, 2017) and Choiniere *et al.* (2014a) who consider that the first manual finger of some coelurosaurs such as *Aorun, Linhenykus,* and *Yi* represents digit II]. Our dataset on theropod manual unguals compiles data on the curvature and elongation of 156 claws from digit I belonging to 133 theropod taxa (mainly non-avian forms; see Supporting Information, S1.5, S5). Some taxa such as *Allosaurus* (4), *Archaeopteryx* (4), and *Anchiornis* (3) are represented by more than one manual ungual I. Both curvature and elongation were measured on the bony core of the manual claw in lateral or medial views using photos taken by us, shared by colleagues, or available in the literature (Supporting Information, S1.5). The claw elongation corresponds in this study to the ratio between the claw length (chord AB), which is the distance between the distalmost point at the tip of the claw (point A) to the point directly proximal to the flexor tubercle (point B), divided by the claw height (chord BD), the distance between the points B and D, where D is the intersection of the perpendicular of the chord AB at the point B on the dorsal curvature of the claw (Supporting Information, S1.5, Fig. SA7). The curvature of the claw was measured using the angle of curvature Y, calculated using Feduccia's (1993) methodology (NB—this method is here applied to the bony core of the manual ungual instead of the

keratinous sheath). Y is the angle between the chord AE' and BE', where A is the distalmost point situated at the tip of the claw and B the point directly proximal to the flexor tubercle at the ventral margin of the claw. Finally, E', is a point created by the intersection of the perpendiculars bisecting the chords AX and BX, where X is located on the ventral margin of the claw's curvature at equal distance between A and B (Supporting Information, S1.5, Fig. SA7). The elongation and curvature of the manual ungual were calculated in Fiji (Schindelin *et al.* 2012, Rueden *et al.* 2017) using custom plugins created by Emanuele Martini (IFOM, FIRC Institute of Molecular Oncology, Milan, Italy) for the claw curvature, and Prof. Dr H. Glünder (Munich Center for Neuroscience and Technische Universität Darmstadt) for the length/width ratio. The results of the various analyses on feeding ecology are presented and discussed after the description of the *Noasaurus* material.

Systematic palaeontology

Dinosauria Owen, 1842

Theropoda Marsh, 1881

Ceratosauria Marsh, 1884

Abelisauroidea Bonaparte, 1991

Noasauridae Bonaparte and Powell, 1980

Noasaurinae Bonaparte and Powell, 1980 *sensu* Rauhut and Carrano, 2016

Genus *Noasaurus* Bonaparte and Powell, 1980

Species *Noasaurus leali* Bonaparte and Powell, 1980

Derivation of generic name: From *NOA*, the acronym for north-western Argentina ('Noroeste Argentino' in Spanish), a geographic and historical region of Argentina composed of the provinces of Catamarca, Jujuy, La Rioja, Salta, Santiago del Estero, and Tucumán (NB—this is the first acronym to be used in the genus of a non-avian theropod; Molina-Pérez and Larramendi 2019), and *sauros* (σαύρα) meaning 'lizard' or 'reptile'. Etymologically, *Noasaurus* translates to 'reptile from north-western Argentina'.

Derivation of specific name: From the family name 'Leal' to honour lab technician and discoverer of the El Brete fossil site Juan Carlos Leal (Fig. 1A).

Holotype: PVL 4061, a left maxilla with five erupted crowns, a right quadrate, a mid-posterior cervical vertebral arch, a mid-cervical rib, a posterior cervical rib, an indeterminate postcervical vertebra, a manual phalanx of digit III, manual unguals possibly belonging to the left and right digit I, and a right metatarsal II (Figs 1E, 3A, B; Tables 2, 3).

Occurrence and age: El Brete Estancia, Department of Candelaria, southern Salta Province, Northeastern Argentina (Fig. 2A, B); Lecho Formation, Balbuena Subgroup, Salta Group; early or mid Maastrichtian, Upper Cretaceous (Bonaparte *et al.* 1977, Bonaparte and Powell 1980, Marquillas *et al.* 2005, Montano *et al.* 2022; Fig. 2C).

Diagnosis: Ceratosaur theropod with the following autapomorphies: (i) a concave alveolar margin of the maxilla; (ii) a diagonally oriented ridge along the dorsal portion of the maxillary fossa; (iii) a strongly arched quadrate body with a dorsoventrally low anterior margin of the pterygoid flange; (iv) maxillary crowns with minute mesial denticles and a low number (<30) of comparatively large distal denticles not diminishing in size basally; (v) a cervical neural arch with anterior epipophyseal prongs (modified from: Bonaparte and Powell 1980); (vi) a well-defined and acute middle longitudinal crest on the ventral surface and at midlength of the manual ungual blade (modified from: Agnolín and Chiarelli 2010); (vii) a strongly ventrally curved manual ungual forming an angle of about 90°; (viii) a manual ungual with a deep C-shaped articular surface in lateral view; and (ix) a deep subtriangular flexor fossa delimited distally by two ridges forming a V on the manual ungual (modified from: Bonaparte and Powell 1980, Agnolín and Chiarelli 2010).

Body length, body mass, and age: As early as its first mention in the literature, *Noasaurus* was seen as a small theropod not exceeding 2 m (Bonaparte *et al.* 1977). The total length of this theropod was later estimated to be <1 m (Bonaparte 1996b, 2007), <1.5 m (Bonaparte 1996a), 1.5 m (Novas 2009, Paul 2010, 2016, 2024), 2.4 m (Lambert 1983, 1990, 1993, Holtz 2007), and 3 m (Benton 1984, Molina-Pérez and Larramendi 2019) in subsequent work. None of these authors, however, applied a formula to estimate the body length of *Noasaurus*. Using our dataset on skull, metatarsal, and body lengths in the most complete theropods (Supporting Information, S1.6), *Noasaurus* is estimated to be around 2 m in length using an estimated cranial length of 185 mm, and 1.6 m using the proximodistal height (115 mm) of metatarsal II. Our formula relies on metatarsal III, which is the tallest metatarsal of the foot and whose measurements are typically given in the literature. Because metatarsal II is slightly proximodistally shorter than metatarsal III in noasaurids (Noasaurinae + Elaphrosaurinae), the body length of *Noasaurus* probably ranged between 1.7 and 2 m (Fig. 3A, C).

No femur or tibia is preserved to calculate the body mass of *Noasaurus* using Benson *et al.*'s (2014), Campione *et al.*'s (2014), or Campione and Evans' (2020) formulas. *Noasaurus*' body mass was estimated to be around 6 kg by Paul (2024), 15 kg by the same author (1988, 2010, 2016), and 38 kg by Molina-Pérez and Larramendi (2019). Likewise, the age of *Noasaurus* could not be assessed as histological analysis on the holotype is currently forbidden. Stiegler (2019), however, suggested that the *Noasaurus* material may belong to an immature individual based on the strongly arched quadrate, a condition restricted to immature individuals of *Limusaurus*.

DESCRIPTION

Cranium

Preserved cranial elements

The cranial elements of *Noasaurus* include a fairly complete left maxilla preserving five partially to almost complete erupted

teeth, as well as a relatively complete right quadrate (Figs 3A, B, 4–6; Tables 2, 3). The squamosal described by Bonaparte and Powell (1980: fig. 7D, E; Fig. 1E) was later identified as a cervical rib by Novas (1989) in his Ph.D. dissertation (Bonaparte 1991) and is consequently described in the section 'Axial skeleton'.

Maxilla

Most of the left maxilla is undistorted and only the posterior extremity of the jugal ramus is out of place (Fig. 4). Multiple fractures are, however, present throughout the bone, the two main ones crossing the middle parts of the ascending and jugal rami horizontally and vertically, respectively. A small piece of bone directly ventral to the ascending ramus was also glued back. The maxilla has been damaged since 2012 (when it was examined the first time by one of us), with an additional fracture at the base of the ascending ramus, while the first maxillary tooth is now loose and kept separately (Fig. 6O, P). The distalmost portion of the ascending ramus illustrated by Bonaparte and Powell (1980) is also missing and most likely lost. A photo of the maxilla provided by Candeiro (2007) shows that this portion of the ascending ramus was already missing before 2007. However, an illustration of the *Noasaurus* material published by Bonaparte (2007), as well as a movie showing some of the specimens shortly after their preparation (Fig. 1D; Supporting Information, S1.2), confirm that the missing part was originally present.

The maxillary bone is fairly complete, missing the dorsal part of the ascending ramus, the anterior portion of the anteromedial process, the medial wall from the posterior extremity of the jugal ramus, small pieces of the alveolar margin and the antorbital ridge, as well as several maxillary teeth (Fig. 4). In lateral view, the maxilla consists of a subtriangular bone with a dorsoventrally tall maxilla body, a short ascending ramus, an anteroposteriorly short pre-antorbital body and long jugal ramus (Fig. 4A). The preserved maxilla is dorsoventrally lower than anteroposteriorly long and the complete bone (Fig. 1E) was longer than tall. The anterior body occupies two-fifths of the maxillary length and is shorter than the jugal ramus. Its anteriormost part is particularly short and dorsoventrally lower than the jugal ramus (Fig. 4A). The anterior margin of the anterior body is weakly concave and posterodorsally inclined at an angle of 53° from the long axis of the alveolar margin. Both the anterior ramus and pre-antorbital body of the maxilla are roughly subtriangular in outline and the angles of the anterior corner of the anterior ramus and pre-antorbital body are approximately 43° and 48°, respectively

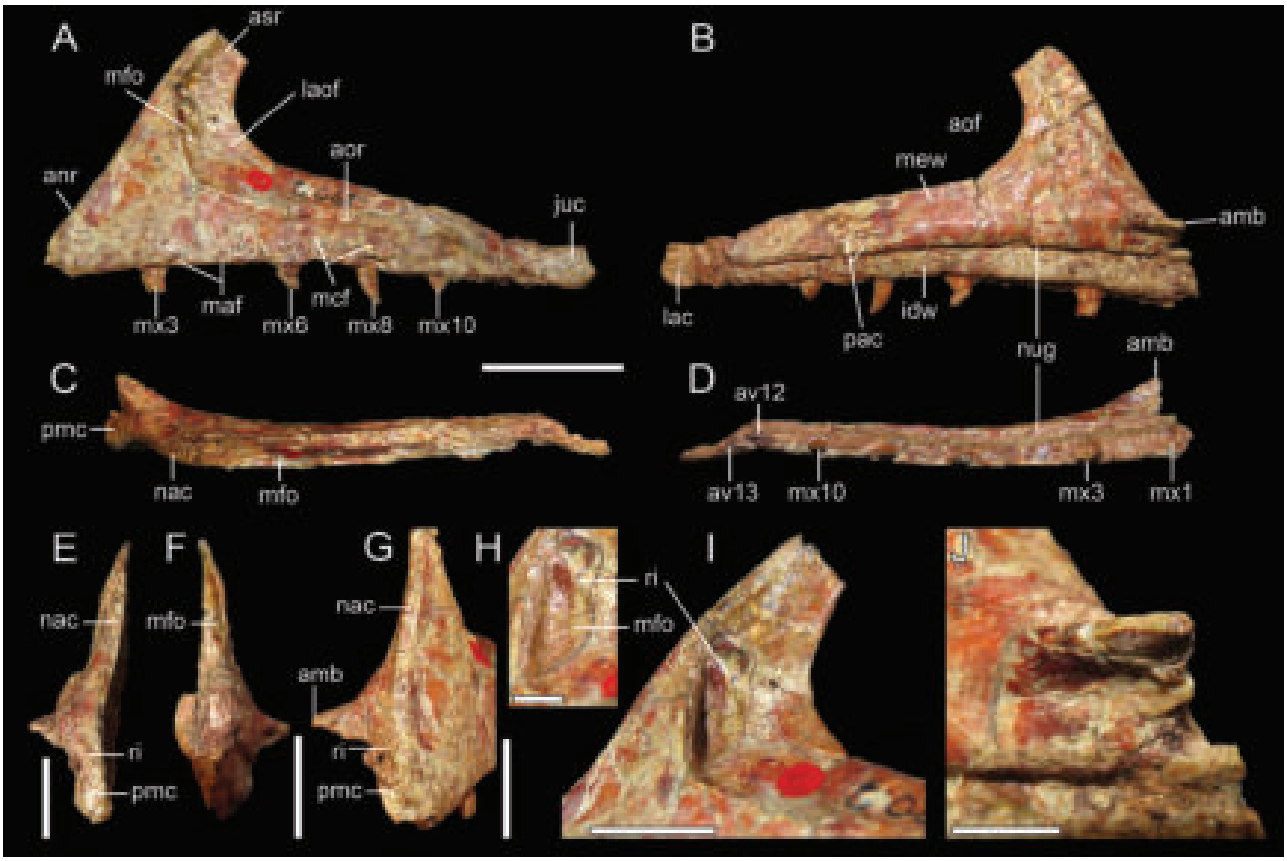

Figure 4. Maxilla of *Noasaurus leali* (PVL 4061). Left maxilla in: A, lateral; B, medial; C, dorsal; D, ventral; E, anterior; and F, posterior views; with F–J, close-up on G, the anterior surface of the maxilla in anterolateral view; H, the maxillary fossa in posterolateral view; I, the maxillary fossa and ascending process in lateral view; J, the anteromedial process in ventromedial view. Abbreviations: amb, anteromedial process; anr, anterior ramus; aof, antorbital fenestra; aor, antorbital ridge; asr, ascending ramus; av12, 12th maxillary alveolus; av13, 13th maxillary alveolus; idw, interdental wall; juc, jugal contact; lac, lacrimal contact; laof, lateral antorbital fossa; maf, maxillary alveolar foramina; mcf, maxillary circumfenestra foramina; mew, medial wall; mfo, maxillary fossa; mx1, first maxillary tooth; mx3, third maxillary tooth; mx6, sixth maxillary tooth; mx8, eight maxillary tooth; mx10, 10th maxillary tooth; nac, nasal contact; nug, nutrient groove; pac, palatine contact; pmc, premaxilla contact; ri, ridge. Scale bars equal 2 cm (A–D), 1 cm (E–G), and 5 mm (H, J).

(Fig. 4A). The anterior ramus occupies one-half of the anterior body and three-fourths of the antorbital body. The anterior margin of the maxilla is weakly sigmoid, with the margin of the anterior body and the ventral one-third of the preserved ascending ramus being slightly concave while the dorsal two-thirds of the remaining ascending ramus is weakly convex. The alveolar margin of the maxilla is gently concave, with the apex of the concavity located around half the length of the bone (Fig. 4A). The jugal ramus, which accounts for ~67% of the maxillary body, corresponds to an elongated subtriangular projection pointing posteriorly and delimited by two weakly sigmoid, almost straight ventral and dorsal margins. The jugal contact at the posterior end of the jugal ramus forms an almost right-angled isosceles triangle pointing anteriorly in lateral view. Based on Bonaparte and Powell (1980: fig. 7A, B; Fig. 1E), the ventral two-thirds of the ascending ramus mainly projects dorsally, perpendicular to the alveolar margin of the maxilla, whereas the dorsal third curves posterodorsally at an angle of ~45° from the long axis of the alveolar margin. The dorsal extremity of the ascending ramus was forked, with the two short dorsal and ventral subtriangular extremities projecting posterodorsally and posteriorly, respectively, as revealed by Bonaparte and Powell's (1980) figure 7A, B (Fig. 1E; NB—the oldest available photo of the maxilla provided by Bonaparte (2007) reveals that the posteriormost extremity of the ascending ramus was already missing before 2007; Supporting Information, S1.1, Fig. SA3). The forked extremity of the ascending ramus was probably articulating with the anterior process of the lacrimal. If we cannot exclude the fact that the ascending ramus illustrated by Bonaparte and Powell (1980) was incomplete and the articulation with the lacrimal, which may have then occurred more posteriorly, had a different shape, a posterior U-shaped fork of the ascending process is the typical morphology for the lacrimal contact of the maxilla in theropods (Rauhut, pers. comm. January 2024), supporting the fact that the ascending ramus figured by Bonaparte and Powell (1980) was complete.

A row of maxillary alveolar foramina is present, directly dorsal to the alveolar margin, parallel to the latter. The foramina are difficult to discern as most of them are obscured by matrix or correspond to a very shallow depression, but they can be seen with razing light. A second row of foramina, the maxillary circumfenestra foramina, is present directly ventral to the antorbital ridge and the most visible foramina are present at the level of mx6-8 (Fig. 4A).

A well-delimited antorbital fossa is present laterally, extending over the posterior one-third of the anterior body, the dorsal one-third of the jugal ramus, and the anterodorsal two-thirds of the ascending process (Fig. 4A). This fossa is ventrally delimited by a low and thick (i.e. dorsoventrally tall) antorbital ridge extending along the dorsal third of the maxillary body ventral to the antorbital fossa. The antorbital ridge narrows and fades anteriorly up to an angular corner formed by the vertically and horizontally orientated borders of the antorbital fossa, at the level of the fourth alveolus. Conversely, the antorbital ridge only slightly narrows posteriorly and remains prominent in its posteriormost part where it curves ventrally to reach the alveolar margin at the level of the tenth alveolus. The jugal contact consists of a rugose and poorly delimited surface located within the posteriormost part of the antorbital fossa, directly dorsal to the posterior extremity of the antorbital ridges. This contact roughly covers the posterior one-fourth of the jugal ramus; however, it is possible that it extended further posteriorly. There is no clear anterior limit of the jugal contact, which is mainly distinguished by its rugose surface and the presence of parallel ridges and grooves directed anteroposteriorly along the posterior half of the articulation surface.

A maxillary fossa is visible in the anterior corner of the lateral antorbital fossa (Fig. 4H, I). This pneumatic structure, interpreted by Stiegler (2019) as the pneumatic recess of the ascending ramus (e.g. but see Discussion below), can be described as a shallow and poorly delimited oval depression on the lateral wall of the antorbital fossa. The maxillary fossa is taller than long and occupies the same height as the dorsoventrally oriented and anteriorly inclined margin of the antorbital fossa. The anterior part of the maxillary fossa is bounded medially by the anterolateral wall of the maxillary body and cannot be seen in lateral view. In the visible posterior half, the fossa is ventrally and dorsally delimited by faint, rounded ridges, which become more prominent and increase in dorsoventral height anteriorly up to the anterior border of the antorbital fossa. A faint and low anteroposteriorly directed and anterodorsally inclined ridge crosses the maxillary fossa at two-thirds of its height (Fig. 4H, I). The maxillary fossa is filled with sediment in its anteriormost part and it is, therefore, unknown whether it extends more anteriorly within the maxillary body. This pneumatic structure does not at least communicate laterally, medially, or anteriorly by any opening. No maxillary, promaxillary or pneumatic fenestra piercing the maxilla are, consequently, present in the maxilla of *Noasaurus*. Likewise, there is no pneumatic excavation within the lateral wall of the ascending ramus.

In medial view, the maxilla is characterized by a tall medial wall dorsally, a short interdental wall ventrally, a prominent anteromedial process in the anteroventral corner of the bone, and faint palatal contact along the posterior two-thirds of the maxilla, directly dorsal to the dorsal wall (Fig. 4B). The medial wall covers the whole jugal ramus and most of the maxillary body, whereas the interdental wall is restricted to the ventral fourth of the maxillary body. The surface of both medial and interdental walls is smooth (i.e. there are no rugosities or ridges) and relatively uniform. The interdental wall is separated from the medial wall by a well-marked step-like nutrient groove sloping ventrally posteriorly and running along the whole maxilla length. The interdental wall, which results from the fusion of the interdental plates, reaches its tallest dorsoventral height at the level of the anterior margin of the maxilla, and gradually diminishes in height dorsally (Fig. 4B). It, however, continuously occupies the ventral third of the jugal ramus all along its length. The ventral margin of the interdental wall extends slightly more dorsally than the alveolar margin of the maxilla. A low and poorly delimited anteroposteriorly directed ridge is visible on the ventralmost surface of the medial wall, directly dorsal to the nutrient groove. This faint ridge is parallel to the interdental wall and shares the same dorsoventral height than the interdental wall along the median wall. The ridge increases in lateromedial thickness before reaching the anteromedial process anteriorly. The latter is located in the anteroventral corner

of the medial wall (Fig. 4J). The anteromedial process consists of a prominent and anteroposteriorly elongated protuberance comprised of two anteroposteriorly oriented ridges separated by a shallow groove. The ventral ridge is more prominent, dorsoventrally taller and lateromedially thicker than the dorsal ridge. It runs anteroposteriorly parallel to the long axis of the nutrient groove. Conversely, the dorsal ridge corresponds to a faint and diagonally oriented prominence curving ventrally towards the ventral ridge up to the anterior margin of the maxilla. The ventral ridge also increases in dorsoventral height and lateromedial thickness anteriorly. The medial process is incomplete and extends further anteriorly beyond the anterior margin of the maxilla (Fig. 4J). The palatal contact of the maxilla is made of two faint and anteroposteriorly directed ridges running along the medial wall of the maxilla, directly dorsal to the nutrient groove, and subparallel to the later (Fig. 4B). The two ridges are faint and badly preserved posteriorly, where they converge, and their preserved parts extend over 14 mm along the central part of the jugal ramus. They become more prominent anteriorly, where they are separated by a distance of around 1 mm, and the dorsal ridge of the palatal contact is prominent enough to delimit a medial antorbital fossa in this part of the maxilla (Fig. 4B).

In ventral and dorsal views, the lateral margin of the maxilla and the medial surface of the medial wall are weakly anteroposteriorly convex and concave, respectively (Fig. 4C, D). The medial process of the maxilla, which strongly protrudes medially from the medial wall, is subtriangular in outline, increasing in lateromedial thickness anteriorly. The posterior extremity of the maxilla where the jugal and lacrimal articulated, is slightly oriented laterally (Fig. 4C, D) but it is unknown if this is due to taphonomic deformations or from the fact that the skull widened at this level of the maxilla. In ventral view, the nutrient groove is filled with sediment and its lateromedial thickness slightly decreases posteriorly to become particularly narrow along the posterior fourth of the medial wall. The maxilla includes 13 alveoli gradually diminishing in size posteriorly (Figs 4D, 6A–C). The alveoli are oval to subrectangular in outline, with weakly to strongly convex medial margins and flatter lateral borders. In dorsal view, the anteromedial process forms a pointy structure directed anteromedially (Fig. 4C). The groove presents on the dorsal surface of the anteromedial process and separates the ventral ridge from the dorsal one, diminishing in lateromedial width anteriorly. The maxillary fossa is lateromedially narrow and delimited laterally by the antorbital ridge. The ascending ramus projects vertically from the maxillary body. The nasal contact, which is present on the anterior border of the ramus, corresponds to a smooth surface with no asperities.

In anterior view, the contact with the premaxilla consists of a relatively uniform and flat surface with no rugosities (Fig. 4E, G). A faint, dorsoventrally elongated, and diagonally oriented ridge extending lateroventrally is present on the dorsal two-thirds of the premaxillary contact (Fig. 4E, G). This ridge extends dorsally from the anteromedial process to the lateral surface of the maxilla ventrally. A dorsoventrally elongated and diagonally oriented depression is present directly medial to this faint ridge and parallel to the later. This depression is shallow ventrally and increases in depth dorsally up to the ventral limit of the anteromedial process. In posterior view, the medial wall delimiting the lateral antorbital fossa is dorsoventrally convex and particularly thin, and the lateral margin of the maxillary fossa forms a symmetrically convex parabola (Fig. 4F). The posterior extremity of the jugal ramus is slightly lateromedially wider in its central part and the lateral border of the jugal ramus is asymmetrically convex anterior to the jugal contact (Fig. 4F).

Quadrate

The fairly complete right quadrate of *Noasaurus* is missing a large portion of the lateral process, most of the entocondyle (i.e. the medial condyle of the mandibular articulation; *sensu* Hendrickx *et al.* 2015a), a central piece of the quadrate ridge, and parts of the pterygoid flange (Fig. 5). The ventral portion of the latter has been strongly reconstructed. This is particularly the case for the medial surface in which the reconstructed portion occupies a large part of the ventral half of the flange (Fig. 5A–D). The pterygoid flange has also suffered multiple damages since 2012. Although the quadrate is not affected by distortion, the bone is broken in several places, with fractures running lateromedially or diagonally along the medial and posterior surfaces. The posterior surface is the least well-preserved of the quadrate, with some

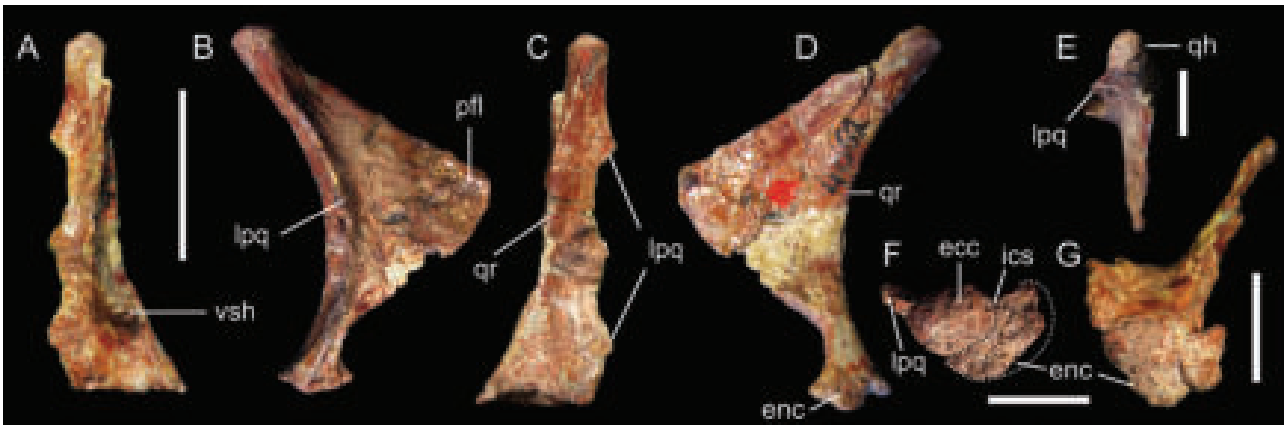

Figure 5. Quadrate of *Noasaurus leali* (PVL 4061). Right quadrate in: A, anterior; B, lateral; C, posterior; D, medial; E, dorsal; F–G, ventral views; with F, tentative reconstruction of the mandibular articulation. Abbreviations: ecc, ectocondyle; enc, entocondyle; ics, intercondylar sulcus; lpq, lateral process, qh, quadrate head; qr, quadrate ridge; pfl, pterygoid flange; vsh, ventral shelf. Scale bars equal 2 cm (A–D) and 1 cm (E–G).

sediment glued to the central portion of the bone. The anterior and dorsal sides of the quadrate are, however, relatively intact.

In posterior view, the *Noasaurus* quadrate is a dorsoventrally elongated bone flaring out ventrally from a lateromedially narrow quadrate head to a wider mandibular articulation (Fig. 5C). It is characterized by a lateromedially narrow, sub-vertical and poorly delimited, rod-shaped quadrate ridge running along the medial edge of the quadrate body. This ridge emerges ventrally at one-third of the body, well-dorsal to the mandibular articulation, and terminates dorsally directly ventral to the quadrate head. The quadrate body is delimited medially by two surfaces meeting at an obtuse angle at two-fifths of the bone height. The surface occupying the ventral two-fifths of the quadrate is flat surface and strongly slopes ventrally. Conversely, the surface along the remaining dorsal three-fifths of the bone is slightly convex and corresponds to the medial margin of the quadrate ridge. An incomplete lateral process is visible in posterior view, projecting strictly laterally from the quadrate body (Fig. 5C). The dorsal margin of the lateral process strongly slopes ventrally and extends from the quadrate body well-ventral to the quadrate head. The ventral margin of the lateral process is sub-horizontal, mediolaterally convex in its preserved part and connects to the quadrate body at the level of the ectocondyle. Although Bonaparte and Powell (1980) described a small quadrate foramen in *Noasaurus* and Carrano and Sampson (2008) scored it as absent in their datamatrix, the presence of a quadrate foramen cannot be determined given that the lateral border of the lateral process contacting the quadratojugal is unpreserved (Fig. 5A, C). It is also unknown whether the quadrate and quadratojugal were fused to each other or not (*contra* Bonaparte 1991; see Discussion). The surface along the central two-thirds of the quadrate and running from the quadrate ridge to the lateral process is lateromedially and dorsoventrally concave. No pneumatic fossa or foramina are visible on this posterior concavity but the surface is too badly preserved to rule out their presence. The articular surface of the quadrate head is convex and restricted to the posteriormost surface of the quadrate body. The ectocondyle extends only slightly posteriorly beneath the quadrate body and its dorsal margin forms a widely convex parabola (Fig. 5C). Based on the preserved portion of the entocondyle, and given that more than a half of this condyle is missing, the mandibular articulation must have protruded strongly medially from the rest of the quadrate body, forming a prominent and pointy medial projection in posterior view. With the entocondyle and the lateral process complete, the quadrate likely had the shape of an Eifel-tower in posterior view.

In medial and lateral views, the posterior margin of the quadrate body is concave and strongly arched, forming an almost perfectly and symmetrically curved parabola (Fig. 5D). Although it is unknown how the quadrate articulated within the cranium, the quadrate head probably strongly projected posterodorsally and was probably positioned well-posterior from the mandibular articulation. The anteroposteriorly short quadrate ridge is only visible along the central two-fourths of the quadrate, being delimited anteriorly by a shallow furrow running dorsoventrally. A subtriangular pterygoid flange projecting anteriorly is visible in medial and lateral views (Fig. 5B, D). The ratio between the anteroposterior length of the flange and the dorsoventral height of quadrate body is 0.45, corresponding to a moderately extended pterygoid flange. The flange projects from the quadrate head dorsally and reaches the quadrate around one-fifth of the quadrate body ventrally, well-dorsal to the mandibular articulation. Although figured as a triangular projection by Bonaparte and Powell (1980: fig. 7C), the pterygoid flange is in fact subtrapezoidal, with a short subvertical anterior margin (Fig. 5D). The dorsal margin of the flange is almost straight, whereas the ventral border is slightly convex. The medial fossa of the pterygoid flange is particularly shallow and no medial pneumatic foramen is present on the preserved part of the flange. A notch corresponding to the intercondylar sulcus between the ento- and ectocondyles is visible on the anterior portion of the mandibular articulation. It is, however, unknown whether this notch was visible when the entocondyle was completely preserved.

In anterior view, the pterygoid flange is subvertical and parallel to the long axis of the quadrate body (Fig. 5A). The flange is straight along most of its lateral and medial surfaces and convex along the ventralmost margin from which projects a lateromedially narrow ventral shelf medially. A concave surface is visible on the lateroventral surface of the mandibular articulation. This concavity extends laterally from the lateral process to the lateral half of the ectocondyle and its dorsal margin forms a lateromedially convex parabola.

In lateral view, the lateral process forms an anteroposteriorly thin and dorsoventrally convex bony projection with a parabolic curvature similar to that of the posterior surface of the quadrate body. The pterygoid flange is devoid of any pneumatic aperture or recess (Fig. 5B). The ventral limit of the ectocondyle is convex, and anterior and posterior pointy projections are visible along the medial portion of the mandibular articulation.

In dorsal view, the quadrate head forms a single, semispherical condyle with a strongly convex posterior margin and a more widely convex, almost subrectangular, anterior margin (Fig. 5E). The pterygoid flange is straight and only projects anteriorly, perpendicular to the laterally projected lateral process. Both pterygoid flange and lateral process are thin bony laminae increasing in width towards the quadrate body.

In ventral view, the mandibular articulation is made of two condyles delimited by a shallow and poorly delimited intercondylar sulcus whose orientation cannot be determined (Fig. 5F, G). Although incomplete, the entocondyle was almost certainly larger than the ectocondyle (Fig. 5F). The latter forms an oval to oblong condyle whose long axis is strongly diagonally oriented from that of the mandibular articulation. The shape of the entocondyle is unknown but its long axis also appears to have been diagonally oriented from the long axis of the mandibular articulation. A lateromedially wide notch is visible on the posterior surface of the mandibular articulation, between the ento- and ectocondyles, whereas the anterior margin of the articulation forms a wide convexity along its preserved portion (Fig. 5F). The lateral process connects to the ectocondyle anteriorly and the ventral shelf of the pterygoid flange is lateromedially narrow (Fig. 5G).

Dentition

Only the left maxillary dentition of *Noasaurus* is preserved. Four isolated theropod teeth (PVL 4062) referred by Bonaparte and Powell (1980) to an indeterminate 'Carnosauria' were also recovered from the El Brete fossil site but their larger size

(CH > 10 mm) and distinct crown and denticle morphologies strongly suggest that they belong to a non-noasaurid theropod, most probably an abelisaurid (C.H. pers. obs.). The maxillary dentition of *Noasaurus* preserves five fully erupted crowns from the first, third, sixth, eighth, and 10th alveoli (Fig. 6A). Bonaparte and Powell (1980) and Novas (2009) suggested that the maxilla had 10 or 11 teeth but 13 maxillary alveoli can be recognized in ventral view (Fig. 6B, C). Only the Lmx8 crown is almost complete as the others are missing a small (Lmx1, Lmx6) or large portion (Lmx3, Lmx10) of the apex. A picture of the *Noasaurus* maxilla illustrated by Bonaparte (2007; Supporting Information, S1.1, Fig. SA3) shows that all the preserved teeth were complete or fairly complete after their preparation. The maxillary dentition currently shows some damages typically consisting of mesiodistally oriented fractures running along the crown-base or the mid-crown. Lmx6 is the least well-preserved, with a large diagonally oriented fracture on the crown and most of the apicodistal surface missing. The denticles present on the best-preserved crowns are also incomplete and sometimes difficult to distinguish, while the enamel is often missing on some portions of the crown surfaces.

The maxillary dentition of *Noasaurus* is ziphodont, i.e. it includes labiolingually compressed, distally recurved, and blade-shaped crowns bearing denticulated carinae. *In situ* teeth of the maxilla are also decumbent (i.e. teeth with no inclination, pointing vertically from the tooth bearing bone; Hendrickx *et al.* 2019, also known as 'orthodont' for the incisors of rodents; Thomas 1919) as it is the case in most theropods. Little variation

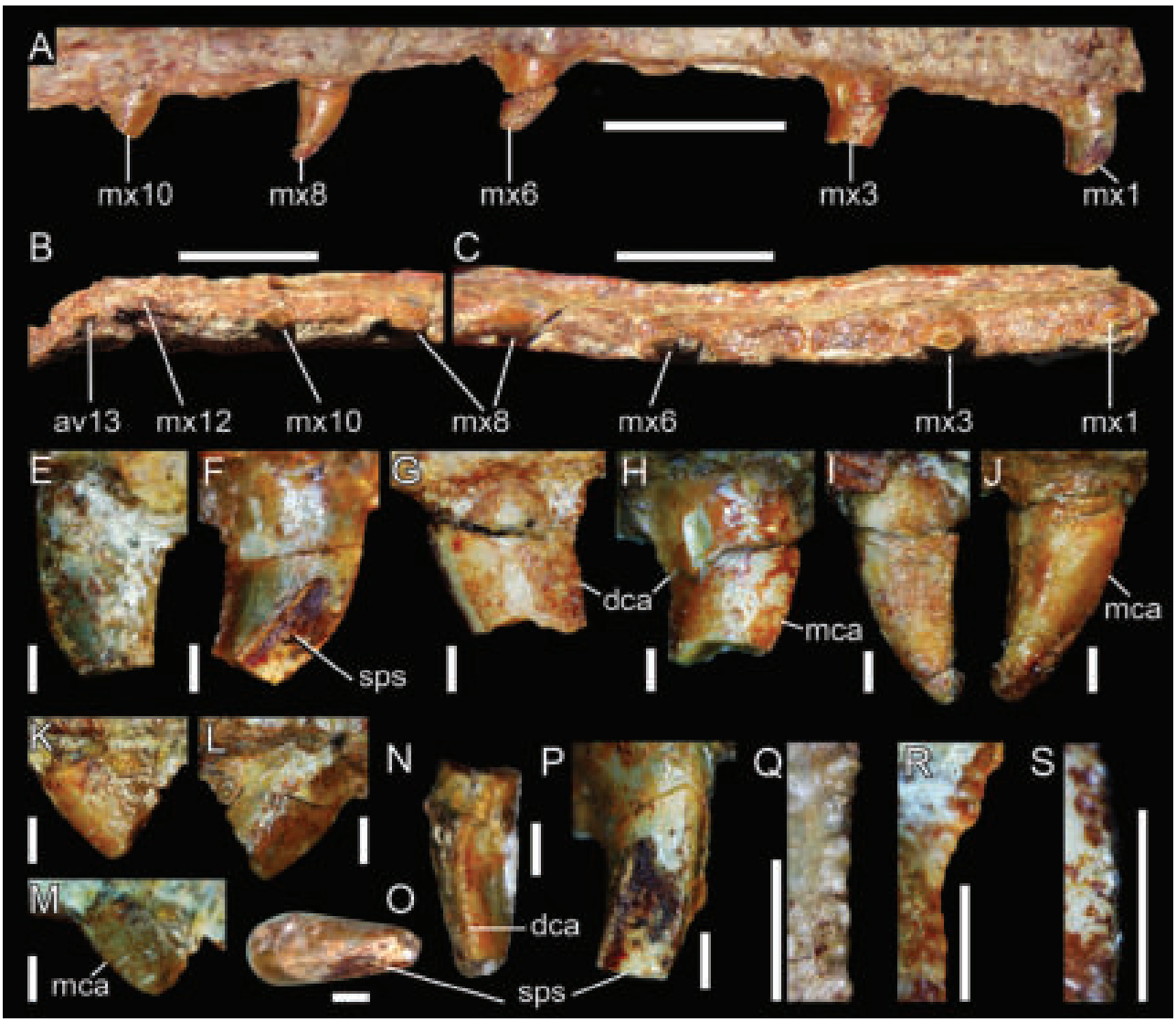

Figure 6. Maxillary dentition of *Noasaurus leali* (PVL 4061). A, maxillary teeth in medial view; B, posterior; C, anterior maxillary teeth in ventral view; close-up on the E, F, first; G, H, third; I, J, eighth; K, M; 10th maxillary teeth in labial (E, G, I, K), lingual (F, H, J, L), and apicolabial (M) views; O, P, close-up on the detached first maxillary crown in N, distal; O, apical; and P, mesiolingual views; Q, R, close-up on the distocentral denticles of the Q, first; and R, third maxillary crowns in labial views; S, close-up on the mesiocentral denticles of the third maxillary crown in lingual view. Abbreviations: av13, 13th maxillary alveolus; dca, distal carina; mca, mesial carina; mx1, first maxillary tooth; mx3, third maxillary tooth; mx6, sixth maxillary tooth; mx8, eight maxillary tooth; mx10, 10th maxillary tooth; mx12, 12th maxillary tooth; sps, spalled surface. Scale bars equal 1 cm (A–C), and 1 mm (D–R), 0.5 mm (S).

exists in the morphology of the preserved maxillary teeth, which mainly differ in their compression and elongation. They are all slightly distally curved, with a weakly concave distal margin, so that the apex of the tooth lies at the same level as the distal margin of the crown at the cervix (Fig. 6A). Although incomplete, none of the maxillary crowns appear to have exceeded 10 mm in height, suggesting that the maxillary dentition was particularly short compared to the cranium's height (Fig. 3B). The best-preserved crown (Lmx8) is almost 5 mm in height, whereas the largest one Lmx3 (CH > 3.12 mm) may have been 5 mm possibly 6 mm in height. Based on the crown–base length (CBL) of the available crowns and the size of the maxillary alveoli, the largest and tallest teeth were probably from the third, fourth, and fifth alveoli, which is typically the case in ziphodont theropods (C.H. pers. obs.). Little variation in size, however, occurred in the maxillary dentition of *Noasaurus* as CBL only varies less than 1 mm, from 2.83 mm in Lmx10 to 3.54 mm in Lmx3. The first maxillary crown (CH > 2.67 mm), which is only missing the apicalmost part of the crown (Fig. 6E, F), was shorter than Lmx3, Lmx6, and Lmx8, and the smallest teeth were probably present in the distalmost maxillary alveoli. With a CBR ranging from 0.54 to 0.65, the maxillary crowns were weakly to moderately compressed, and Lmx1 was the thickest. The crown compression does not seem to follow a trend along the maxilla but the most compressed teeth appear to have been present in the distalmost portion of the maxilla (Table 3). Little is known of the elongation of the maxillary crowns. The only complete tooth Lmx8 (Fig. 6I, J) has a normal elongation (CHR = 1.64) and the other partially preserved crowns seem to have had similar elongation. A cross-section of mx3, which is missing the apex, reveals that the cross-sectional outline of this crown was lenticular, with almost symmetrically convex labial and lingual margins (Fig. 6B). The labial side is only slightly more angular in its central part than the lingual one. All the preserved maxillary teeth are believed to have a lenticular or lanceolate cross-sectional outline at the base and at mid-crown.

The maxillary crowns all have straight or weakly apicobasally arched mesial and distal carinae (Fig. 6N). The mesial carina is centrally positioned on the mesial surface in all preserved crowns other than Lmx8 in which it slightly twists on to the mesiolingual surface basally (Fig. 6C). The distal carina is also either centrally positioned or slightly labially displaced, as seen in Lmx1 (Fig. 6N) and Lmx8. A denticulated distal carina is present in all teeth, whereas mesial denticles can be observed in at least Lmx3 and Lmx8 (Fig. 6H–J). As noted by Candeiro (2007), the mesial denticles are significantly smaller than those of the distal carina. We calculated a denticle density of 20 to 25 distal denticles and 32.5 mesial denticles per 5 mm at mid-crown (Fig. 6S), giving a DSDI of 1.3 to 1.44 for the maxillary crowns. The distal denticles can be seen along the whole crown height in all preserved crowns. Mesial denticles are more difficult to discern but the denticulated mesial carina also appears to extend to the cervix in Lmx3, Lmx8, and Lmx10, and possibly Lmx1. The mesial carina of Lmx10 is devoid of denticles suggesting the fact that mesial denticles were probably absent in the distalmost maxillary teeth (Fig. 6M). With an estimation of less than 30 denticles along the whole distal carina, the distal denticles are particularly large compared to the crown height (Fig. 6G). We counted 10 distal denticles on the basal half of Lmx3, indicating that the number of denticles on the distal carina was probably close to 20. The distal denticles do not diminish in size basally (Fig. 6G). When complete, the distal denticles project perpendicularly from the distal carina and are subquadrangular in outline, with a parabolic and symmetrically convex external margin (Fig. 6Q, R). The interdenticular space is narrow, and short and diagonally oriented interdenticular sulci are present on the labial side of Lmx8, between the baso- and centrodistal denticles. Interdenticular sulci, however, appear to be absent between the distal denticles of the other preserved crowns. The mesial denticles are minute and difficult to distinguish in Lmx3 and Lmx8, whereas their presence is unknown in Lmx1. The most complete and best-preserved mesial denticles are seen in Lmx3 at mid-crown where they are short, poorly defined, apicobasally subrectangular in outline, and with a symmetrically convex external margin (Fig. 6S). No interdenticular sulci are present between the mesial denticles.

The maxillary crowns do not show any ornamentation such as marginal or transverse undulations, flutes, longitudinal ridges or grooves, basal striations, concave surfaces adjacent to the carinae, or labial and lingual depressions on the crown surface. The enamel surface texture also does not have any particular pattern and is, therefore, described as irregular (*sensu* Hendrickx *et al.* 2015d). An extensive spalled surface is, nevertheless, visible on the lingual surface of Lmx1 (Fig. 6F, O, P). This surface is oval in shape in its basal part, diagonally oriented from the long axis of the crown, and extends on the mesial half and apical two-thirds of the crown. No other spalled surface or wear facets are neither present on the labial side of the maxillary teeth nor on the lingual surface of the other crowns.

Axial skeleton

Cervical vertebral arch

The cervical vertebral arch of *Noasaurus* was briefly described by Bonaparte and Powell (1980), whereas Novas (1989) expanded the description of this element in his Ph.D. dissertation. The neural arch is virtually complete, lacking some structures such as the left diapophysis, the neural spine, which is broken at its base, the anterior tip of the right epipophysis, and a small area of the dorsomedial aspect of the left prezygapophysis. Novas (2009) identified this element as being presumably from the sixth cervical vertebra. We agree with this author that this neural arch probably belongs to a mid-posterior cervical element, probably to the sixth or seventh cervical. The presumed position is based on the inclination of the transverse processes, which are lateroventrally projected, forming an angle of 53° from the mid-sagittal plane, as well as the slightly ventral bending of the prezygapophyseal–epipophyseal lamina, the wide distance between pre- and postzygapophyses (this distance is short in more caudal cervical vertebrae), the epipophyses surpassing posteriorly the postzygapophyses, and the resemblance with mid-posterior cervical vertebrae of other abelisauroids (Carrano *et al.* 2002, 2011, O'Connor 2007, Langer *et al.* 2019). This change is evidenced by the prezygapophyses and centroprezygapophyseal fossae, which are more dorsally placed relative to the neural canal.

Distinctive features of this element (Fig. 7) include an enlargement of the neural arch mainly resulting from the strong elongation of epipophyses, which occupies nearly 65% of the maximum length of the arch, a markedly concave surface of the transverse processes, an anteroposteriorly short neural spine, distinctly separated dorsal and lateral aspects of the neural arch due the development of the epipophyseal prezygapophyseal lamina, and numerous pneumatic features represented by several laminae and fossae.

In dorsal view, the general bone surface is well preserved, except for the missing neural spine (Fig. 7E, K). The dorsal surface of the neural arch has a rectangular profile due to the enlarged lateral epipophyses and the slightly divergent prezygapophyses. The anterior and posterior sides are characterized by the V-shaped incisions inwards the arch, formed by the zygapophyses and the spinopre- and spinopostzygapophyseal fossae. The preserved base of the neural spine is transversely compressed and anteroposteriorly short. The anterior extent of the spine base does not meet the spinoprezygapophyseal fossa, whereas it hardly contacts the spinopostzygapophyseal fossa posteriorly.

The dorsal surface of the neural arch is separated from the lateral sides by a well-developed epipophyseal–prezygapophyseal

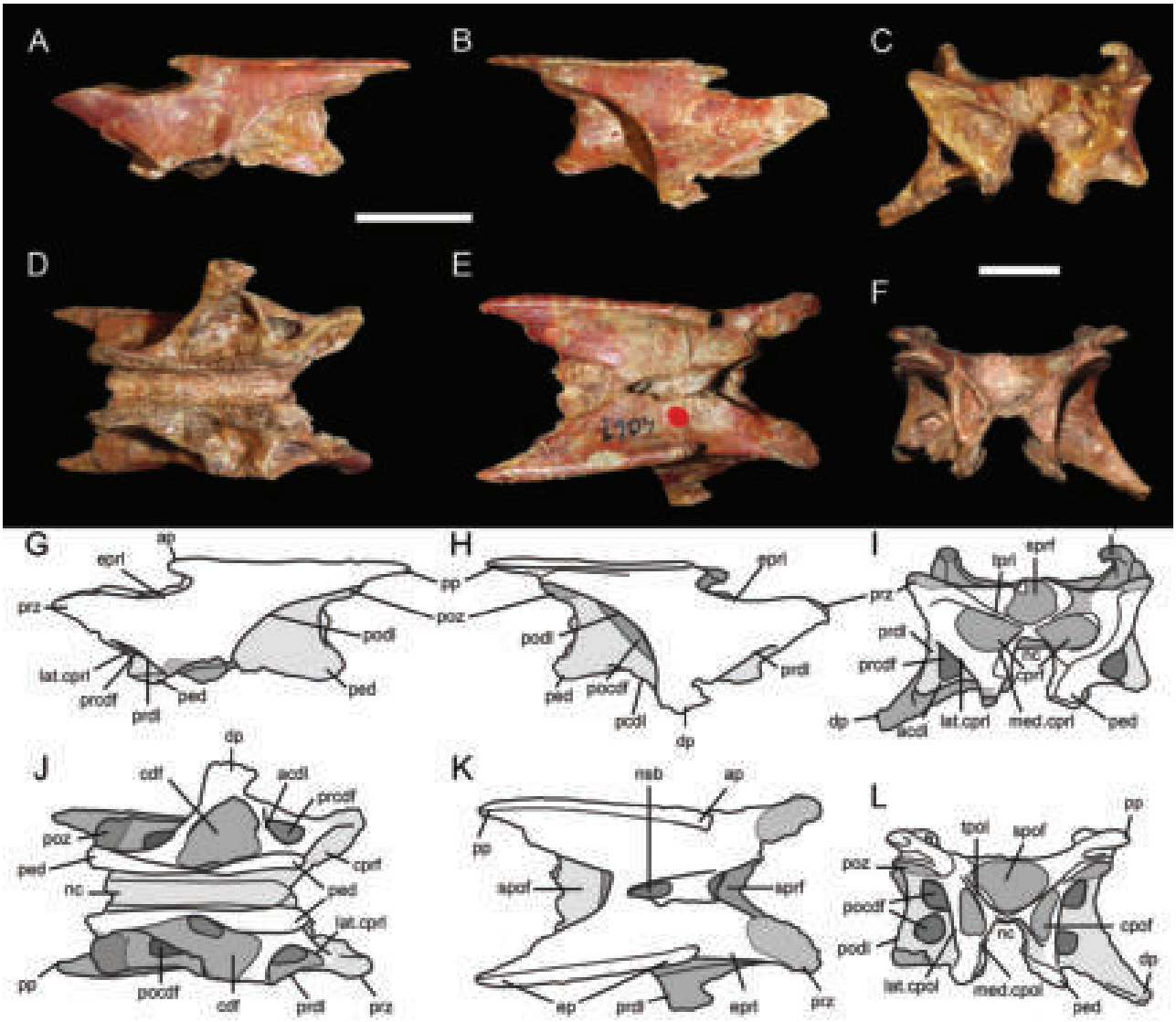

Figure 7. Mid-posterior cervical vertebral arch of *Noasaurus leali* (PVL 4061). Sixth or seventh cervical vertebra without (A–F) and with labels (G–L) in A, G, left lateral; B, H, right lateral; C, I, anterior; D, J, ventral; E, K, dorsal; and F, L, posterior views. Abbreviations: acdl, anterior centrodiapophyseal lamina; ap, anterior prong; cdf, centrodiapophyseal fossa; cpof, centropostygapophyseal fossa; cprf, centroprezygapophyseal fossa; dp, diapophysis; ep, epipophysis; eprl, epipophyseal–prezygapophyseal lamina; lat. cpol, lateral centropostzygapophyseal lamina; lat. cprl, lateral centroprezygapophyseal lamina; med. cpol, medial centropostzygapophyseal lamina; med. cprl, medial centroprezygapophyseal lamina; nc, neural canal; nsb, neural spine base; pcdl, posterior centrodiapophyseal lamina; ped, pedicle; pocdf, postzygapophyseal centrodiapophyseal fossa; pp, posterior prong; prcdf, prezygapophyseal centrodiapophyseal fossa; poz, postzygapophysis; podl, postzygodiapophyseal lamina; prdl, prezygodiapophyseal lamina; prz, prezygapophysis; sprf, spinoprezygapophyseal fossa; spof, spinopostzygapophyseal fossa; tpol, intrapostzygapophyseal lamina; tprl, intraprezygapophyseal lamina. Scale bars equal 2 cm (A, B, D, E) and 1 cm (C, F).

lamina (eprl) (Fig. 7K), as occurs in all abelisauroids (Sereno *et al.* 2004, Langer *et al.* 2019). The epipophyses are particularly hypertrophied, with anterior and posterior prongs ('spike-like structures' *sensu* Bonaparte and Powell 1980) that are autapomorphic of *Noasaurus* within noasaurids. Although the epipophyses are almost subparallel to each other, their main axis is oriented anteromedially to posterolaterally, so that they slightly diverge posteriorly.

The anterior projections of the epipophyses flare slightly medially and extend anteriorly to the level of the diapophysis; both anterior and posterior projections of the epipophyses are acuminate on their ends. The surface between the epipophyses and the base of the neural spine is roughly flat and smooth. The prezygapophyses are divergent from each other, each one having a lobate shape. Both spinopre- and spinopostzygapophyseal fossae are broad and V-shaped, and the spinopostzygapophyseal fossa is superficially broader. The angle of aperture of the spinoprezygapophyseal fossa is about of 60°, whereas the spinopostzygapophyseal fossa reaches 46°.

In lateral view, the epipophyseal–prezygapophyseal lamina has a faintly undulating profile (Fig. 7A, B, G, H), posterior to the prezygapophyses; it, however, does not form a markedly concave margin as in the mid-cervicals of other noasaurids (e.g. *Laevisuchus* and *Masiakasaurus*). The anterior prong of the epipophysis forms a marked and deep notch on the dorsolateral side of the arch. The epipophysis is well differentiated from the rest of the lateral surface of the transverse process and is particularly marked on its posterior half towards the posterior prong. The surface between the epipophysis and the transverse process is mostly smooth (Fig. 7A, G). As for the prezygapophyses, they are well below the level of the epipophyses.

The prezygodiapophyseal lamina (prdl) has a lightly curved anterior margin reaching the prezygapophyses at an angle of 29°. Its dorsoventral development completely obscures the anterior centrodiapophyseal lamina (acdl), as well as the lateral centroprezygapophyseal lamina (lat.cprl) partially in lateral view (Fig. 7A, B, G, H). The prezygapophyseal centrodiapophyseal fossa (prcdf) is also partially visible laterally. As for the postzygodiapophyseal lamina (podl), the margin with its contact with the postzygapophyses is strongly curved. This lamina overhangs the postzygapophyseal centrodiapophyseal fossa (pocdf), which is superficially broad in lateral view (Fig. 7B, H). The subfossae within are, however, hidden by the postzygodiapophyseal lamina. The posterior centrodiapophyseal lamina (pcdl) extends from the posterior surface of the transverse process to the posterior pedicles, describing a curved shape. The lateral centropostzygapophyseal lamina (lat.cpol) has slightly curved and vertically directed margins on its contact with the dorsal aspect of pedicles. The diapophysis is triangular, ventrally projected with a rounded distal end.

In anterior view, the dorsal surface of the neural arch is almost flat, with the anterior projections of the epipophyses flaring medially (Fig. 7C, I). The articular surfaces of the prezygapophyses are dorsomedially oriented at an angle of approximately 40° relative to the horizontal plane. The spinoprezygapophyseal fossa is mediolaterally wide and separates both centroprezygapophyseal fossae (cprf) on its dorsal sector by the junction of the intraprezygapophyseal laminae (tprl). The latter join together at an angle of 140°, forming the ventral limit of the spinoprezygapophyseal fossa. The centroprezygapophyseal fossae are located lateroventrally to the spinoprezygapophyseal fossa and dorsolaterally to the neural canal, forming large ovoidal excavations on the anterior side of the neural arch; it is unclear whether these fossae are blind or pierced by foramina as they are partially filled with sediment. Each centroprezygapophyseal fossa is delimited by the lateral (lat.cprl) and medial centroprezygapophyseal laminae (med.cprl). Both laminae meet at the neural canal mid-height at an angle of almost 90°. The medial centroprezygapophyseal lamina contacts the intraprezygapophyseal lamina at an angle of 71°, whereas the lateral centroprezygapophyseal lamina joins the prezygodiapophyseal lamina at 52°. The prezygapophyseal centrodiapophyseal fossa (prcdf) is broadly exposed and subtriangular [the 'cavidad antediapofisial' of Novas (1989)]. The centrodiapophyseal fossa (cdf) has a minimal expression when seen in anterior view due to the fact that it is hidden by the anterior centrodiapophyseal lamina (acdl). The latter has a slight ventral curvature towards its contact with the diapophyses. Because all described fossae are currently filled with sediment, it remains unclear whether they lead to pneumatic camerae, as in the cervical vertebrae of other noasaurids (Brum *et al.* 2018, Smyth *et al.* 2020).

In posterior view, the spinopostzygapophyseal fossa (spof) is mediolaterally broad, deep, and wider than tall (Fig. 7F, L). The intrapostzygapophyseal laminae (tpol) join at an angle of 110°. The centropostzygapophyseal fossae (cpof) appear below these laminae and dorsolaterally to the neural canal. These fossae are deep but relatively small in area when compared with the centroprezygapophyseal counterpart. The centropostzygapophyseal fossae have a scalene triangle contour and are delimited by the lateral (lat.cpol) and medial (med.cpol) centropostzygapophyseal laminae. The medial centropostzygapophyseal lamina is transversally thinner than the lateral one, which becomes thicker towards its contact with the postzygapophysis. These laminae contact each other at an angle of 41°. The medial centropostzygapophyseal lamina joins the intrapostzygapophyseal lamina forming an angle of 108°. The articular surfaces of the postzygapophyses are oriented ventrolaterally at an angle of 28°, which is less than the inclination of the prezygapophyses. The posterior projection of the epipophysis is laterally offset from the postzygapophysis and a shallow groove running mediolaterally separates the posterior surface of both structures. The postzygodiapohyseal lamina is also strongly curved in posterior view, contacting dorsally the postzygapophysis at an angle of 46°, and ventrally joins the posterior centrodiapophyseal lamina at an angle of 36°. The postzygapophyseal centrodiapophyseal fossa (pocdf) is located on the posterior surface of the transverse process. A peculiarity is that two smaller subfossae are differentiated by a median lamina that runs mediolaterally within this fossa. Both subfossae were previously identified by Novas (1989) as the 'postdiapophysial cavities' ('cavidades postdiapofisiales'; Novas 1989). The subfossae are circular and one is positioned below the other. They appear to be deep but it is unclear if they lead to pneumatic cavities. These subfossae of the postzygapophyseal centrodiapophyseal fossa are present on both sides of the neural

arch but they are less apparent on the right as both excavations remain filled with sediment.

In ventral view, the neurocentral suture is well discernible along the ventral surface of the neural arch (Fig. 7D, J). The centroprezygapophyseal fossae and lateral centroprezygapophyseal laminae are partially visible. The latter meet the prezygodiapophyseal lamina at an angle of almost 56° in that view. The anterior centrodiapophyseal lamina, which is located anteriorly to the diapophysis, is obliquely oriented and meets the prezygodiapophyseal lamina at an angle of 62°. These laminae form the lateral and posterior walls of the prezygapophyseal centrodiapophyseal fossa, which is bean-shaped, deep, and larger than wide. The centrodiapophyseal fossa, which is clearly visible in ventral view, is wider than long, being much larger that the previously described fossae of the anterior aspect of the neural arch. The centrodiapophyseal fossa is subdivided by a median swelling of bone rather than a lamina, delimiting a relatively large subfossa posteromedially and a smaller one anterolaterally, close to the anterior centrodiapophyseal lamina. The postzygapophyseal centrodiapophyseal fossa, which is only partially visible, shows that the larger subfossa is anteroposteriorly long and almost reaches the postzygapophysis. The posterior projections of the epipophyses project far posteriorly the articular facets of the postzygapophyses.

Mid-cervical rib

This element was correctly identified as a cervical rib by Bonaparte and Powell (1980: fig. 8I, J) who, however, did not specify its position within the cervical series. Novas (2009) stated that this bone may pertain to more anterior cervical ribs based on its morphological similarity with other abelisauroids. Carrano *et al.* (2011), however, suggested that this element may pertain to a fourth cervical rib, resembling those of *Masiakasaurus*. We agree with the latter authors in the fact that this bone most likely represents a mid-cervical rib, probably a fourth or fifth cervical element, based on the short distance between the capitulum and tuberculum, a thin capitulotubercular web, and the short neck of the capitulum (when compared with the longer neck of the posterior cervical rib of *Noasaurus*). The cervical rib corresponds to a left proximal end (Fig. 8), with some fractures on the anterolateral process and lacking the styliform process.

In medial view, the tuberculum is ellipsoidal, anteroposteriorly longer than the capitulum, and slightly exceeds the horizontal plane of the main rib body (Fig. 8B). The capitulum is less ellipsoidal and is not at the same level than the tuberculum, which is displaced posterodorsally relative to the former. Both structures are linked by the transversally thin and oblique capitulotubercular web. This lamina gets thicker towards its connection with the capitulum and tuberculum. The anterolateral process of the cervical rib tapers anteriorly into a blunt end and connects with the capitulum through a concave lamina. In lateral view, the rib has a ridge-like buttress with a nearly constant transverse section except anteriorly where it gradually diminishes after the tuberculum (Fig. 8A). The lateral surface of the rib is mostly smooth but some faint striations are visible. Due to the poor preservation of the bone, it is unclear whether a bifurcated process was present in the rib of *Noasaurus*, as commonly present in other abelisauroids (O'Connor 2007, Carrano *et al.* 2011).

In ventral view, the lateral buttress of the rib extends from the anterolateral to the posterolateral processes (Fig. 8D). The angle that the capitulum forms with the main axis of the rib ['neck-shaft angle' *sensu* O'Connor (2007)] is approximately 105°. It is clear that the tuberculum is strongly concave and the capitulum is irregularly convex. In dorsal view, the lateral buttress also forms a slightly ornamented keel (Fig. 8E).

In anterior view, the rib has a wide fossa between the capitulotubercular web and anterolateral process (Fig. 8C); however, this fossa is non-invasive. The lateral surface of the rib body is strongly concave in this view. Conversely, a broad pneumatic fossa with two large foramina piercing the surface can be seen in posterior view (Fig. 8F). The larger (5 mm) is located close to the capitulum whereas the smaller (~2 mm) is present near the tuberculum.

Posterior cervical rib

Bonaparte and Powell (1980) originally identified the cervical rib as a right squamosal (Novas, 1989, 2009). The cervical rib of *Noasaurus* represents a well-preserved proximal left element only lacking some areas of the capitulum surface and the whole rib shaft (Fig. 9). This element corresponds to a caudal cervical rib, probably from the ninth or 10th cervical vertebra, based on the wide distance of the capitulotubercular web, the presence of the sharp anterolateral process, a capitulotubercular web pierced by a pneumatic foramen on tis anterior surface, and the obtuse angle (128°) formed between the main axis of the rib body and the capitulum (Fig. 9A, E; see: O'Connor 2007). Carrano *et al.* (2011) argued that this element may pertain to a tenth cervical or even the first dorsal element based on a comparison with *Masiakasaurus*.

In dorsal view, the dorsolateral process (dlp) is mediolaterally wide posterior to the contact with the tuberculum and becomes less expanded towards the anterolateral process (alp; Fig. 9C). The latter is developed as a pointy and blunt end with slightly concave and convex medial and lateral margins, respectively. The anterolateral process is marked on its dorsal and ventral surfaces by a lateral buttress that extends posteriorly as a faintly ornamented ridge toward the dorsolateral process. The capitulum is robust and projects anterolaterally (in this view) from the main shaft at an angle of 128°; both anterior and posterior margins are straight and ornamented with rugosities, whereas the distal end is eroded and it is not possible to observe whether it was convex as in other abelisauroids. The tuberculum is also robust, dorsomedially projected, and has a short neck when compared with the tuberculum. Its distal end, which is damaged, is circular in cross-section. The capitulotubercular web is hidden by the tuberculum in this view.

In ventral view, the tuberculum and capitulotubercular web are not observable due to the strong development of the capitulum (Fig. 9F). The overall surface between the capitulum and the main rib body is smooth, except for the lateral buttress (which is continuous from the anterolateral to the dorsolateral processes), which exhibits some slight rugosities. The margin that connects the anterolateral process and tuberculum has a strongly concave contour, almost

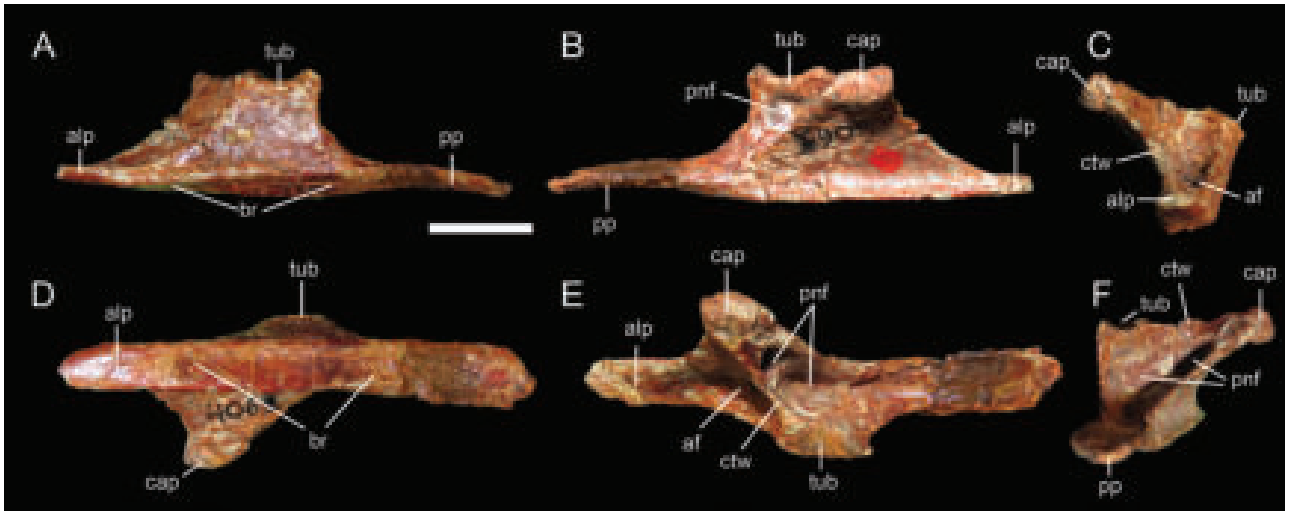

Figure 8. Mid-cervical rib of *Noasaurus leali* (PVL 4061). Left proximal end of a fourth or fifth cervical rib in: A, lateral; B, medial; C, anterior; D, ventral; E, dorsal; and F, posterior views. Abbreviations: af, anterior fossa; alp, anterolateral process; br, buttressed ridge; cap, capitulum; ctw, capitulotubercular web; pnf, pneumatic foramina; pp, posterior process; tub, tuberculum. Scale bar equals 1 cm.

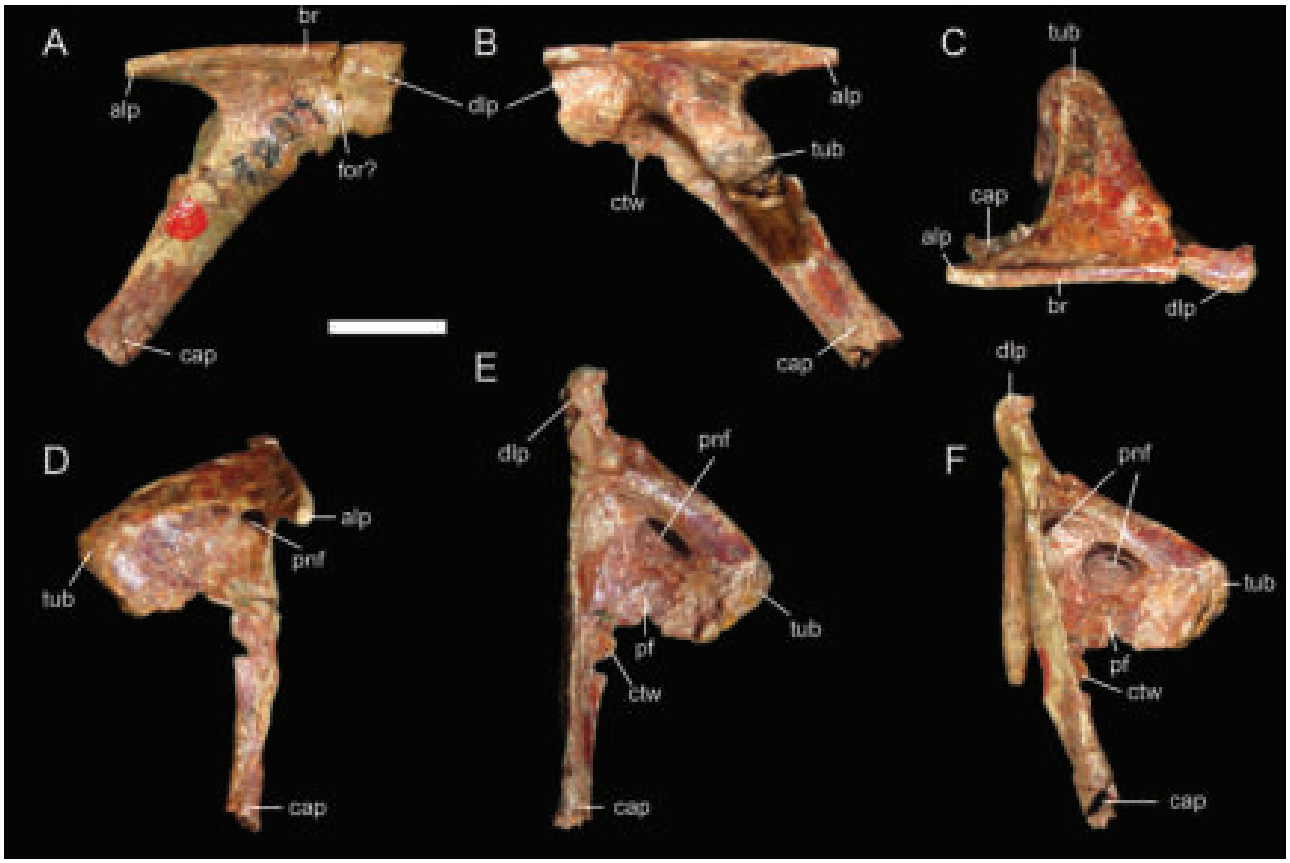

Figure 9. Posterior cervical rib of *Noasaurus leali* (PVL 4061). Left ninth or 10th cervical rib in: A, lateral; B, medial; C, dorsal; D, anterior; E, posterior; and F, ventral views. Abbreviations: alp, anterolateral process; br, buttressed ridge; cap, capitulum; ctw, capitulotubercular web; dlp, dorsolateral process; for?, putative foramen; pf, posterior fossa; pnf, pneumatic foramen; tub, tuberculum. Scale bar equals 1 cm.

forming a notch in this area. On the other hand, the central area of the dorsolateral process is pierced by a small and distinct pneumatic foramen (~2mm).

In anterior view, the tuberculum and capitulum meet at an angle of 84° (Fig. 9D). The capitulotubercular web is mostly missing but its preserved portion proves that it was broad and transversally thin near the tuberculum. The surface between the tuberculum and the anterolateral process is concave; the same condition occurs for the ventral surface that joins the capitulum and the anterolateral process. The pointy anterior

end of the anterolateral process flares laterally and its distal tip has a circular cross-section. A conspicuous pneumatic foramen (~2 mm) is present within a small fossa. This foramen pierces the anterior surface between the capituloturbecular web and the anterolateral process and enters into the main rib body.

In posterior view, a smooth and elliptical fossa characterizes the capitulotubercular web (Fig. 9E). This fossa bears a large and teardrop-shaped pneumatic foramen (~5 mm) adjacent to the tuberculum. This foramen also enters the rib body and is probably connected internally with the aforementioned pneumatic structures. The tuberculum is transversally thicker than the capitulum in this view.

Indeterminate postcervical vertebra

This element was originally mentioned by Bonaparte and Powell (1980) as part of the holotype but was neither described nor figured. This isolated vertebral body is poorly preserved, with largely eroded areas reconstructed with plaster (Fig. 10). The centrum probably belongs to the series between the middle and posterior trunk vertebrae owing to the absence of parapophyses and a blind excavation on its lateral surface (O'Connor 2007, Langer *et al.* 2019). However, we cannot reject the possibility that it may come from the caudal series based on the presence of a lateromedial constriction at mid-length and articular surfaces that are taller than wide, as seen in *Masiakasaurus* (Carrano *et al.* 2011). Nevertheless, although being damaged, the ventral surface does not show clear evidence of haemal facets while a shallow sulcus is partially visible (see description below).

In lateral view, the centrum, which is a relatively simple element, is elongated (1.7× longer than deep) and weakly amphicoelous, despite both articular surfaces being slightly eroded (Fig. 10A, B). The lateral surface is characterized by smooth and poorly-developed pleurocentral fossae, lacking other distinctive features. Although not completely observable in this view, the constriction of the centrum on its midlength is visible by the concave ventral margin connecting both articular surfaces. The articular surfaces are ovoid (Fig. 10C, F), taller than wide, with the posterior articular surface projecting slightly more ventrally relative to the anterior one. In ventral view, the centrum is spool-shaped due to its transversally compressed nature. A shallow and elongate sulcus characterizes the anterior half of the centrum surface (Fig. 10D). This sulcus is bounded laterally by thin ridges that gradually fade at the midlength of the centrum.

Appendicular skeleton

Manual phalanges

In the original description of the *Noasaurus* material, Bonaparte and Powell (1980) concluded that the available phalanges came from the foot and given its trenchant aspect, the ungual may probably correspond to a sickle-like claw, similar to, but convergently acquired with that of deinonychosaur theropods (Bonaparte 1991). The claw of *Noasaurus* was found as very different from that of other theropods in being notably curved and in having an excavated ventral surface devoid of flexor tubercles. The morphology of the *Noasaurus* pedal claw remained a unique trait of this carnivorous theropod. The raptorial claw of *Noasaurus* pes is, however, regarded as being from the manus by several authors, an opinion we here follow (Agnolín *et al.* 2004, Carrano *et al.* 2004, Carrano and Sampson 2008, Agnolín and Chiarelli 2010).

The manual phalanges of *Noasaurus leali* are represented by a non-ungual phalanx probably from digit III, as well as a partial and a complete ungual possibly from digit I (Figs 11–13). Because the manus anatomy of noasaurid is still poorly known (Langer *et al.* 2019) and abelisaurid digits are strongly modified, the homology and position of *Noasaurus*' manual elements

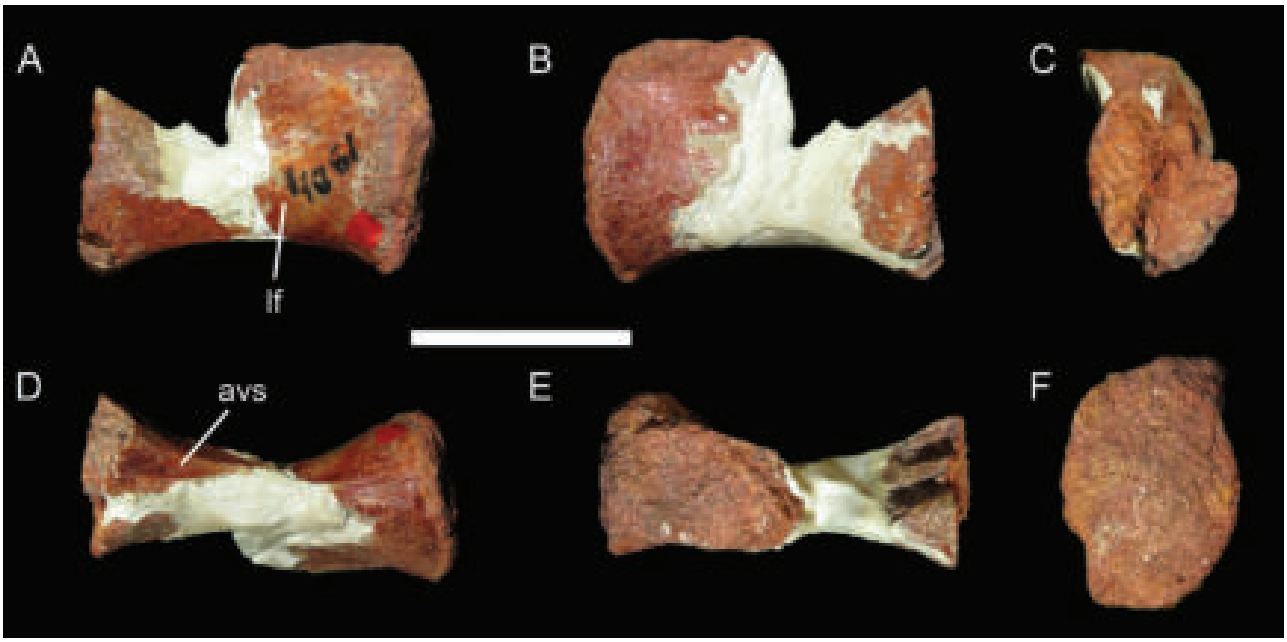

Figure 10. Indeterminate postcervical vertebra of *Noasaurus leali* (PVL 4061). Centrum in A, left lateral; B, right lateral; C, anterior; D, ventral; E, dorsal; and F, posterior views. Abbreviations: avs, anteroventral sulcus; lf, lateral fossa. Scale bar equals 2 cm.

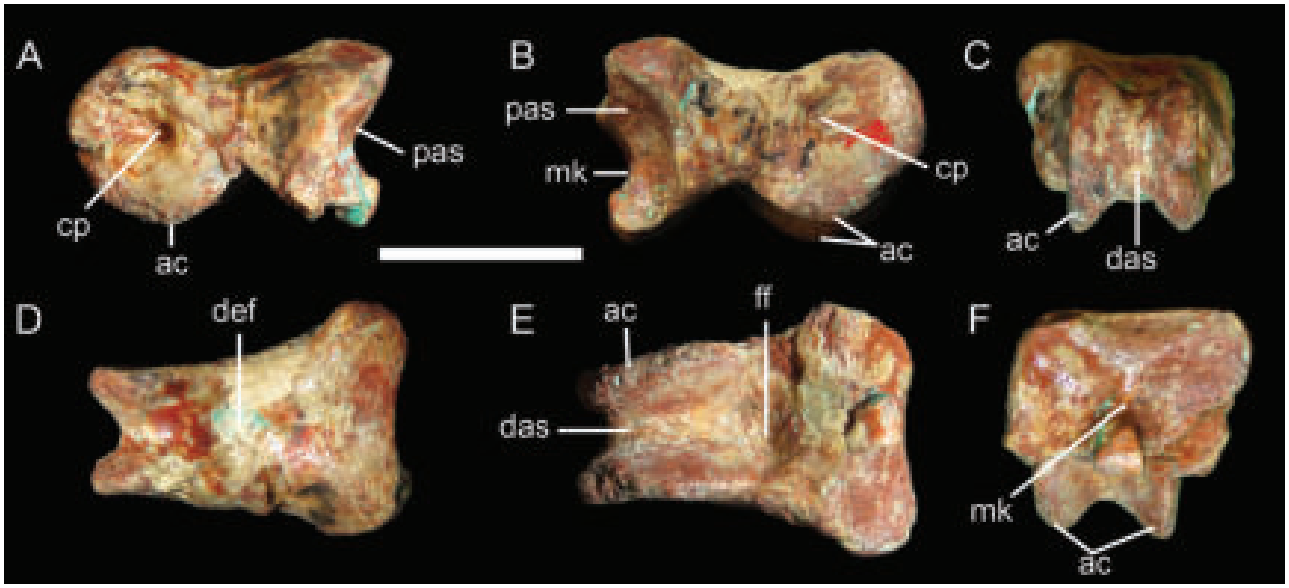

Figure 11. Manual phalanx of *Noasaurus leali* (PVL 4061). Left manual phalanx III-1 in: A, lateral; B, medial; C, distal; D, dorsal; E, ventral; and F, proximal views. Abbreviations: ac, articular condyles; cp, collateral pits; das, distal articular surface; def, dorsal extensor fossa; ff, flexor fossa; mk, median keel; pas, proximal articular surface. Scale bars equal 1 cm.

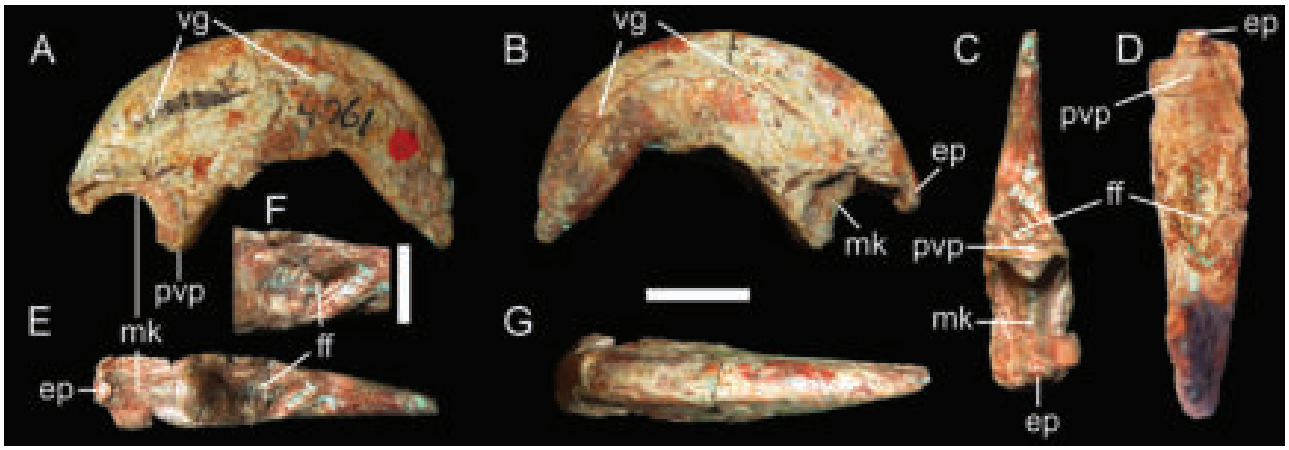

Figure 12. Manual ungual of *Noasaurus leali* (PVL 4061). Complete right? manual ungual I? in: A, lateral; B, medial; C, proximal; D, distal; E, F, ventral; G, dorsal views; with F, close-up on the flexor fossa. Abbreviations: ep, extensor process; ff, flexor fossa; mk, median keel; pvp, posteroventral process; r, ridge; vl, ventral lip; vg, vascular groove. Scale bars equal 1 cm (A–E, G) and 5 mm (F).

is uncertain. In contrast to the original interpretation, and following Agnolín and Chiarelli (2010), the non-ungual and ungual phalanges are not considered as being consecutive. In fact, when put in articulation, their mobility is strongly reduced, precluding important flexor or extensor mobility.

Non-ungual manual phalanx

A single non-ungual phalanx was recovered (Fig. 11). In contrast to recently published foot phalanges of noasaurids (e.g. *Velocisaurus* and *Vespersaurus*; Brissón Egli *et al.* 2016, Langer *et al.* 2019), the phalanx of *Noasaurus* resembles those of the manus in having the collateral ligamental pit dorsally displaced and the distal articular condyles ventrally located with respect to the main axis of the phalanx shaft (Agnolín and Chiarelli 2010). Based on its size and the well-differentiated proximal and distal articular surfaces (Fig. 11A, B), this phalanx probably does not belong to manual digit IV. Phalanx IV-1 is indeed nub-shaped, with a rounded distal end, as seen in other ceratosaurs such as *Ceratosaurus*, *Aucasaurus*, and *Majungasaurus* (Gilmore, 1920; Coria *et al.*, 2002; Burch and Carrano, 2012; Carrano and Choiniere, 2016). Likewise, it cannot belong to digit I as the manual phalanges of the first manual finger are strongly asymmetrical in ceratosaurs (Coria *et al.* 2002, Burch and Carrano 2012, Langer *et al.* 2019). Comparison with the corresponding phalanx of *Vespersaurus* suggests that the non-ungual phalanx of *Noasaurus* probably belongs to the left hand. As seen in the *Noasaurus* phalanx, the lateral surface of phalanx III-1 of *Vespersaurus* is straighter than the medial one, which is more deeply excavated and shows a more prominent bony edge in the proximal end (Langer *et al.* 2019). We, therefore, identify the non-ungual phalanx of *Noasaurus* as a left manual phalanx III-1.

The phalanx is proportionally short, dorsoventrally compressed and robust (Fig. 11A, B). In dorsal and ventral views, it

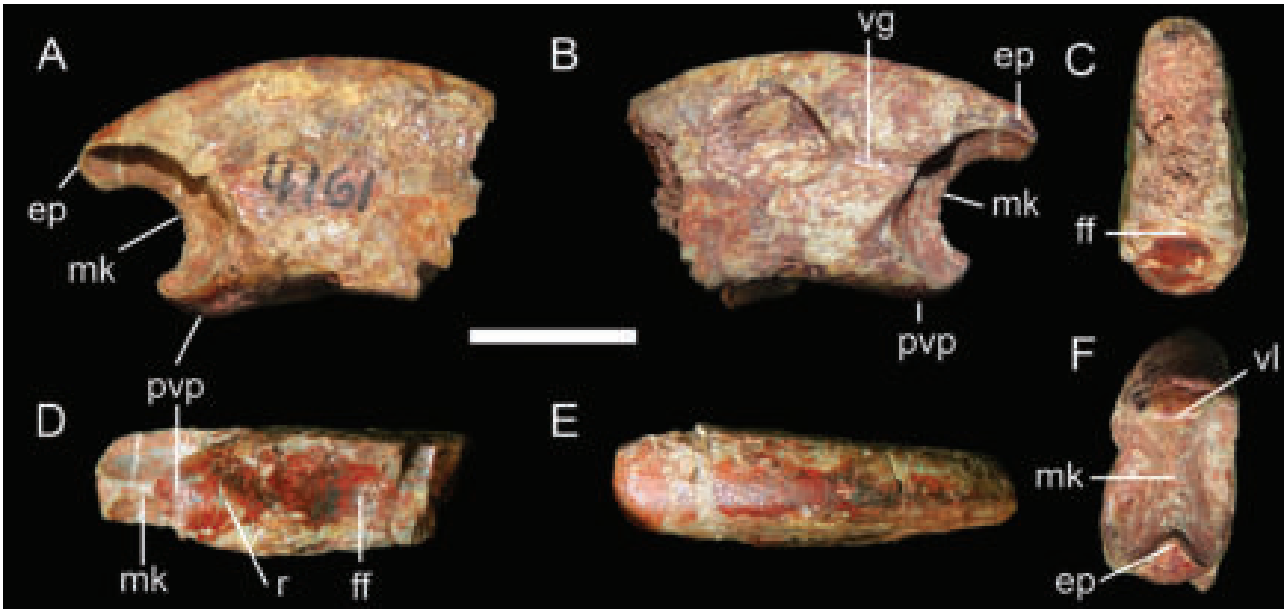

Figure 13. Manual ungual of *Noasaurus leali* (PVL 4061). Incomplete left? manual ungual I? in: A, medial; B, lateral; C, distal; D, ventral; E, dorsal; F, proximal views. Abbreviations: ep, extensor process; ff, flexor fossa; mk, median keel; pvp, posteroventral process; r, ridge; vl, ventral lip; vg, vascular groove. Scale bar equals 1 cm.

is roughly subtriangular in outline (Fig. 11D, E). In side view, the proximal and distal articular surfaces are separated by a well-developed phalangeal neck (Fig. 11A, B). The proximal articular surface shows nearly straight to subparallel dorsal and ventral surfaces (Fig. 11F). This results in an inverted trapezoidal shape. The proximal end shows an extensor process that is dorsally flat and strongly transversely expanded. In contrast, the flexor process is subquadrangular in outline and transversely narrow, representing less than one-third of the proximal phalangeal width. The medial surface of the extensor process is thicker and forms a bump absent on its lateral surface.

The proximal articular surface is strongly excavated and subdivided by a deep and subvertically oriented keel (Fig. 11F). Both surfaces are well-excavated and are subequal in size and shape, the medial one being slightly narrower than the lateral one on its ventral surface. This results in the fact that the proximal articular surface is more exposed in medial than in lateral view.

The distal ginglymoid is notably expanded and shows very narrow and acute articular condyles. The latter are separated by a deep and wide groove (Fig. 11E), forming a pulley-like distal articular surface. In distal view, the distal end of the phalanx is subquadrangular in outline (Fig. 11C). The articular condyles are subparallel to each other and slightly medially oriented. Both condyles are subequal in shape, the medial one being only slightly larger than the lateral one. Both flexor and extensor fossae are deep and well defined, resulting in a deep separation between the proximal and distal articular surfaces. Collateral ligamental pits are deep and ellipsoidal in contour and the medial one is wider but shallower than the lateral one.

Manual unguals

The *Noasaurus* holotype includes two manual unguals (Figs 12, 13). Unguals of *Noasaurus* were originally interpreted as belonging to the foot (Bonaparte and Powell 1980, Bonaparte 1991, 1996a). The available unguals can, however, be referred to the manus based on the following combination of traits: notably curved blade with a narrow cross-section, a deep and transversely narrow proximal articular surface, with a prominent and well-defined median keel (Agnolín and Chiarelli 2010). The particular morphology of the unguals of *Noasaurus*, which strongly differ from those of other ceratosaur claws, makes a referral to any digit of the hand particularly challenging. However, the available complete ungual is tentatively referred to digit I based on its strong blade curvature, as well as a nearly symmetrical proximal articular surface. Indeed, ungual I is often the most curved claw of the hands in non-avian theropods (e.g. *Afrovenator*, *Allosaurus*, *Balaur*, *Buitreraptor*, *Coelophysis*, *Herrerasaurus*, *Megaraptor*, *Nqwebasaurus*, therizinosaurs, *Suchomimus*, troodontids, and *Yutyrannus*; Sereno 1994, 2017, Zanno 2006, Barta *et al.* 2018, Chinzorig *et al.* 2018, Kubota *et al.* 2024; C.H. pers. obs.), especially those with enlarged ungual I. The ungual is also tentatively assigned to the right digit based on the slightly medial/inner curvature of the distal extremity of the claw in ventral, dorsal, proximal, and distal views (Fig. 12C–E, G). The other claw, despite only preserving the proximal half (Fig. 13), is tentatively identified as ungual I from the left manus owing to the fact that it shares with the complete ungual the same size and curvature, and the slight medial curvature of the claw in proximal view (Fig. 13F).

The manual claw of *Noasaurus* shows a strongly curved blade that forms an arch of about 90° along its ventral margin (Fig. 12). The proximal end of the dorsal margin of the blade is nearly straight, with a curvature starting approximately at one-third of the length of the bone (Fig. 12A, B). The ungual blade is strongly laterally compressed and shows a roughly ovoidal to subtriangular cross-sectional outline. One surface of the blade is nearly flat, whereas the other is slightly convex, suggesting that the former probably corresponds to the medial aspect of the

ungual, whereas the latter is the lateral surface (Figs 12E, 13D). There is a single collateral vascular groove extending along the dorsal third of the blade. The medial collateral vascular groove appears to be deeper than the lateral one; this may, however, be an artefact of preservation.

The ventral surface of the manual ungual is notably complex and lacks any sign of flexor tubercle and flexor facets (Figs 12A, B, 13A, B). It, however, shows a very deep and subtriangular fossa which is delimited by a poorly raised posteroventral process proximally and by two well-defined ridges distally. These two ridges contact each other distally to form a 'V'-shape (Fig. 12F) whose anteriorly directed apex extends as a midline ridge up to the distal point of the claw. Such peculiar morphology of the ventral surface of the manual ungual is unknown in any other theropod, including other noasaurids such as *Vespersaurus* (Langer *et al.* 2019), and is here considered as an autapomorphy of *Noasaurus*.

The proximal articular surface of the ungual is subrectangular in proximal view (Figs 12C, 13F). The subvertical midline keel separates two deep and subrectangular concave cotyles for the articulation with the condyles of the non-ungual phalanx. The cotyles are well defined, particularly deep, and result in a 'C'-shaped articular surface when viewed from the sides (Figs 13A, B, 14A, B). The lateral cotyle is transversely narrower and dorsoventrally taller than the medial one. Both cotyles are delimited at their sides by narrow and acute ridges. The midline keel is notably prominent and forms a small wall separating the cotyles in side view. This keel is well-separated from the flexor process [the 'proximoventral process' of Agnolín and Chiarelli (2010)] in this same view. The extensor process [the 'proximodorsal process' of Agnolín and Chiarelli (2010)] is prominent and well defined and no depression is present distal to this process.

Only the proximal third of the left? manual ungual is preserved (Fig. 13). The ungual blade shows a subtriangular outline in cross-section (Fig. 13C), being strongly laterally compressed and showing a flat ventral surface delimited by the medial and lateral ridges. The medial collateral vascular groove appears to be deeper than the lateral one, although this might be a preservation artefact. The ventral surface is poorly preserved (Fig. 13D) and lacks a flexor tubercle. Parts of the ridges are preserved and form the 'V' delimiting a prominent ventral fossa, as seen in the complete manual ungual. The proximal articular surfaces of both unguals are almost identical.

Metatarsal II

The second right metatarsal (here abbreviated Mt) of *Noasaurus* is the only preserved element of the hind limb (Fig. 14). It is a long, gracile, and particularly well-preserved bone with only some fractures over the diaphysis (Fig. 14A–D). The proximal end of MtII is ovoidal and mediolaterally narrow (Fig. 14E), with a flat lateral surface for the contact with MtIII. The medial surface is convex and the posterior and anterior margins end in a rounded tip. A relatively small, flat facet is present on the proximolateral area of the shaft and may correspond to the attachment site for some pedal muscle. The metatarsal shaft, which is anteroposteriorly deep, becomes mediolaterally compressed over two-thirds of its length distal to the proximal end. The transverse section is D-shaped at two-thirds of the shaft due to the flat lateral facet that received MtIII and the convex lateral margin which extends distally. The distal one-third of MtII expands mediolaterally to form a slightly convex anterior surface, resulting in a subquadrangular transverse profile (Fig. 14A, C). In medial/lateral views, a faint inflexion point with a very low angle (i.e. <5°) is seen shortly after the widening of the shaft (Fig. 14A, C).

The flat lateral surface of the shaft becomes slightly concave (Fig. 14C) forming a wide groove towards the distal end, though it is unclear if this is a taphonomical artefact. A barely visible and subquadrangular hyperextensor fossa is present on the anterior surface of the distal end (Fig. 14B). The most conspicuous feature of the medial surface of MtII (Fig. 14A) is a low elliptical bulge ornamented by small tubercles corresponding to a muscle attachment and where some of the short extensors of digit II (m. extensor digiti II?) probably originated. In posterior view, the mediolaterally compressed shaft is represented by a sharp edge expanding mediolaterally on the distal half (Fig. 14D). An elongate and faintly sculptured muscle scar, which probably represents one of the insertions of the mm. gastrocnemii, is present at the midlength of MtII (Carrano and Hutchinson 2002). A few muscle striations are similarly present on the posterior surface of the distal half, proximal to the ginglymus. Both collateral pits ['ligamentous fossae' in Bonaparte and Powell (1980)] are subcircular and subequal in size. While the medial collateral pit is shallow (Fig. 14G), the lateral pit is deep and contained within a proximodistally large fossa that is continuous with the 'groove' formed by the lateral surface (Fig. 14H).

The distal end of the metatarsal has a roughly quadrangular shape, being only slightly longer anteroposteriorly than mediolaterally (Fig. 14F). The ginglymus is well defined on the plantar aspect and both condyles are well-developed posteriorly. They are, however, strongly asymmetrical, with the lateral condyle being lateromedially buttressed and more posteriorly projected than the small and blunt medial condyle. The deep U-shaped sulcus that separates both condyles is relatively shallow and more developed medially. This sulcus probably corresponds to the passage of the main flexor muscles of the second toe.

RESULTS

Phylogenetic analyses

The cladistic analysis performed on our update version of the datamatrix of Agnolín *et al.* (2022) yielded 3000 most parsimonious trees (MPTs) (overflowed tree buffer; tree length = 1106) whose strict consensus recovered a large polytomy in Ceratosauria (Supporting Information, S3.1.4, Fig. SA1). The latter includes more than 10 taxa among which are the noasaurids *Noasaurus*, *Masiakasaurus*, and *Vespersaurus*, as well as the poorly to fully resolved clades Ceratosauridae (*Ceratosaurus* and *Genyodectes*), Berthasauridae clade nov. (*Berthasaura*, *Afromimus*, and *Austrocheirus*; see definition in Table 1), Elaphrosaurinae (MNN TIG6, *Limusaurus* and *Elaphrosaurus*), and Abelisauridae. Pruning seven unstable OTUs (Table 4), other than the wildcard taxa *Laevisuchus* and *Velocisaurus*, yielded a better-resolved tree in which *Kryptops* (only represented by the postcranium) is classified as the basalmost Ceratosauria and the sister-taxon

Figure 14. Metatarsal II (MtII) of *Noasaurus leali* (PVL 4061). Right MtII in: A, medial; B, anterior; C, lateral; D, posterior; E, proximal; F, distal views; with close-up on the G, medial and; H, lateral collateral pits in medial (G) and lateral (H) views. Abbreviations: cmtI?, possible contact for MtI; cmtIII, contact for MtIII; cp, collateral pit; dg, distal groove; ef, extensor fossa; gc, scar for m. gastrocnemius; lc, lateral condyle; mc, medial condyle; ms, muscle scar; su, sulcus. Scale bars equal 2 cm (A–D) and 1 cm (bar on the top for E, F; bar on the bottom for G, H).

of the clade Elaphrosaurinae + Neoceratosauria (Fig. 15A). The latter includes ceratosaurids at the base, as well as a few basal taxa in a ladder-like position, namely *Berberosaurus*, *Eoabelisaurus*, and *Ligabueino*, the latter being the sister-taxon of the clade Berthasauridae + Abelisauroidea (= Noasauridae + Abelisauridae). Noasauridae include five taxa namely, *Noasaurus*, *Masiakasaurus*, *Laevisuchus*, *Velocisaurus*, and *Vespersaurus*, all recovered in a polytomy (Fig. 15A). Conversely, Abelisauridae are a much larger clade with *Spectrovenator* and *Rugops* as the basalmost taxa, followed by a series of subclades such as Brachyrostra and Majungasaurinae (Fig. 15A). Excluding all nine unstable taxa (Table 4) recovered a well-resolved Noasauridae made of three

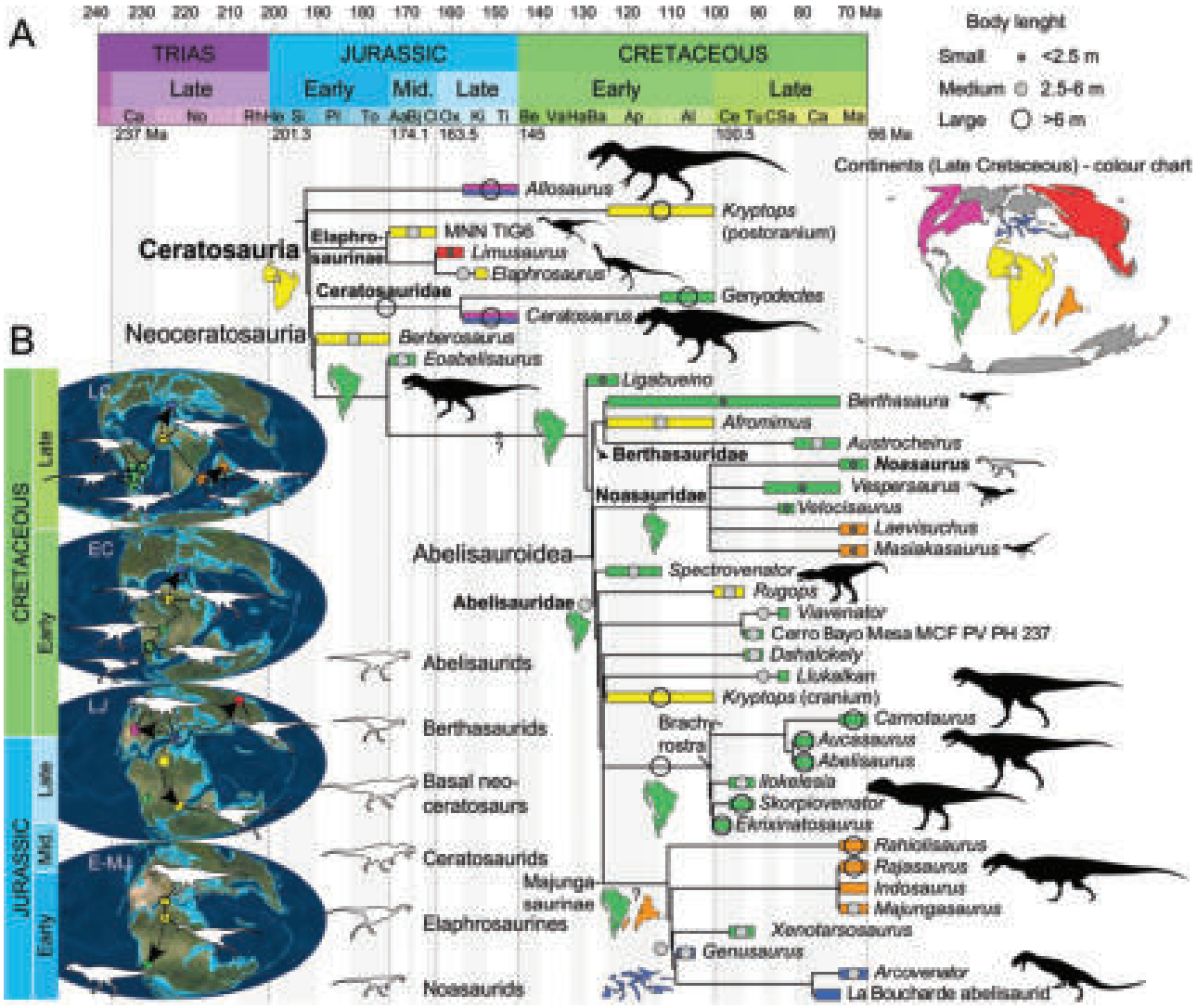

Figure 15. Phylogenetic placement of *Noasaurus* among ceratosaurs and palaeogeographic history of ceratosaurs based on the result of the cladistic analysis conducted on a revised version of Agnolín *et al.*'s (2022) datamatrix. A, strict consensus tree of 3000 trees (tree length = 1106) from the cladistic analysis after pruning seven unstable taxa and keeping the wildcard taxa *Laevisuchus* and *Velocisaurus* (Table 4). The coloured bars and circles for each taxon represent the continent of origin (South America in green, North America in purple, Europe in blue, Africa in yellow, Asia in red, and Madagascar/India in orange) and body length (<2.5 m for the small black dot, 2.5–6 m for the medium grey dot, and >6 m for the large black circle; Supporting Information, S2.2, S5 for data on body length), respectively. Continents beneath the stems represent the possible origin of the clades; B, hypothetical palaeogeographic history of ceratosaurs during the Early–Middle Jurassic, Late Jurassic, Early Cretaceous, and Late Cretaceous (palaeogeographic reconstructions from CPGeosystems of Rob Blakey). Abbreviations: EC, Early Cretaceous; E-MJ, Early–Middle Jurassic; LC, Late Cretaceous; LJ, Late Jurassic. Theropod silhouettes approximately to scale. Black silhouettes from Funkmonk (*Elaphrosaurus*), Iain Reid (*Eoabelisaurus*), Jagged Fang Designs (*Ekrixinatosaurus*), Jaime Headden (*Arcovenator*), Julio Garza (*Dilophosaurus*), Geovane Alves de Souza (*Berthasaura*; modified), Tasman Dixon (*Masiakasaurus*, *Spectrovenator*, *Vespersaurus*), Ville-Veikko Sinkkonen (*Limusaurus*), and Scott Hartman (all the others). See Supporting Information, S1.7 for the silhouette's licence attribution.

taxa where *Noasaurus* is the basalmost and the sister-taxon of a clade gathering *Masiakasaurus* and *Vespersaurus* (Supporting Information, S3.1.4, Fig. SA2). The inclusion of the wildcard taxon *Deltadromeus* in the analysis collapses the clade Ceratosauria, which encompasses the clades Elaphrosaurinae, Ceratosauridae, Berthasauridae + Abelisauroidea, and various ceratosaur taxa (e.g. *Deltadromeus*, *Eoabelisaurus*, *Berberosaurus*) in a polytomy (Supporting Information, S3.1.4, Fig. SA3). This result might be due to the fact that *Deltadromeus* is possibly not a ceratosaur but a basally branching carcharodontosaurian, as recovered by Apesteguía *et al.* (2016). The same occurs when *Huinculsaurus* is included in the analysis, with Abelisauroidea corresponding to a polytomy comprised of the taxa *Noasaurus*, *Huinculsaurus*, and *Ligabueino* as well as the clades Abelisauridae, Berthasauridae and *Vespersaurus* + *Masiakasaurus* (Supporting Information, S3.1.4, Fig. SA4).

The cladistic analysis conducted on our updated version of Baiano *et al.*'s (2023) datamatrix provided the same results as these authors, with a strict consensus from 3000 MPTs (tree length = 606) recovering Ceratosauria fully unresolved

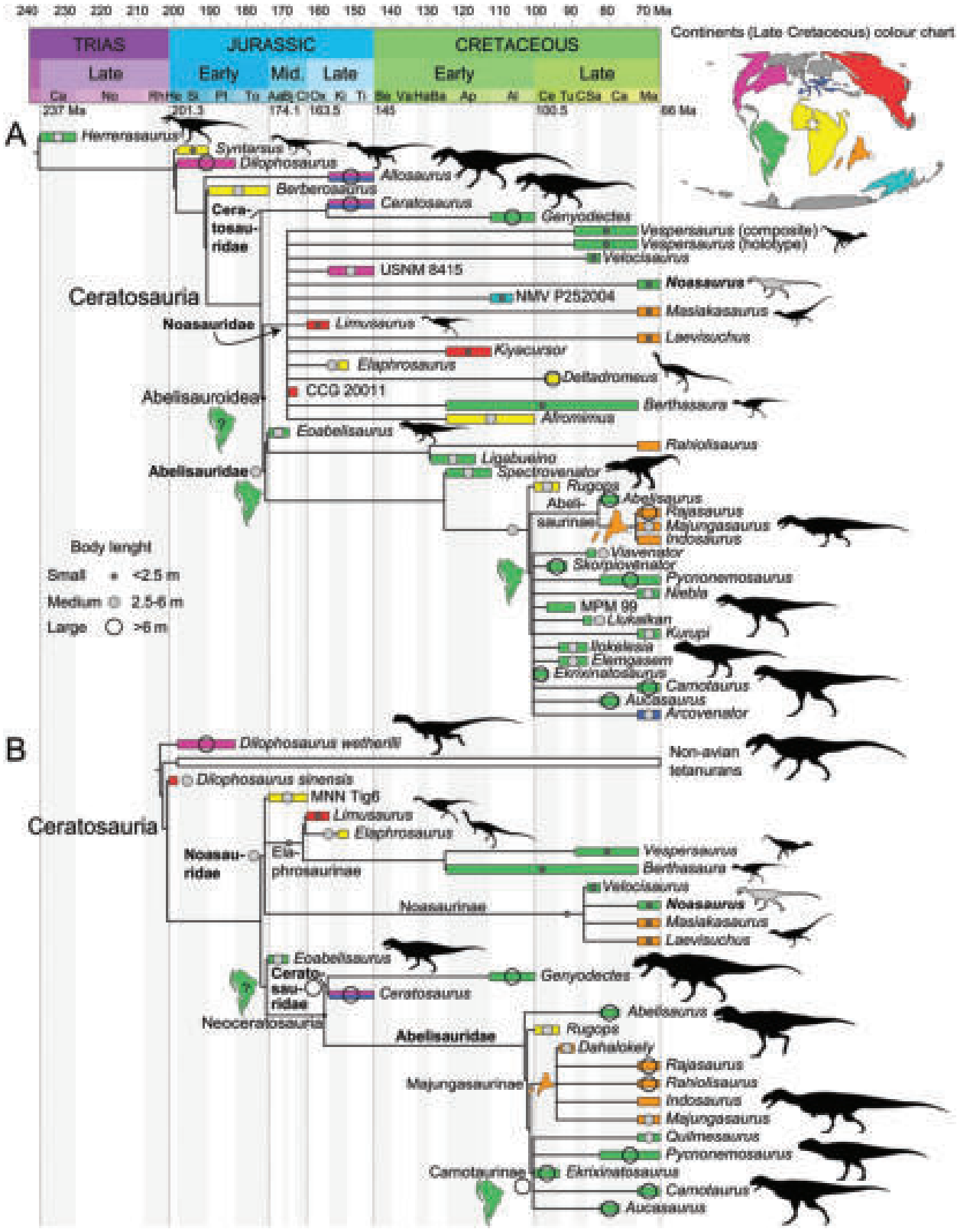

Figure 16. Phylogenetic placement of *Noasaurus* among ceratosaurs based on two separate datamatrices on theropod relationship. A, strict consensus tree of 3000 trees (tree length = 606) from the cladistic analysis performed on a revised version of Baiano *et al.*'s (2023) datamatrix after pruning ten unstable taxa and keeping ten others (i.e. *Afromimus*, *Deltadromeus*, *Elemgasem*, *Kurupi*, *Laevisuchus*, *Masiakasaurus*, MPM 99, *Pycnonemosaurus*, USNM 8415, and the holotype of *Vespersaurus*; Table 4); B, strict consensus tree, here reduced to *Dilophosaurus wetherilli* and averostran theropods (see Supporting Information, S3.3.4, Fig. SA8 for the whole tree), of 3000 trees (tree length = 4797) from the cladistic analysis performed on a revised version of Rauhut and Pol's (2021) datamatrix after pruning 28 unstable taxa (Table 4). The coloured bars and circles for each taxon represent the continent of origin (South America in green, North America in purple, Europe in blue, Africa

(Supporting Information, S3.2.4, Fig. SA5). Pruning 20 wildcard taxa (Table 4) yielded a better resolved topology in which Ceratosauria include the basally branching *Berberosaurus*, followed by the clades Ceratosauridae (*Genyodectes*, *Ceratosaurus*) and Abelisauroidea (= Noasauridae + Abelisauridae; Fig. 16A). Noasauridae remain unresolved due to the unstable position of *Noasaurus*, with the clades Elaphrosaurinae (*Limusaurus*, *Elaphrosaurus*, CCG 20011), *Kiyacursor* + NMV P25204, and the rest of the noasaurid taxa grouped in a polytomy (Supporting Information, S3.2.4, Fig. SA6). Keeping 10 out of the 20 wildcard taxa (i.e. *Afromimus*, *Deltadromeus*, *Elemgasem*, *Kurupi*, *Laevisuchus*, *Masiakasaurus*, MPM 99, *Pycnonemosaurus*, USNM 8415, and the holotype of *Vespersaurus*), however, recovered the same general ceratosaur topology where *Berberosaurus* is the sister-taxon of Ceratosauria (= Ceratosauridae + Abelisauroidea) (Fig. 16A). Noasauridae are here fully unresolved and include 15 OTUs all recovered in a polytomy (Fig. 16A).

A huge polytomy was similarly obtained in the strict consensus tree of 3000 MPTs (tree length = 4797) resulting from the cladistic analysis performed on our revised version of Rauhut and Pol's (2021) dataset (Supporting Information,S 3.3.4, Fig. SA7). Theropoda is made of a pectinate succession of clades, with *Eodromaeus* and the group *Tawa* + Herrerasauridae classified as basalmost theropods, followed by a polytomy with *Segisaurus*, *Sarcosaurus*, *Panguraptor*, and Coelophysoidea, a clade comprised of *Zupaysaurus*, *Lophostropheus*, and *Liliensternus*, forming the sister-group of a huge and relatively unresolved clade gathering the fully or partially-resolved clades Megalosauroidea, Megaraptora, Metriacanthosauridae, Carcharodontosauridae, Tyrannosauridae, Ornithomimosauria, Therizinosauria, Alvarezsauria, Oviraptorosauria, Microraptorinae, Troodontidae, and Avialae, as well as all other averostran taxa. The resolution was significantly improved after pruning 28 taxa (Table 4) as the analysis recovered the typical theropod topology summarized by Hendrickx *et al.* (2015b) (Supporting Information, S3.3.4, Fig. SA8). In this configuration, Ceratosauria are made of the basally branching *Dilophosaurus sinensis*, followed by a polytomy gathering Noasauridae and Etrigansauria (*sensu* Delcourt 2018), a clade made of *Eoabelisaurus* and Neoceratosauria (= Ceratosauridae + Abelisauridae; Fig. 16B). Noasauridae are here comprised of MNN TIG6 and two subclades, namely Elaphrosaurinae and Noasaurinae, in a polytomy, with Noasaurinae being formed by *Noasaurus*, *Velocisaurus*, *Masiakasaurus*, and *Laevisuchus* all in a polytomy (Fig. 16B).

Feeding ecology analyses

The cladistic analysis performed on the dentition-based datamatrix yielded 10 000 MPTs (tree length = 1217) whose strict consensus tree recovered *Noasaurus* and many other ziphodont taxa (e.g. basal theropods, non-abelisaurid ceratosaurs, non-tyrannosaurid tyrannosauroids, compsognathids, and megaraptorans) in a large polytomy (Supporting Information, S1.4.4, Fig. SA4). Removing 15 unstable taxa from the analysis (see Table 4) resulted in a better-resolved strict consensus tree from 10 000 MPTs where *Noasaurus* is classified with the basally branching coelurosaur *Bicentenaria* at the base of a large dentition-based clade made of the putative juvenile specimen of *Dracovenator* BP/1/5272 (basalmost taxon) and two dental-based clades, one gathering *Dracoraptor*, *Ornitholestes*, *Eodromaeus*, *Bambiraptor*, and microraptorines, and another relatively unresolved group encompassing *Archaeopteryx* and juvenile *Limusaurus* at the base, as well as *Berthasaura*, ornithomimosaurs, oviraptorosaurs, and unenlagiines (Supporting Information, S1.4.4, Fig. SA5). Keeping the wildcard taxa *Caudipteryx*, *Compsognathus*, and *Scipionyx* in this analysis recovered the same general topology (Supporting Information, S1.4.4, Fig. SA6) with the difference that the two latter taxa are classified at the base of a poorly resolved clade encompassing *Archaeopteryx*, *Berthasaura*, unenlagiines, ornithomimosaurs, and oviraptorosaurs (Fig. 17A).

The analysis on curvature and elongation of manual unguals I in non-avian theropods found *Noasaurus* in a zone of the graph gathering poorly elongated (elongation ratio <2) but extremely curved (curvature angle >120°) claws (Fig. 17B; Supporting Information, S1.5.4, Fig. SA8). The 2D plot on the curvature (X-axis) and elongation (Y-axis) of the theropod manual ungual I shows that the bony claw of *Noasaurus* shares similar curvature and elongation to those belonging to the basally branching alvarezsaur *Tugulusaurus*, the allosaurid *Allosaurus*, the megalosaurid *Torvosaurus* (whose ungual may belong to a large-bodied *Allosaurus*; see Discussion), and the basal coelurosaur *Bicentenaria*, and close curvature and elongation to the manual ungual I of the megalosaurid *Afrovenator*, the spinosaurid *Baryonyx*, the basally branching alvarezsaur *Haplocheirus*, the unenlagiine dromaeosaurid *Buitreraptor*, and the troodontid *Xixiasaurus* (Fig. 17C).

DISCUSSION

Comparative anatomy

Cranial and dental elements

Noasauridae Bonaparte and Powell 1980, and Noasaurinae Rauhut and Carrano 2016, were created using *Noasaurus* as the type genus of the two nominal taxa, and the inclusion of *Noasaurus leali* among these two clades, therefore, needs no justification. Comparing this species to other taxa classified among noasaurids, especially those recovered among non-elaphrosaurine noasaurids in recent phylogenetic analyses on ceratosaurs (i.e. *Masiakasaurus*, *Laevisuchus*, *Velocisaurus*, and

in yellow, Asia in red, Madagascar/India in orange, and Australia in turquoise) and body length (<2.5 m for the small black dot, 2.5–6 m for the medium grey dot, and >6 m for the large black circle; Supporting Information, S2.2, S5 for data on body length), respectively. Continents beneath the stems represent the possible origin of the clades. Theropod silhouettes approximately to scale. Black silhouettes from Alessio Ciaffi (*Abelisaurus* in figure B), Funkmonk (*Deltadromeus*), Iain Reid (*Eoabelisaurus*), Jagged Fang Designs (*Ekrixinatosaurus*), Jaime Headden (*Arcovenator*), Julio Garza (*Dilophosaurus*), Geovane Alves de Souza (*Berthasaura*; modified), Tasman Dixon (*Masiakasaurus*, *Spectrovenator*, *Vespersaurus*), Ville-Veikko Sinkkonen (*Limusaurus*), and Scott Hartman (all the others). See Supporting Information, S1.7 for the silhouette's licence attribution.

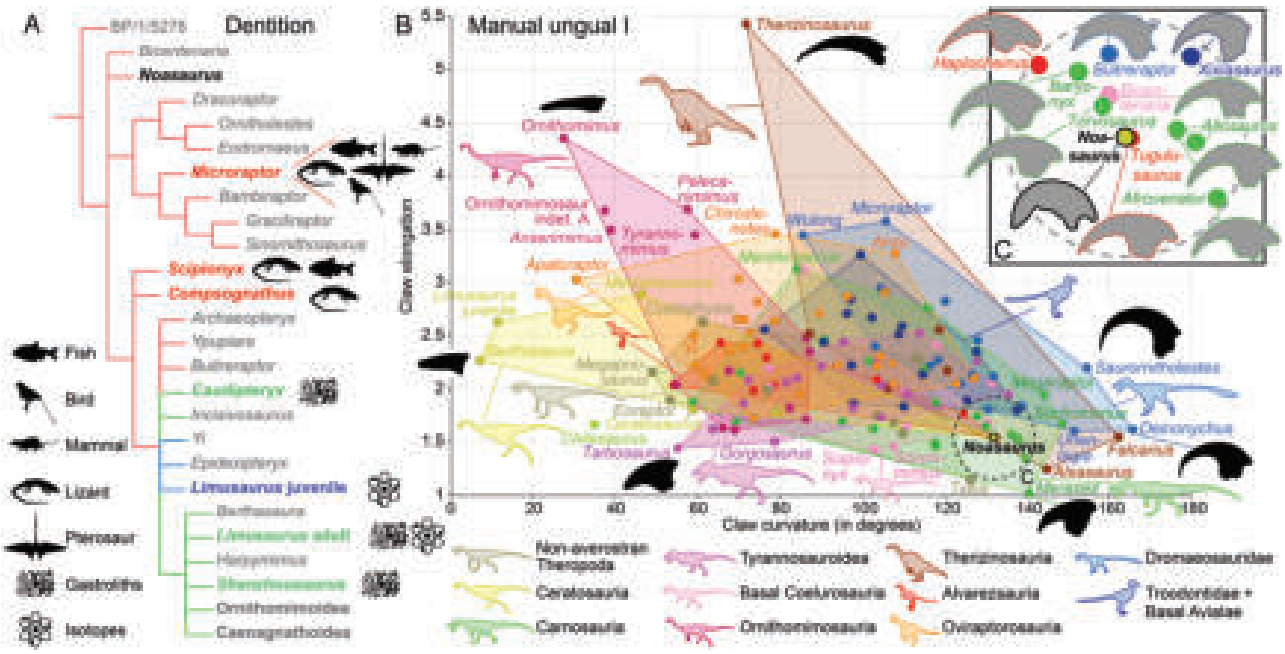

Figure 17. Results of the analyses on feeding ecology in *Noasaurus*. A, strict consensus tree resulting from 10 000 most parsimonious trees (tree length = 1217) obtained in the cladistic analysis performed on a dentition-based datamatrix of 125 non-avian theropod taxa after pruning 12 unstable taxa and keeping the wildcard taxa *Caudipteryx*, *Compsognathus*, and *Scipionyx* (Table 4; see Supporting Information, S1.4.4, Fig. SA6 for the whole tree). The dentition-based clade including *Noasaurus* is the only one to be illustrated, with information on the diet of the taxa retrieved in this clade based on direct evidence (stomach content and isotopic analyses). Taxa in red, blue, and green represent carnivorous, omnivorous, and herbivorous theropods, respectively, for which we have direct evidence of diet. Taxa in light grey represent theropods with only indirect evidence of diet. Tree lines in red and green indicate probable carnivorous and herbivorous feeding ecologies, respectively, based on indirect and direct evidence of diet. B, 2D plot of the curvature vs. the elongation of the bony manual ungual I from 156 specimens belonging to 133 non-avian theropod taxa. The manual claws of a few theropods such as *Noasaurus*, *Dilong*, *Berthasaura*, and *Masiakasaurus* are tentatively referred to the first finger but might pertain to another one. C, close-up on the region of the graph occupied by *Noasaurus*. Remark: *Torvosaurus*' claw might represent the manual ungual of a particularly large-bodied *Allosaurus*. Silhouettes from Funkmonk (Therizinosauria, Alvarezsauria), Ingo Braasch (fish), Jaime Headden (Oviraptorosauria), Jose Carlos Arenas-Monroy (lizard), Matt Martyniuk (Troodontidae + Basal Avialae; bird), Mark P. Witton and Darren Naish (pterosaur), Nobu Tamura (mammal), Ville-Veikko Sinkkonen (Ceratosauria), Scott Hartman (all the others). See Supporting Information, S1.7 for the silhouette's licence attribution.

Vespersaurus; Rauhut and Carrano 2016, Wang *et al.* 2017a, Langer *et al.* 2019), is, however, pivotal for our understanding of noasaurid phylogeny.

The maxilla of *Noasaurus* shares with the noasaurids *Masiakasaurus* (FMNH PR 2183; Fig. 18H, I) and *Berthasaura* (MN 7821-V), as well as the putative noasaurid *Limusaurus* (Stiegler, 2019) (Fig. 18O, P), a pointy pre-antorbital body, a dorsoventrally low and anteroposteriorly long jugal ramus, an extensive and well-delimited lateral antorbital fenestra bounded by a prominent antorbital ridge, as well as an anteromedial process situated almost directly dorsal to the nutrient groove and mainly made of a single and strongly medially protruding (ventral) ridge. Conversely, ceratosaurids and abelisaurids such as *Ceratosaurus* (USNM 4735, MNH VP 5278; Madsen and Welles 2000; Fig. 18.2, 18.3), *Spectrovenator* (MZSP-PV 833), *Rugops* (MNN IGU1; Sereno *et al.* 2004), and *Majungasaurus* (FMNH PR 2100; Sampson and Witmer 2007; Fig. 18U, V) have a convex alveolar margin, taller subrectangular or parabolic pre-antorbital body, a taller and often shorter jugal ramus (especially in brachyrostran abelisaurids), as well as a lower antorbital ridge when the latter is present. The anteromedial process of non-noasaurid ceratosaurs is also made of two less prominent ridges (*Ceratosaurus*; USNM 4735, UMNH VP 5278) or situated much more dorsally than the nutrient groove (abelisaurids). Abelisaurids additionally have a lateral antorbital fossa extending mainly anteriorly and slightly ventrally (especially in the anteriormost portion of the fossa, e.g. *Tralkasaurus*) or with no ventral extension at all (Sereno *et al.* 2004, Sampson and Witmer 2007, Sereno et al. 2008, Cerroni *et al.* 2020a, b, Zaher *et al.* 2020). Unlike other noasaurids, but similar to *Ceratosaurus* (Fig. 18.2), the lateral antorbital fossa of *Noasaurus* only covers a small portion of the anterior body anteriorly and the maxillary body ventrally. As in *Masiakasaurus* (Fig. 18H) and *Berthasaura*, the maxillary fossa of *Noasaurus* is closed medially, differing from the opened maxillary fenestra of the elaphrosaurine *Limusaurus* (Stiegler 2019; Fig. 18O). *Noasaurus* also shares with the noasaurine *Masiakasaurus* a dorsoventrally low and continuous interdental wall showing a smooth surface (Fig. 18B, I). Interdental plates are present and separated in the juvenile *Limusaurus*, whereas they are absent in adult individuals. Conversely, the interdental wall of ceratosaurids and abelisaurids is significantly taller and its surface is smooth and anteroposteriorly undulated (e.g. ceratosaurids, *Spectrovenator*, UCPC 10; Fig. 18.3), rugose (*Kryptops*), or ornamented with vertical striae (e.g. *Rugops*, *Abelisaurus*, *Majungasaurus*, *Ekrixinatosaurus*, and *Llukalkan*; Fig. 18V). The maxilla of *Noasaurus* differs from all other

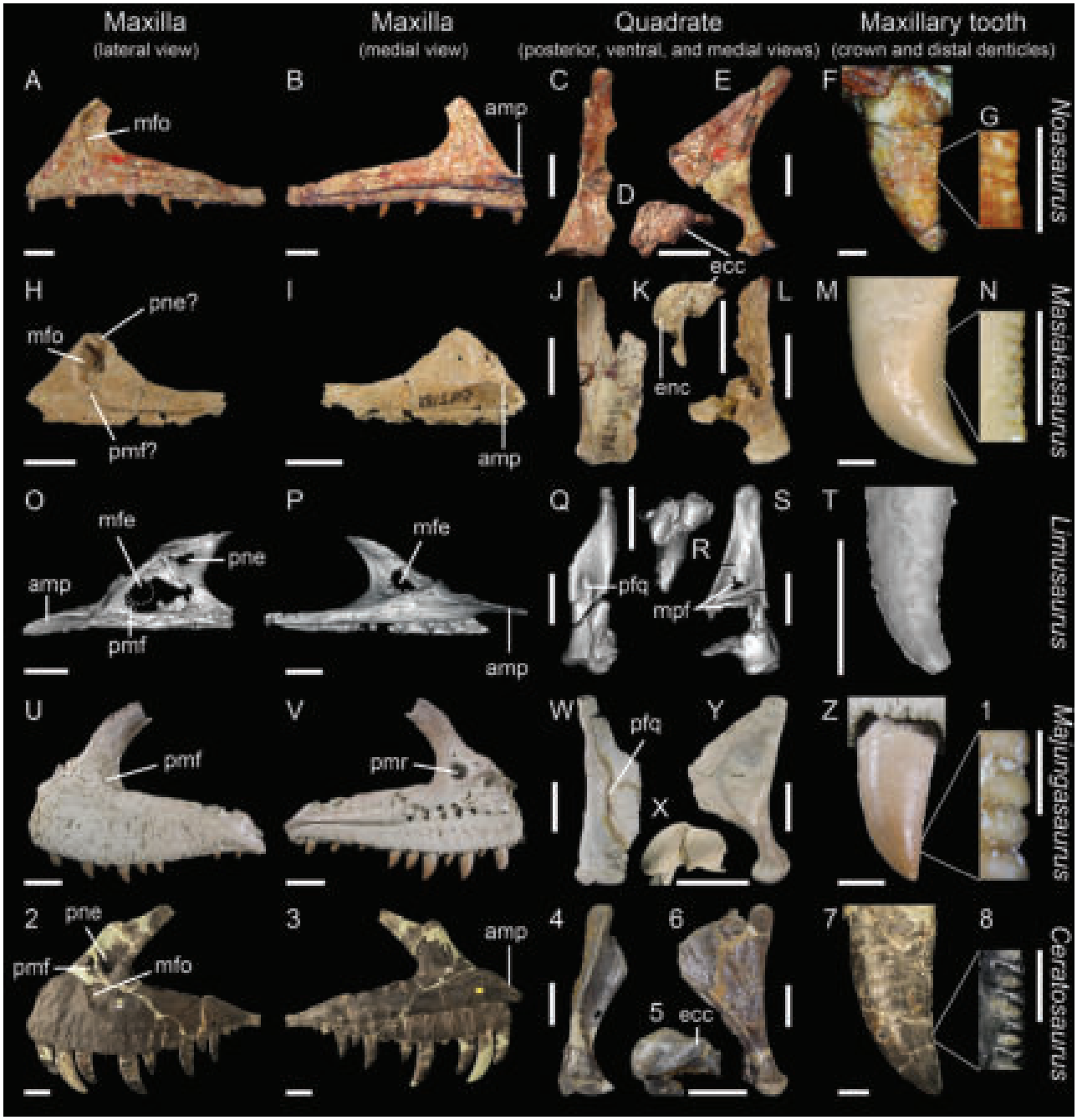

Figure 18. Comparative cranial and dental anatomy in ceratosaur theropods. Maxillae in lateral and medial views of: A, B, *Noasaurus leali* (left; PVL 4061); H, I, *Masiakasaurus knopfleri* (right, reversed; FMNH PR 2183); O, adult *Limusaurus inextricabilis* (right, reversed, in lateral view; IVPP V15923; from Stiegler 2019, modified); P, juvenile *Limusaurus inextricabilis* (left, in medial view; IVPP V15301; from Stiegler 2019, modified); U, V, *Majungasaurus crenatissimus* (left; FMNH PR 2100); 2, 3, *Ceratosaurus nasicornis* (left; UMNH VP 5278); quadrates in posterior, ventral, and medial views of C–E, *Noasaurus leali* (right; PVL 4061); J–L, *Masiakasaurus knopfleri* (right; FMNH PR 2496); Q–S, *Limusaurus inextricabilis* (left, reversed; IVPP V15297; from Stiegler 2019, modified); W–Y, *Majungasaurus crenatissimus* (right; FMNH PR 2100); 4–6, *Ceratosaurus nasicornis* (right; MWC 1; courtesy of Oliver Rauhut); maxillary crowns and distal denticles in lateral view of F, G, *Noasaurus leali* (lmx8; PVL 4061); M, N, *Masiakasaurus knopfleri* (isolated lateral crown; UA 9091); T, *Limusaurus inextricabilis* (lmx2 or 3; IVPP V15301; from Stiegler 2019, modified); Z-1, *Majungasaurus crenatissimus* (lmx4; FMNH PR 2100); 7, 8, *Ceratosaurus nasicornis* (lmx8; UMNH VP 5278). Abbreviations: amp, anteromedial process; ecc, ectocondyle; enc, entocondyle; mfe, maxillary fenestra; mfo, maxillary fossa; mpf, medial pneumatic foramina; pmf, promaxillary fenestra; pfq, posterior fossa; pne, pneumatic excavation. Scale bars equal 5 cm (U–Y, 2–6), 1 cm (A–E, H–L, O, Q–S, Z, 7), 2 mm (P), and 1 mm (F, G, M, N, T, F, 1, 8).

ceratosaurs in having a concave alveolar margin in lateral view, a tall, shallow, suboval, and poorly delimited maxillary fossa whose anterior half is covered by the lateral rim of the maxilla, as well as a dorsoventrally low interdental wall made of fused interdental plates with straight ventral margins. Conversely, the alveolar margin of *Masiakasaurus*, the closest relative of *Noasaurus* with

a preserved maxilla, is almost perfectly straight and the maxillary fossa is deep, subrectangular, and particularly well delimited (Fig. 18H). A small pneumatic opening (which may be homologous to the promaxillary fenestra of *Limusaurus*; Stiegler 2019) also invades the anteroventral surface of the lateral antorbital fossa of *Masiakasaurus* (Fig. 18H). The fused interdental plates of the latter have V-shaped ventral margins (Fig. 18I), whereas they are straight in *Noasaurus* whose ventral border of the interdental wall forms a straight line along the maxilla (Fig. 18B).

Stiegler (2019) interprets the maxillary fossa of *Noasaurus* and *Masiakasaurus* as a pneumatic excavation ['pneumatic recess' *sensu* Stiegler (2019: 47)] present in the ascending ramus and similar to that of *Ceratosaurus*. The homology of pneumatic openings and recesses in the maxilla of theropods is well-known to be particularly difficult to assess (Witmer 1997). We, nonetheless, follow Hendrickx and Mateus' (2014b) and de Souza *et al.*'s (2021) opinions and tentatively interpret the shallow or well-delimited depressions present in the anterior corner of the lateral antorbital fossa as the maxillary fossa in the noasaurids *Noasaurus*, *Masiakasaurus*, and *Berthasaura* for the following reasons. (i) This pneumatic depression is situated directly posterior to the anteriormost margin of the lateral antorbital fossa and most of the depression is located ventral to the anteriormost point of the antorbital fossa. The pneumatic depression with a similar location is identified as the maxillary fossa by Hendrickx and Mateus (2014b) [the 'maxillary sinus' *sensu* Madsen and Welles (2000)] for *Ceratosaurus* and as the maxillary fenestra (homologous to the maxillary fossa, from which it only differs by its perforation) by Stiegler (2019) for *Limusaurus*. (ii) The pneumatic excavation of both *Ceratosaurus* and *Limusaurus* occupies a large portion of the ascending ramus both anteroposteriorly and dorsoventrally, and its ventral limit is situated at the same level or dorsal to the anteriormost point of the antorbital fenestra, which is not the case of the pneumatic depressions in both *Noasaurus* and *Masiakasaurus*. (iii) Although *Noasaurus* does not have any pneumatic depression in the ascending ramus of the maxilla, a small depression is present directly dorsal to the larger pneumatic depression that we interpret as the maxillary fossa in *Masiakasaurus* (Fig. 16H). Given its location, this small depression is most likely homologous to the pneumatic recess of *Ceratosaurus* and *Limusaurus*, which would thus confirm the fact that the large and well-delimited pneumatic depression of *Noasaurus* and *Masiakasaurus* is the maxillary fossa.

The quadrate of *Noasaurus* displays many ceratosaurian features, such as the presence of a laterally oriented lateral process reaching the quadrate body well ventral to the quadrate head (also present in allosauroids and a few coelurosaurs such as *Shuvuuia* and *Ornitholestes*; Hendrickx 2015), a mediolaterally narrow, straight, sub-vertical, and poorly delimited quadrate ridge emerging ventrally at the level of the entocondyle, around one-third of the quadrate body, and reaching the quadrate head dorsally, as well as a ventral shelf projecting from the anteroventral margin of the pterygoid flange (Hendrickx 2015) [NB—a poorly developed ventral shelf is present in both *Masiakasaurus* and *Limusaurus*; *contra* Carrano *et al.* (2011) and Stiegler (2019); Fig. 18C–E, J–L, Q–S, W–Y, 4–6]. As seen in the mandibular articulation of other abelisauroids, the ectocondyle of *Noasaurus* is subcircular and significantly smaller than the entocondyle, which was almost certainly mediolaterally thick and oval in shape (Hendrickx 2015; Fig. 18D, K, R, X, 5). Unlike *Limusaurus* (Fig. 18Q, S) and similar to other ceratosaurs, the quadrate of *Noasaurus* is apneumatic (Hendrickx *et al.* 2015a). The quadrate of *Limusaurus* indeed includes a deep medial pneumatic foramen delimited dorsally by a prominent ridge running anterodorsally along the middle part of the pterygoid flange (Fig. 18R), a feature absent in other ceratosaurs (Hendrickx *et al.* 2015a, Stiegler 2019). Similar to *Ceratosaurus* (Fig. 18.6) and abelisaurids (Fig. 18Y), but unlike *Limusaurus* and *Masiakasaurus*, the pterygoid flange of *Noasaurus* reaches the quadrate body well-dorsal to the mandibular articulation and the ventral margin of the flange is diagonally and anterodorsally oriented from the long axis of the quadrate body. In *Limusaurus* and *Masiakasaurus*, the ventral margin of the pterygoid flange extends mainly anteriorly, perpendicular to the posterior margin of the quadrate body, and almost directly dorsal to the mandibular articulation. In dorsal view, the subcircular quadrate head of *Noasaurus* additionally differs from the triangular head of *Masiakasaurus* and *Limusaurus*. The noasaurines *Noasaurus* and *Masiakasaurus*, however, have in common a shallow posterior fossa extending dorsoventrally along the whole quadrate body, as well as a narrow intercondylar sulcus separating the mandibular condyles. The quadrate of *Noasaurus* is apomorphic in having a trapezoidal and almost subtriangular pterygoid flange with a particularly dorsoventrally low anterior margin and a ventral margin extending at an acute angle from the quadrate body. All ceratosaurs preserving the pterygoid flange entirely (e.g. *Limusaurus*, *Ceratosaurus*, *Eoabelisaurus*, *Majungasaurus*, *Carnotaurus*, and possibly *Berthasaura*) have a much taller anterior margin of the quadrate (C.H. pers. obs.). Another autapomorphy of *Noasaurus* is the strongly arched quadrate body (Fig. 18E). A curved quadrate body is shared with juvenile individuals of *Limusaurus* (Stiegler, 2019) but the degree of curvature displayed by them does not seem to be as important as in *Noasaurus*. A quadrate with a small quadrate foramen and unfused to the quadratojugal were two autapomorphies proposed by Bonaparte (1991) to diagnose *Noasaurus*. Both quadrate foramen and quadratojugal contact of the quadrate are, nevertheless, unpreserved and these synapomorphies are consequently invalid.

If the maxilla of *Noasaurus leali* was described by Bonaparte and Powell (1980) and Novas (2009) as bearing 10 to 11 teeth, a character used by Carrano and Sampson (2008) to diagnose this species, there are 13 maxillary tooth positions. This number is comparable to that of *Ceratosaurus* (Madsen and Welles, 2000) and *Aucasaurus* (Hendrickx *et al.*, 2020b) among ceratosaurs, as well as several carnosaurs (e.g. *Asfaltovenator*, *Dubreuillosaurus*, *Monolophosaurus*, and *Wiehenvenator*; Allain 2002, Brusatte *et al.* 2010, Rauhut *et al.* 2016, Rauhut and Pol 2019), many tyrannosauroids (e.g. *Daspletosaurus*, *Gorgosaurus*, *Jinbeisaurus*, *Raptorex*, *Suskityrannus*, and *Tarbosaurus*; Currie 2003, Sereno *et al.* 2009, Nesbitt *et al.* 2019, Wu *et al.* 2020), and a few dromaeosaurids (e.g. *Microraptor* and *Tsaagan*; Norell *et al.* 2006, Pei *et al.* 2014). Given that ceratosaurid are recovered as a basally branching radiation of ceratosaurs in some phylogenies (Figs 16A, 17A), and that *Noasaurus* and some specimens of *Ceratosaurus* (i.e. MWC 1; Madsen and Welles 2000) bore the same number of maxillary teeth, it is possible that, unlike some elaphrosaurines that lost them entirely (Wang *et al.* 2017a, b),

a reduction of the number of maxillary teeth may not have occured throughout the evolution of noasaurine ceratosaurs. The dentition of *Noasaurus* shares with the large majority of ceratosaurs the presence of a mesial carina reaching the cervix in the lateral crowns (Hendrickx *et al.* 2019, 2020b), a dental feature present in most other large-bodied ziphodont theropods such as non-megalosaurid megalosauroids, most allosauroids, and some tyrannosauroids (e.g. Hendrickx *et al.* 2015c, 2019, 2020a, b). As in abelisaurids, but unlike ceratosaurids and all other elaphrosaurines and noasaurines preserving lateral teeth (i.e. juvenile *Limusaurus* and *Masiakasaurus*; Fig. 18M), the distal profile of all preserved lateral crowns of *Noasaurus* is straight, while only a few lateral teeth of ceratosaurids (Fig. 18.7) and *Limusaurus* show this condition (Stiegler 2019, Hendrickx *et al.* 2019, 2020b). The dentition of *Noasaurus* and other noasaurids departs from that of non-noasaurid ceratosaurs and most non-coelurosaur theropods in the particularly small size of the crowns (i.e. <20 mm; Fig. 18F, M, Z, 7), a condition shared with most neocoelurosaur theropods other than eudromaeosaurids (Hendrickx *et al.* 2019). In dentulous elaphrosaurines and noasaurines, the teeth of *Noasaurus* and *Masiakasaurus* differ from those of the juvenile *Limusaurus* in the presence of carinae and denticles (Carrano *et al.* 2002, Wang *et al.* 2017a, Stiegler 2019, de Souza *et al.* 2021; Fig. 18F, M, T). The two noasaurines also share a size discrepancy between mesial and distal denticles (i.e. DSDI > 1.2), a condition present in the mesial dentition of *Ceratosaurus* and, among abelisaurids, in the lateral crowns of *Arcovenator* and juvenile *Majungasaurus* (Hendrickx *et al.* 2019, 2020b). Outside Ceratosauria, a size discrepancy between mesial and distal denticles is also typical of the teeth of piatnitzkysaurids, basal tyrannosauroids, and the majority of eudromaeosaurs (Currie *et al.* 1990, Rauhut *et al.* 2010, Hendrickx *et al.* 2019). The lateral crowns of *Noasaurus* show the derived feature of having a low number (<30) of large distal denticles relative to the crown height and a similar number of distal denticles at mid-crown and more basally, two dental features absent in non-coelurosaur theropods (C.H. pers. obs.). Lateral crowns with less than 30 distal denticles not decreasing in size basally have also been observed in the compsognathid *Juravenator* (JME Sch 200), the dromaeosaurids *Microraptor* (IVPP 2008.5; IVPP V13475), and *Deinonychus* (YPM 5232), as well as the troodontids *Sinusonasus* (IVPP V1527) and *Zanabazar* (Norell *et al.* 2009: fig. 30).

Axial skeleton

The elongation of the cervical vertebrae of *Noasaurus* was previously mentioned as indicative of a long and sigmoidal necks in noasaurids (Carrano *et al.* 2011, Rauhut and Carrano 2016). In fact, the long neck and other features of the appendicular skeleton, such as the slender tibia and the gracile metatarsus, led several authors to interpret noasaurids as coelurosaur theropods possibly related to ornithomimosaurs, as occurred with *Elaphrosaurus* (Janensch 1925, Nopcsa 1928, Galton 1982; Fig. 19Q). However, the posterior cervical vertebra of *Noasaurus* (Fig. 7) is relatively less elongate than in some elaphrosaurines such as *Elaphrosaurus*, *Limusaurus*, and the specimen NMV-P252004 from Victoria, Australia (Rauhut and Carrano 2016, Wang *et al.* 2017b, Poropat *et al.* 2020). Another general feature of the cervical elements of noasaurids is related to their relatively low height, since the cervical neural spines are dorsoventrally low and the transverse processes became flattened; the resultant dorsal surface is thus clearly differentiated from the lateral aspect by the development of the prezygapophyseal epipophyseal lamina, as seen in *Noasaurus* and other closely related abelisauroids, such as *Masiakasaurus*, *Spinostropheus*, and *Laevisuchus*.

A main difference between the neural arch of the holotype of *Noasaurus* and other noasaurines is the lateral profile of the prezygapophyseal epipophyseal lamina, which is faintly curved posterior to the prezygapophyses in the Argentine taxon (Figs 7A, B, 19A), whereas this area of the lamina is anteroposteriorly shorter and forms a markedly concave margin in the sixth cervical vertebra of some noasaurines (e.g. *Laevisuchus* and *Masiakasaurus*; Novas *et al.* 2004, Carrano *et al.* 2011, Mohabey *et al.* 2024; Fig. 20I). In the middle cervical of *Vespersaurus*, this margin is similar in shape to that of *Noasaurus*, although it is not as anteroposteriorly extensive (Langer *et al.* 2019). Conversely, the middle cervical vertebrae of *Elaphrosaurus* and *Limusaurus* show a poorly developed prezygapophyseal epipophyseal lamina (Rauhut and Carrano 2016, Stiegler 2019; Figs 20Q, 20S). The anterior prong of the epipophysis is probably one of the most remarkable features of *Noasaurus* (Fig. 10A), given its absence in all known cervicals of noasaurids (Fig. 19I); the presence of this prong may be related to the insertion of the m. longus colli dorsalis (Snively and Russell 2007) or the ossification of the tendons attached to the epipophyses (Novas 2009). The centroprezygapophyseal fossae are large and well developed in the neural arch of *Noasaurus* (Fig. 19C), *Masiakasaurus* (Fig. 19K), *Laevisuchus*, as well as in several indeterminate noasaurids ('pneumatic fossa' in: Novas *et al.* 2004, Brum *et al.* 2018, Smyth *et al.* 2020, Mohabey *et al.* 2024). These fossae seem, however, to be poorly developed in the middle cervicals of *Vespersaurus* ('peduncular fossa'; Langer *et al.* 2019). Another feature from the mid-cervicals shared by *Noasaurus*, *Masiakasaurus*, and *Berthasaura* is the fact that the epipophyses exceeds far beyond the postzygapophyses (de Souza *et al.* 2021), which is not the case in the sixth cervical vertebra of *Masiakasaurus* (Fig. 19I); as for *Elaphrosaurus*, there are no epipophyses on the cervical postzygapophyses (Rauhut and Carrano 2016; Fig. 19Q, R).

The postzygapophyseal centrodiapophyseal fossa from the mid-posterior cervical of *Noasaurus* is broadly developed with two distinct pockets or subfossae located dorsally and ventrally (Fig. 10F). It is unclear if these structures communicate via foramina within the internal structure of the neural arch, as in some noasaurid material from Brazil (Brum *et al.* 2018). Conversely, this large fossa is simple and undivided but also present a foramen in the mid-posterior cervical vertebrae of *Vespersaurus* and *Elaphrosaurus* (Rauhut and Carrano 2016; Langer *et al.* 2019; Fig. 19Q). The postzygapophyseal centrodiapophyseal fossa ['infrapostzygapophyseal fossa' of Carrano *et al.* (2011)] is also undivided and large, but less pronounced in the sixth cervical of *Masiakasaurus* (Fig. 19I). In the middle cervical of *Berthasaura*, the centrodiapophyseal fossa is similarly divided into two fossae, which in turn are hidden laterally by the postzygodiapophyseal lamina, a condition similar in *Noasaurus*, but both excavations have different size in *Berthasaura* (de Souza *et al.* 2021) whereas they are subequal in *Noasaurus*.

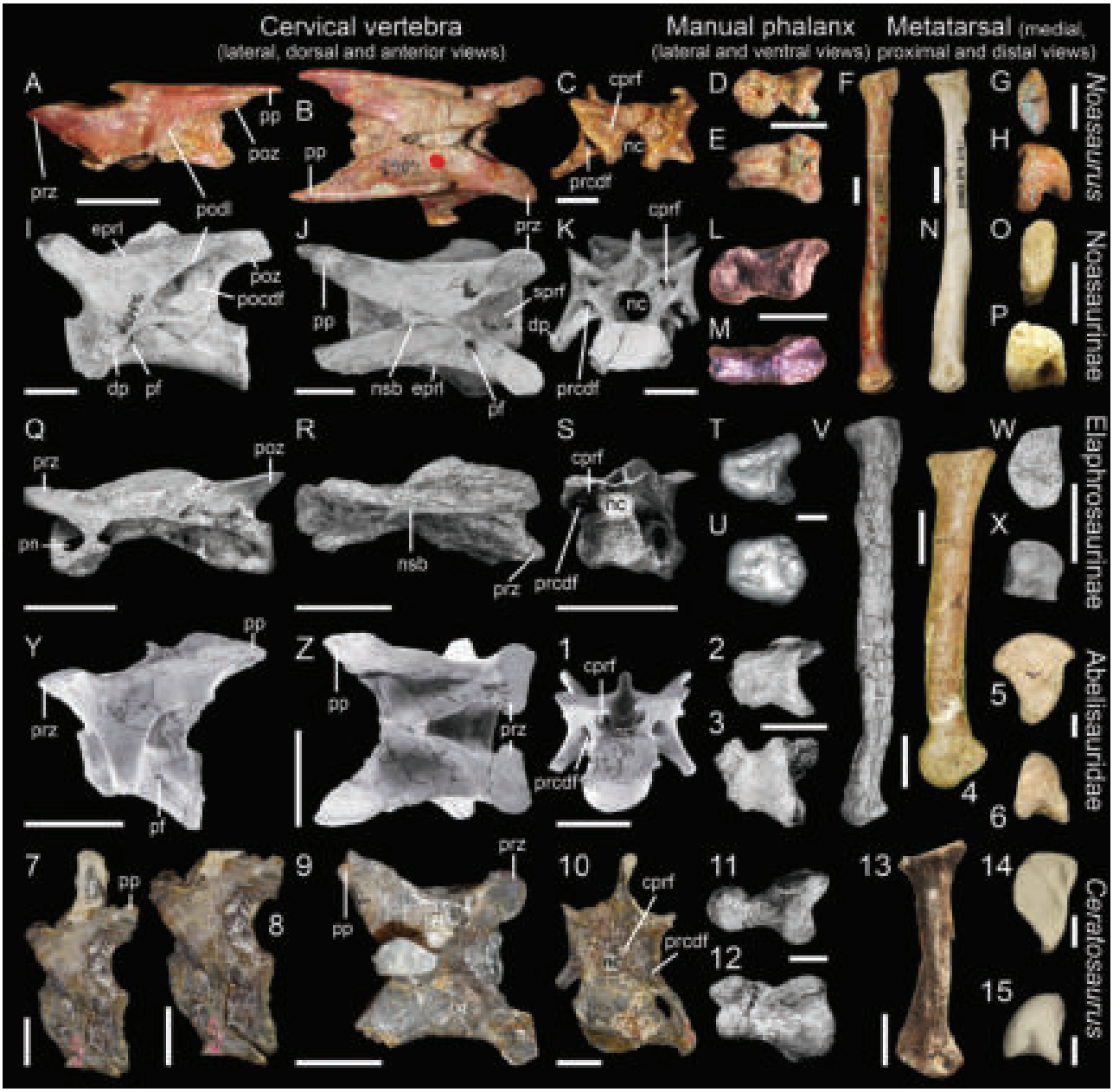

Figure 19. Comparative postcranial anatomy in ceratosaur theropods. Cervical vertebrae in lateral, dorsal and anterior views of: A–C, *Noasaurus leali* (sixth or seven vertebral arch; PVL 4061); I–K, *Masiakasaurus knopfleri* (sixth cervical vertebra; FMNH PR 2481; courtesy of Matthew Carrano); Q–S, *Elaphrosaurus bambergi* (sixth cervical; MB R 4260; from Rauhut and Carrano 2016, modified); Y-1, *Majungasaurus crenatissimus* (fifth cervical; UA 8678; from O'Connor, 2007); 7–10, *Ceratosaurus nasicornis* [fifth cervical, with close-up on the centrum in 8; MWC 1; courtesy of Oliver Rauhut (7, 8, 10) and Matthew Carrano (9)]; manual phalanx in lateral and ventral views of: D, E, *Noasaurus leali* (III-1; PVL 4061); L, M, *Ligabueino andesi* (digit III?, reversed; MACN PV-N 42); T, U, *Limusaurus inextricabilis* (III-1; IVPP V15924; from Stiegler 2019); 2, 3, *Majungasaurus crenatissimus* (II-1; FMNH PR 2836; from Burch and Carrano 2012); 11, 12, *Ceratosaurus nasicornis* (III-1; USNM 4735; from Carrano and Choiniere 2016); MtII in medial, proximal, and distal views of F–H, *Noasaurus leali* (PVL 4061); N–P, *Masiakasaurus knopfleri* (FMNH PR 2151, cast); V–X, *Elaphrosaurus bambergi* (MB R 4260, reversed; from Rauhut and Carrano (2016), modified); 4–6, *Aucasaurus garridoi* (MCF-PVPH-236; courtesy of Matthew Lamanna); 13–15, *Ceratosaurus nasicornis* (UMNH VP 5278, reversed; courtesy of Matthew Carrano for 13; from Gilmore (1920) for 14, 15). Abbreviations: cprf, centroprezygapophyseal fossa; dp, diapophysis; eprl, epipophyseal–prezygapophyseal lamina; nc, neural canal; nsb, neural spine base; pf, pneumatic foramen; pocdf, postzygapophyseal centrodiapophyseal fossa; podl, postzygodiapophyseal lamina; poz, postzygapophysis; pp, parapophysis; prcdf, prezygapophyseal centrodiapophyseal fossa; prz, prezygapophysis; sprf, spinoprezygapophyseal fossa. Scale bars equal 5 cm (Q–S, V–Z, 1, 4, 7–10, 13), 2 cm (A, B, 5, 6, 14, 15), 1 cm (C–K, N–P, T, U, 2, 3, 11, 12), and 5 mm (L, M).

Little information has been published regarding the cervical and dorsal ribs of noasaurids, except for the original publication of *Noasaurus* (Bonaparte and Powell 1980), the briefly described *Spinostropheus* (Sereno *et al.* 2004), and the extensive revision of the new materials of *Masiakasaurus* (Carrano *et al.* 2011). Thus, rib comparisons in Noasauridae are limited by the

current published information, though many features are shared with abelisaurids. At first glance, a sharp and well-developed anterior projection in the dorsolateral process of the cervical ribs seem to characterize both noasaurines (e.g. *Noasaurus* and *Masiakasaurus*), elaphrosaurines (e.g. *Spinostropheus*), and abelisaurids (e.g. *Carnotaurus* and *Majungasaurus*). Furthermore, the pneumatization of the anterior and posterior surfaces of the cervical rib of *Noasaurus* (Figs 9C, F, 10C, F) is also present in most abelisauroids preserving this element (Sereno *et al.* 2004, O'Connor 2007). The lateral buttressing of the cervical rib of *Noasaurus* is another feature that may be widespread among abelisauroids, being present in several taxa such as *Masiakasaurus*, *Majungasaurus*, and *Skorpiovenator*. Because the cervical ribs of *Noasaurus* do not preserve the styliform process, it is unknown whether this process was distally bifurcated, as commonly seen in Abelisauroidea (Sampson *et al.* 1998, Zaher *et al.* 2020).

Appendicular skeleton

The only available non-ungual phalanx of *Noasaurus* shows a well-defined, strikingly narrow, and short flexor process (Fig. 11), as occurs in known abelisaurid manual phalanges (e.g. *Carnotaurus* and *Aucasaurus*; Bonaparte *et al.* 1990, Coria *et al.* 2002, Ruiz *et al.* 2011), as well as in *Eoabelisaurus* (Pol and Rauhut 2012) and *Dilophosaurus* (Marsh and Rowe 2020). Conversely, this process is absent or transversely wide, with its transverse width being subequal to that of the distal articular surface in other theropods (Agnolín and Chiarelli 2010). The extensor process is transversely expanded and subrectangular in contour in *Noasaurus*, a condition shared with *Ligabueino* and once regarded as diagnostic of noasaurids (Coria and Salgado 1998). A similar condition is, however, present in *Berthasaura* and *Limusaurus*, as well as abelisaurids such as *Majungasaurus* and *Aucasaurus* (Coria *et al.* 2002, Xu *et al.* 2009, Burch and Carrano 2012, de Souza *et al.* 2021). The extensor process is subrectangular in outline and strongly transversely expanded in all these taxa, contrasting with the extensor process of other theropods such as *Allosaurus* and *Sinraptor* (Madsen 1976, Currie and Zhao 1993) in which it is transversely narrower than the flexor process and typically subtriangular in outline in dorsal view. The same condition is observed in the manual phalanges of *Ceratosaurus* (Carrano and Choiniere 2016).

As highlighted in the original description of *Noasaurus*, the unguals of this taxon are particularly different from those of any known theropods, especially ceratosaurs (Fig. 20; Bonaparte and Powell 1980, Bonaparte 1991, Carrano and Sampson 2008, Agnolín and Chiarelli 2010). The manual claws of ceratosaurs are poorly known and restricted to a handful of taxa (e.g. *Ceratosaurus*, *Masiakasaurus*, *Limusaurus*, *Berthasaura*, *Vespersaurus*, and *Eoabelisaurus*; Xu *et al.* 2009, Pol and Rauhut 2012, Carrano and Choiniere 2016, Langer *et al.* 2019, de Souza *et al.* 2021; Fig. 20B–D, F, G), while the presence of manual unguals remains uncertain in abelisaurids but might be present in some taxa such as *Carnotaurus* (Fig. 20H; Agnolín and Chiarelli 2010, Ruiz *et al.* 2011, Burch and Carrano 2012). Importantly, the elongated and poorly curved claws of *Masiakasaurus* identified as manual unguals by Carrano *et al.* (2002, 2011) are now considered as pedal unguals (Carrano, pers. comm. 2022). Their morphology, however, suggests that they could pertain to the manus as they are low and proximodistally elongated, while noasaurid pedal unguals tend to be taller and shorter (NB—the presence of a single or two 'blood grooves' along the surface of the transverse surface of the claw cannot be used to differentiate manual from pedal unguals in ceratosaurs as this feature can change in different digits of the same manus and, for the pes, vary individually; Langer *et al.* 2019, Stiegler 2019). We, therefore, tentatively follow Carrano *et al.*'s (2002, 2011) initial identification of these elements as manual unguals, possibly from digits II or III given that they strongly differ from the strongly curved manual ungual I of the closely related *Noasaurus*. As noted in previous works (e.g. Novas and Bandyopadhyay 2001), *Noasaurus*' manual claws resemble those of abelisauroids in lacking a flexor tubercle, which is replaced by an excavation, two ungual features considered synapomorphic for the clade (Novas and Bandyopadhyay 2001, Novas *et al.* 2004). Although strongly variable in shape, the manual unguals of *Noasaurus* and other noasaurids (i.e. noasaurines and elaphrosaurines), such as *Limusaurus*, *Berthasaura*, and *Vespersaurus*, appear to have in common a distal portion with a convex ventral margin (Fig. 20A–D) [see Stiegler (2019: fig. 2.62D and 2.63Q) for juvenile and adult *Limusaurus*, respectively]. This ventrodistal surface is indeed flat in non-abelisauroid theropods (Fig. 20F, G) and possibly biconvex in abelisaurids if the distalmost triangular element in *Carnotaurus* digit III (Fig. 20H; Ruiz *et al.* 2011: fig. 1) is revealed to be a manual ungual.

Despite these morphological similarities, the manual unguals of *Noasaurus* are particularly apomorphic in being strongly ventrally curved (forming a ventral arch of about 90°; Fig. 20A) and having a transversely compressed blade that ends in a very acute tip (see: Agnolín and Chiarelli 2010), several features reminiscent to those of other theropod dinosaurs such as *Baryonyx* (Fig. 20L) and *Allosaurus* (Fig. 20E; Madsen 1976, Charig and Milner 1997). The manual unguals of *Noasaurus* particularly differ from those of *Limusaurus*, *Masiakasaurus*, *Berthasaura*, and *Vespersaurus* in which the ungual is dorsoventrally low, transversely thick, and poorly curved (Fig. 20B–D). Additionally, the ventral excavation replacing the flexor tubercle is particularly deep and subtriangular in contour and anteriorly delimited by two ridges forming a 'V' in *Noasaurus* (Fig. 12E). This morphology in unknown in other abelisauroids, in which the ventral excavation is devoid of delimiting ridges and notably shallower and wider (e.g. Novas and Bandyopadhyay 2001, Novas *et al.* 2004, 2005). The manual ungual of *Noasaurus* also bears a ridge along its ventral surface (Fig. 12C), a feature vaguely reminiscent to the sharp ventral edge formed by the marked asymmetry of manual unguals I in some megaraptorid tetanurans, such as *Megaraptor* (Novas 1998, Novas *et al.* 2016). Unlike megaraptorids, the ridge is much shorter and extends from the anterior end of the flexor fossa up to the tip of the ungual blade in *Noasaurus*. Because they are distantly related, we consider the presence of this feature in *Noasaurus* and megaraptorids as convergent. In contrast, the ventral margin of the claw lacks any sign of longitudinal ridge in other ceratosaurs, such as the noasaurid *Vespersaurus* (Langer *et al.* 2019).

The manual unguals of *Noasaurus* show a very deep and C-shaped articular surface for the preceding phalanx when

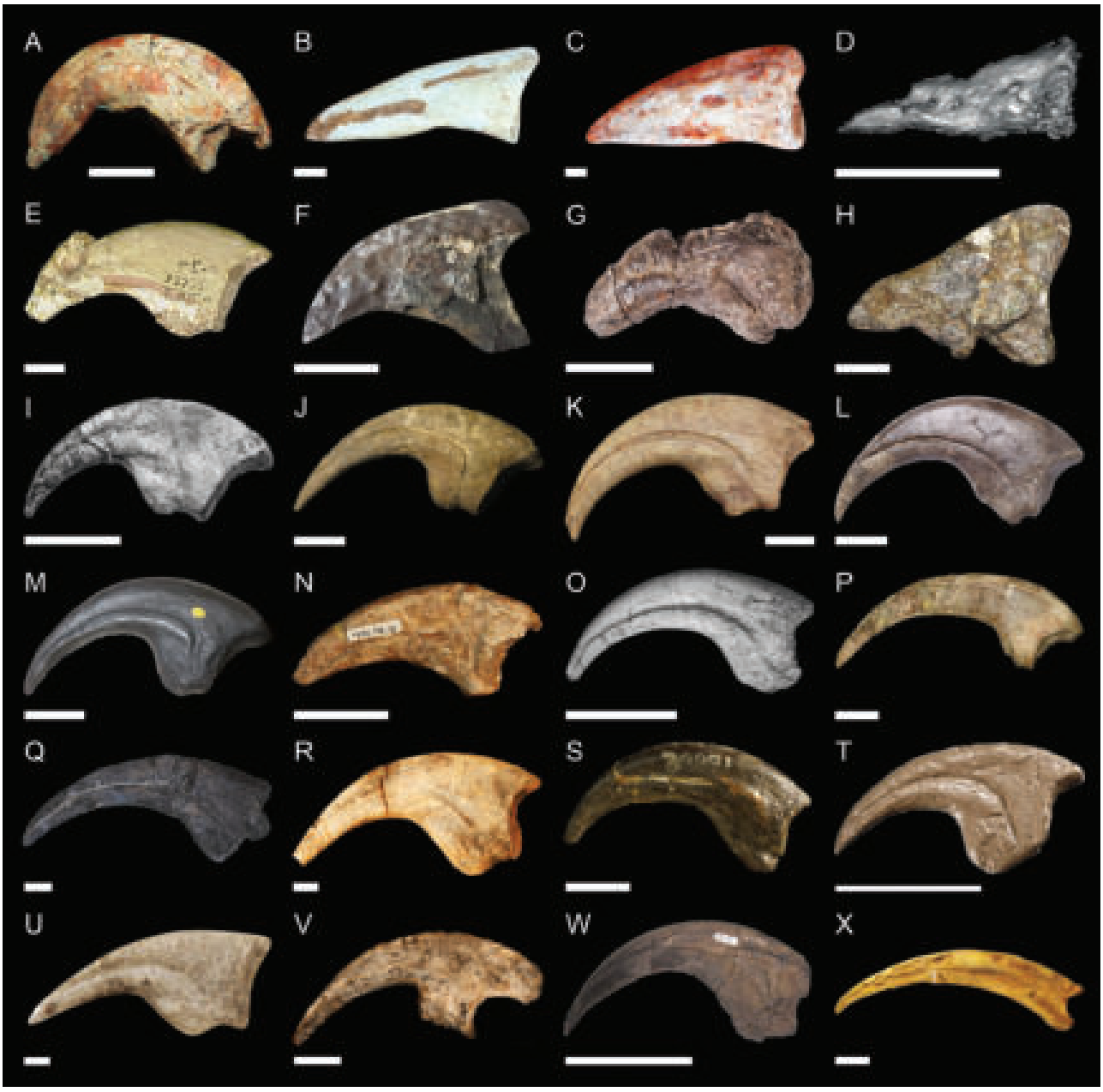

Figure 20. Manual ungual diversity in non-paravian theropods. Manual unguals in side view of: A, *Noasaurus leali* (digit I?; PVL 4061); B, *Berthasaura leopoldinae* (digit unknown; MN 7821-V; courtesy of Geovane A. de Souza); C, *Vespersaurus paranaensis* (digit II?, reversed; MPCO.V 0006j); D, *Limusaurus inextricabilis* (digit I of juvenile; IVPP V15301; from Stiegler 2019: fig. 2.62D); E, *Dilophosaurus wetherilli* (digit I, reversed; UCMP 37302; courtesy of Philip Currie); F, *Ceratosaurus nasicornis* (reversed; digit unknown; MWC 1; courtesy of Julia B. McHugh); G, *Eoabelisaurus mefi* (digit I; MPEF PV 3990; from Pol and Rauhut 2012); H, *Carnotaurus sastrei* (digit III?; MACN CH 894); I, *Afrovenator abakensis* (digit I; MNN UBA1; courtesy of Paul Sereno); J, claw I? referred to *Torvosaurus tanneri* by Galton and Jensen (1979) and possibly belonging to *Allosaurus* sp. (digit I?; BYU-VP 17697); K, *Suchomimus tenerensis* (digit I; reversed; MNN GDF 500; courtesy of Serjoscha Evers); L, *Baryonyx walkeri* (digit I; NHMUK R9951); M, *Allosaurus fragilis* (digit I; NHMUK R10868, cast); N, *Mapusaurus roseae* (digit unknown; MCF-PVPH-108.14); O, *Chilantaisaurus tashuikouensis* (digit I; IVPP V.2884.2; from Benson and Xing 2008); P, *Megaraptor namunhuaiquii* (digit I; MCF PVPF 79); Q, *Tanycolagreus topwilsoni* (digit I; TPII 2000-09-29; courtesy of Mark Loewen); R, *Eotyrannus lengi* (digit I?; IWCMS 1997.550; courtesy of Roger Benson); S, *Dryptosaurus aquilunguis* (digit I?, reversed; ANSP 9995; courtesy of Roger Benson); T, *Tyrannosaurus rex* (digit I; FMNH PR 2081; from Longrich and Saitta 2024); U, *Compsognathus longipes* (digit I, reversed; BSPG AS I 563; courtesy of Oliver Rauhut); V, *Haplocheirus sollers* (digit I; IVPP V14988; courtesy of Jonah Choiniere); W, *Nothronychus mckinleyi* (digit I; UMNH VP 16420.98; from Hedrick *et al.* 2015); X, *Therizinosaurus cheloniformis* (digit III, reversed; SMA coll., cast of PIN 551–483). Scale bars equal 10 cm (O, W, X), 5 cm (F, J–N, P, S, T), 1 cm (A, E, G–I, Q, R, V), and 1 mm (B–D, U).

viewed from the side (Figs 13A, 14A). This contrasts with the condition seen in other ceratosaurs (e.g. *Vespersaurus*, *Limusaurus*, and *Berthasaura*) in which the proximal end is poorly excavated and results in an open bracket-shaped articular surface when viewed from the side (Fig. 20B–D, F–H). The relatively small and well-delimited articular surface exhibited by

Noasaurus suggests a restricted articulation with the preceding phalanx and, thus, the movement between both elements was probably severely restricted. This contradicts the original interpretation by Bonaparte and Powell (1980) who regarded the claw as having a very wide angle of movement. In sum, as indicated by previous workers, the manual ungual of *Noasaurus* clearly departs from that of other ceratosaur theropods.

The second metatarsal of *Noasaurus*, the only preserved hindlimb element in this taxon, is similar to that of other noasaurid taxa in having slender proportions (Fig. 19F, N, V) and a lateromedially compressed shaft leading to a nearly laminar cross-section. Because MtII is the only pedal element to be preserved, the overall proportions of the whole metatarsus of *Noasaurus* cannot be known. Among ceratosaurs, it is worth noting that noasaurids are characterized by gracile metatarsi whose central element MtIII is long and slender, whereas MtII and IV are more lateromedially compressed (Bonaparte 1991, Langer *et al.* 2019) (NB—such a feature is also present in *Valdoraptor* and the Angeac material referred to Ornithomimosauria; Allain *et al.* 2014). The degree of compression of *Noasaurus*' MtII is similar to that seen in *Masiakasaurus* (Carrano *et al.*, 2002) and *Velocisaurus* (Baiano and Coria 2019; *contra* Brissón Egli *et al.* 2016). It, however, did not reach the extreme laminar condition seen in *Vespersaurus* (Langer *et al.* 2019), whereas the shaft of MtII in *Elaphrosaurus* and *Limusaurus* is not as reduced as in *Noasaurus* (Xu *et al.* 2009, Rauhut and Carrano 2016). The slender MtII of *Noasaurus* clearly departs from the stouter and less mediolaterally compressed bone of most abelisaurids (e.g. *Aucasaurus* and *Skorpiovenator*; Fig. 19.4) and *Ceratosaurus* (Novas 2009, Cerroni *et al.* 2022; Fig. 19.13). The posterior surface of the shaft in *Noasaurus* has faint striations, which may correspond to the insertion site of mm. gastrocnemii (Fig. 17D), as seen in the other noasaurid's MtII (e.g. *Vespersaurus*, *Masiakasaurus*, and *Elaphrosaurus*). However, noasaurids did not develop a marked and wrinkled step for the insertion of these muscles, which is present in the MtII of abelisaurids (Carrano 2007, Cerroni *et al.* 2022). The proximal end of MtII is ovoid and mediolaterally narrow in *Noasaurus* (Fig. 19G), a condition shared with *Masiakasaurus* (Fig. 19O), *Velocisaurus*, and *Vespersaurus*. Conversely, the proximal end of MtII is more expanded mediolaterally, with a strong D-shaped contour in *Elaphrosaurus* (Rauhut and Carrano 2016; Fig. 19W), whereas that of abelisaurids (e.g. *Majungasaurus*, *Aucasaurus*, and *Skorpiovenator*; Fig. 19.5) and *Ceratosaurus* (Fig. 19.14) are strongly developed as a rounded triangle. The distal end of MtII has a subquadrangular outline in distal view, with a deep intercondylar sulcus and a mediolaterally broad lateral condyle in *Noasaurus* (Fig. 19H). This condition is also present in *Masiakasaurus* (Carrano *et al.* 2002; Fig. 19P) but not in *Vespersaurus* in which the sulcus and lateral condyle are shallower and narrower, respectively (Langer *et al.* 2019). This subquadrangular morphology of the distal end of MtII departs from that of *Ceratosaurus* (Fig. 19.15) and abelisaurids (Fig. 19.6), in which it is subtriangular and almost V-shaped. However, the lateral condyle of *Noasaurus* and some noasaurines, such as *Masiakasaurus* (Fig. 19P), is bulky and similarly mediolaterally expanded as in abelisaurids (e.g. *Aucasaurus* and *Majungasaurus*; Fig. 19.6), whereas both condyles share similar size in *Ceratosaurus* (Fig. 19.15) and *Elaphrosaurus* (Fig. 19.10).

Taxonomic affinity of MACN-PV 622

MACN-PV 622 (Fig. 21) is a cervical vertebra recovered from the same fossil site from which the holotype of *Noasaurus* was found (Bonaparte *et al.* 1977, Bonaparte and Powell 1980). The specimen is generally well preserved other than the missing postzygapophyses, epipophyses, and the neural spine (Fig. 21) and a thorough description of this element is provided in the Supporting Information, S4. Frankfurt and Chiappe (1999) originally identified MACN-PV 622 as the fourth or fifth cervical vertebra of an oviraptorosaur. The vertebra was later reinterpreted as the third or fourth cervical of a noasaurid by Agnolín and Martinelli (2007), who noted that MACN-PV 622 shares some features with Abelisauroidea (e.g. broader than tall centrum in anterior view and deep spinoprezygapophyseal fossa), especially with noasaurids (e.g. *Masiakasaurus*), such as a wide neural canal, a U-shaped space between prezygapophyses in dorsal view (Fig. 21A), and a low and anteroposteriorly elongated neural arch. According to Agnolín and Martinelli (2007), some of the traits previously considered by Frankfurt and Chiappe (1999) as characteristic of oviraptorosaurs, such as the presence of 'peduncular foramina' [i.e. centroprezygapophyseal fossae, *sensu* Wilson *et al.* (2011)] and the U-shaped space between prezygapophyses, are also present in *Elaphrosaurus* and several noasaurids. Agnolín and Martinelli (2007) concluded that the specimen MACN-PV 622 may belong to the anteriormost cervical vertebra of *Noasaurus leali* based on the close association with the holotype, the presence of noasaurid features, and a similar size with the cervical elements of the *Noasaurus* holotype. Novas (2009) later questioned the assignment of this element to the holotype of *Noasaurus* based on the strong morphological differences between the neural arches of MACN-PV 622 and *Noasaurus*' vertebra, leading him to assign MACN-PV 622 to an indeterminate Abelisauroidea. Brum *et al.* (2018) more recently referred MACN-622 to a noasaurid but noted that the specimen shared some traits with *Elaphrosaurus*, including a reduced pattern of laminae in the neural arch, a centroprezygapophyseal fossa (cprf) restricted to the neural arch, and a poorly developed epipophyseal–prezygapophyseal lamina (eprl). The presence of an epipophyseal–prezygapophyseal lamina, however, cannot be determined given that the only visible structures observable in MACN-PV 622 probably correspond to the prezygodiapophyseal lamina (prdl) and part of the spinoprezygapophyseal lamina (sprl). Brum *et al.* (2018) further observed that a distinctive characteristic of MACN-PV 622 is its U-shaped spinoprezygapophyseal fossa in dorsal view (Fig. 21A), which contrasts with the V-shaped fossa of other abelisauroids (e.g. *Masiakasaurus*, *Majungasaurus*, and *Dahalokely*). This difference is also reflected in the isolated neural arch of the holotype of *Noasaurus*, in which the spinoprezygapophyseal fossa is V-shaped.

Another feature that potentially links MACN-PV 622 to noasaurids is the dorsoventrally low centrum in anterior view (Fig. 21C; also noted by: Agnolín and Martinelli 2007). Some noasaurids have anterior cervical vertebrae with low centra of variable shapes, such as the reniform centrum of *Vespersaurus* (Langer *et al.* 2019: fig. 4f) or the subrectangular centra of *Masiakasaurus* (Carrano *et al.* 2011: 13) and NMV P252004 (Poropat *et al.* 2020). Other features supporting MACN-PV 622 as the anterior cervical vertebra of Noasauridae include the

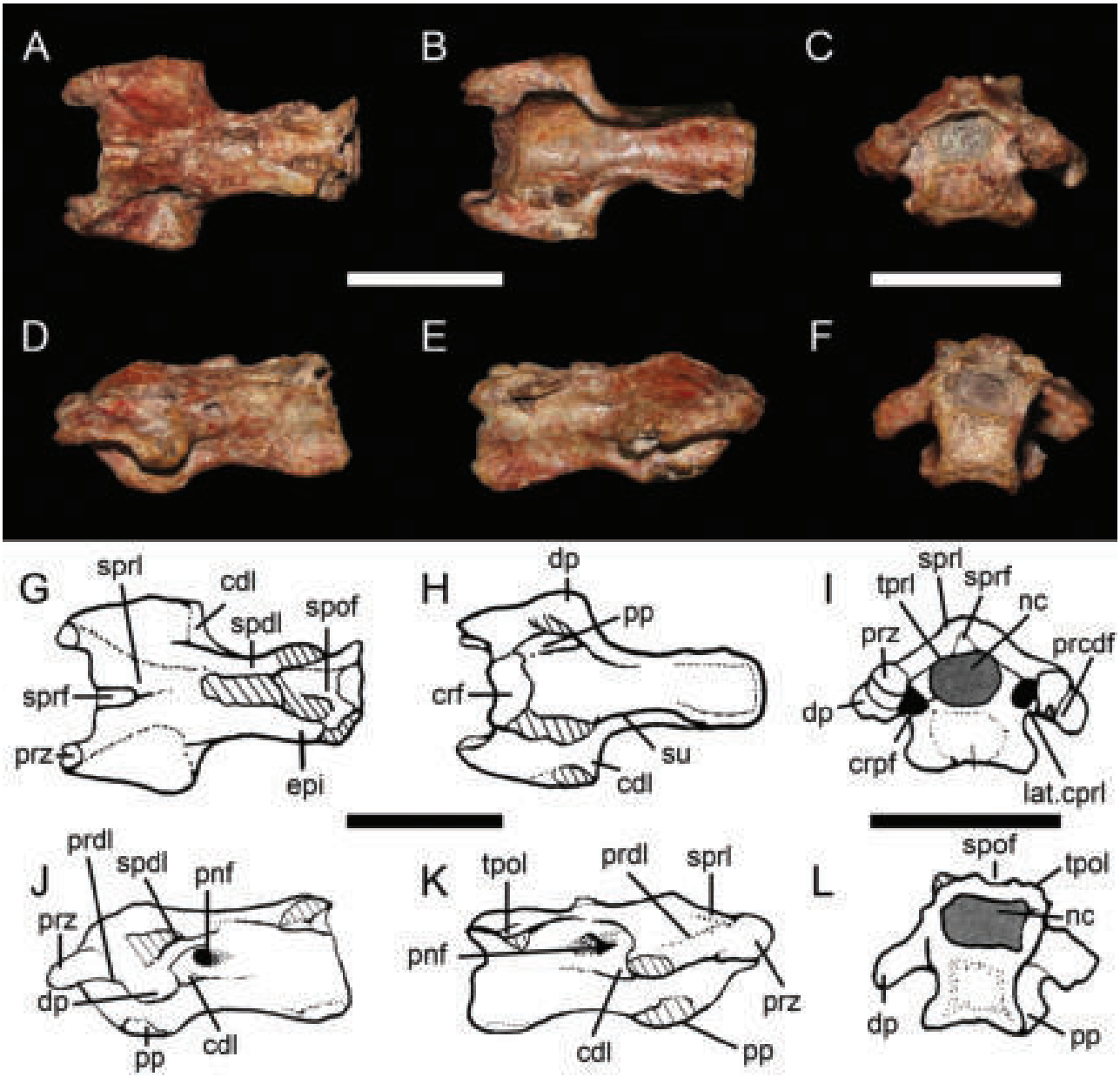

Figure 21. Anterior cervical vertebra (MACN PV 622) possibly belonging to a noasaurid or a pterosaur. A–F, cervical vertebra; G–L, line drawings of the specimen, in dorsal (A, G), ventral (B, H) anterior (C, I), left lateral (D, J), right lateral (E, K), and posterior (F, L) views. Line drawings in G–L from Frankfurt and Chiappe (1999). Abbreviations: cdl, centrodiapophyseal lamina; cprf, centroprezygapophyseal fossa; dp, diapophysis; lat. cprl, lateral centroprezygapophyseal lamina; nc, neural canal; pnf, pneumatic foramen; pp, parapophysis; prcdf, prezygapophyseal centrodiapophyseal fossa; prdl, prezygodiapophyseal lamina; prz, prezygapophysis; spdl, spinodiapophyseal lamina; sprf, spinoprezygapophyseal fossa; sprl, spinoprezygapophyseal lamina; spof, spinopostzygapophyseal fossa; su, sulcus; tpol, intrapostzygapophyseal lamina; tprl, intraprezygapophyseal lamina. Scale bars (on the right for A, B, D, E; on the left for C, F) equal 2 cm.

strong inclination of the anterior articular surface of the centrum and its offset position relative to the posterior one, a short gap separating the parapophysis from the diapophyses, and the presence of centroprezygapophyseal fossae [known as 'peduncular foramina' of Frankfurt and Chiappe (1999) and, Agnolín and Martinelli (2007)] lateral to the neural canal. Further traits diagnosing MACN-PV 622 as an anterior cervical vertebra of a noasaurid include the large size of the neural canal in anterior view (Fig. 21C), the lateral placement of the prezygapophyses from the neural canal, and lateroventrally sloping neural arches in anterior view. This latter feature is present in the postaxial anterior cervical of *Vespersaurus* (Langer *et al.* 2019: fig. 4f) and the cervical vertebrae of two indeterminate noasaurids (Poropat *et al.* 2020, Smyth *et al.* 2020). Notably, the size of the neural canal of MACN-PV 622 is nearly as large as the articular surface of the centrum in anterior view, a feature resembling that described by Carrano *et al.* (2011: 13) in the third cervical of *Masiakasaurus*, suggesting that MACN-PV 622 may represent a third cervical element. Interestingly, the anterior cervical vertebrae of indeterminate noasaurids from Brazil (Brum *et al.* 2018) and Morocco

(Smyth *et al.* 2020) similarly show large neural canals compared to the size of their centra.

Even if a drastic morphological change between the neural arch of MACN-PV 622 and that of *Noasaurus* is considered, some features of the former appear unusual among noasaurids, namely: a posteriorly constricted neural arch in dorsal view (Fig. 21A; differing from the subquadrangular vertebra of *Noasaurus*), a prezygapophysis lateral to the neural canal, a large pneumatic foramen on the lateral surface of the neural arch, a lateroventrally sloping neural arch in anterior view, as well as a large centroprezygapophyseal fossa lateroventral to the neural canal. These features are similar to those observed in the cervical vertebrae of several pterosaurs from the Cretaceous of South America (Veldmeijer 2006, Kellner *et al.* 2019, Ortiz David *et al.* 2022, Buchmann and Rodrigues 2024) and may indicate pterosaurian affinities for MACN-PV 622. We, however, note that some of them might be convergent with noasaurids. For instance, if a laterally positioned prezygapophysis is an unusual trait of MACN-PV 622, this may be explained by the anterior position of the cervical, whereas the prezygapophysis is positioned dorsal to the neural canal in more posterior cervical vertebrae (as in the isolated neural arch of *Noasaurus*). A laterally placed prezygapophysis is also found in a noasaurid cervical from Australia (Poropat *et al.* 2020) and a prezygapophysis slightly laterodorsal to the neural canal is seen in a postaxial cervical vertebra of *Vespersaurus* (Langer *et al.* 2019: fig. 4F). The pneumatic foramen of MACN-PV 622 may also be homologous to the deep and ventrally positioned pneumatic excavation present in the neural arch of the holotype (Fig. 7F, L). Noasaurids with similar pneumatic foramina on the cervical neural arch include *Vespersaurus* (MPCO.V0035; Langer *et al.* 2019) and *Berthasaura* (de Souza *et al.* 2021: fig. 5c), which both show large pneumatic excavations on the lateral surface of the neural arch, ventral to the transverse process. We additionally note that the anterior cervical vertebrae of some indeterminate noasaurids show a lateroventrally sloping neural arch (Poropat *et al.* 2020, Smyth *et al.* 2020) similar to that of a postaxial anterior vertebra of *Vespersaurus* (Langer *et al.* 2019: fig. 4f). The cervical vertebrae of pterosaurs further display several anatomical features absent in MACN-PV 622, such as the presence of hypapophysis, preexapophysis and postexapophysis, a strongly dorsoventrally depressed centra in anterior view, a particularly small neural canal relative to the size of the centrum, as well as a complex pattern of pneumatization (Buchmann and Rodrigues 2019, 2024, Buchmann *et al.* 2019, Kellner *et al.* 2019). The cervical vertebra of some pterosaurs (e.g. azdarchoids) are characterized by a dorsally positioned pneumatic excavations close to the neural canal (Buchmann *et al.* 2019, Kellner *et al.* 2019), a feature clearly absent in MACN-PV 622.

In conclusion, we remain uncertain whether MACN-PV 622 belongs to a noasaurid theropod or a pterosaur, and further observations and comparisons with new and more complete noasaurid and pterosaur material are, therefore, necessary to clarify the taxonomic affinities of MACN-PV 622. A noasaurid affinity for this specimen, nonetheless, appears more likely based on our current knowledge of noasaurid and pterosaur cervical anatomy.

Palaeoecology of *Noasaurus*

The ecology of *Noasaurus* was briefly discussed by Bonaparte and Powell (1980: 25) who interpreted this new taxon as 'a running and lightly built animal' and 'a carnivore able to prey upon rather small forms, i.e. young sauropods and birds' based on its dental and pedal morphology. Bonaparte (1996a: 90) further commented that a few characters of the maxilla and phalanges (ungual and pre-ungual) 'strongly suggest *Noasaurus* as a predator which used the hindlimbs to catch and wound the prey'. If the gracile and swift nature suggested by Bonaparte and Powell (1980) for *Noasaurus* was later confirmed by the discovery of more complete noasaurids, the misidentification of the peculiar claw as a pedal ungual misled them about its feeding strategy. The strongly curved ungual was, indeed, compared to the enlarged raptorial pedal ungual II of dromaeosaurids, such as *Deinonychus*, so that *Noasaurus* was reconstructed with such a raptorial claw at the foot in several popular-science books (Lambert 1990, 1993, Novas *et al.* 1992, Orbis Publishing 1994; Fig. 22A–C). This misidentification led Bonaparte and Powell (1980), Paul (1988), and Bonaparte (1996a) to imagine *Noasaurus* and dromaeosaurids with the same feeding strategy, i.e. hunting medium-sized prey items with the large sickle pedal claw, with Paul (1988) further hypothesizing the fact that noasaurines were the South-American counterparts of the sickle-clawed dromaeosaurids from the northern Hemisphere. The re-identification of the unguals as manual claws (Agnolín *et al.* 2004, Carrano *et al.* 2004, Carrano and Sampson 2008, Agnolín and Chiarelli 2010), combined with a much better understanding of the dental anatomy of closely related species, enable the proposal of a different feeding ecology for *Noasaurus*.

The two preserved elements of the skeleton providing indirect information on the diet of *Noasaurus*, the maxillary dentition and the manual ungual, both show a derived morphology that may be indicative of a specialized diet. The ziphodont maxillary crowns are particularly small (CH < 10 mm) and poorly compressed labiolingually (CBR ~0.6 in average) compared to those of most other ziphodont theropods (C.H. pers. obs.). In addition, the mesial denticles of the crowns are minute and significantly smaller than the distal denticles (DSDI ~1.3), whereas the latter are particularly large relative to the crown, with less than 30 denticles along the whole distal carina. Ziphodont lateral crowns with denticulated carinae clearly support a carnivorous feeding ecology (D'Amore 2009, D'Amore and Blumenschine 2009, Hendrickx *et al.* 2019) and the small size of the crowns suggests that *Noasaurus* most likely fed on small prey items. Fowler *et al.* (2011) argued that the size reduction of denticles from the mesial carina relative to the distal carina in the dromaeosaurid *Deinonychus* would enhance the piercing function of the crowns. Hendrickx *et al.* (2019) also noted that a discrepancy in size between mesial and distal denticles is commonly found among small-sized (<5 m in length) carnivorous theropods (e.g. noasaurids, basal tyrannosauroids, eudromaeosaurs, juvenile abelisaurids, and tyrannosaurids), possibly reflecting similar functional factors among small-bodied theropods with relatively close feeding strategies. Results of the cladistic analysis performed on the dentition-based datamatrix after pruning 12 wildcard taxa and keeping three (*Caudipteryx*, *Compsognathus*, and *Scipionyx*) suggest that the maxillary dentition of *Noasaurus*

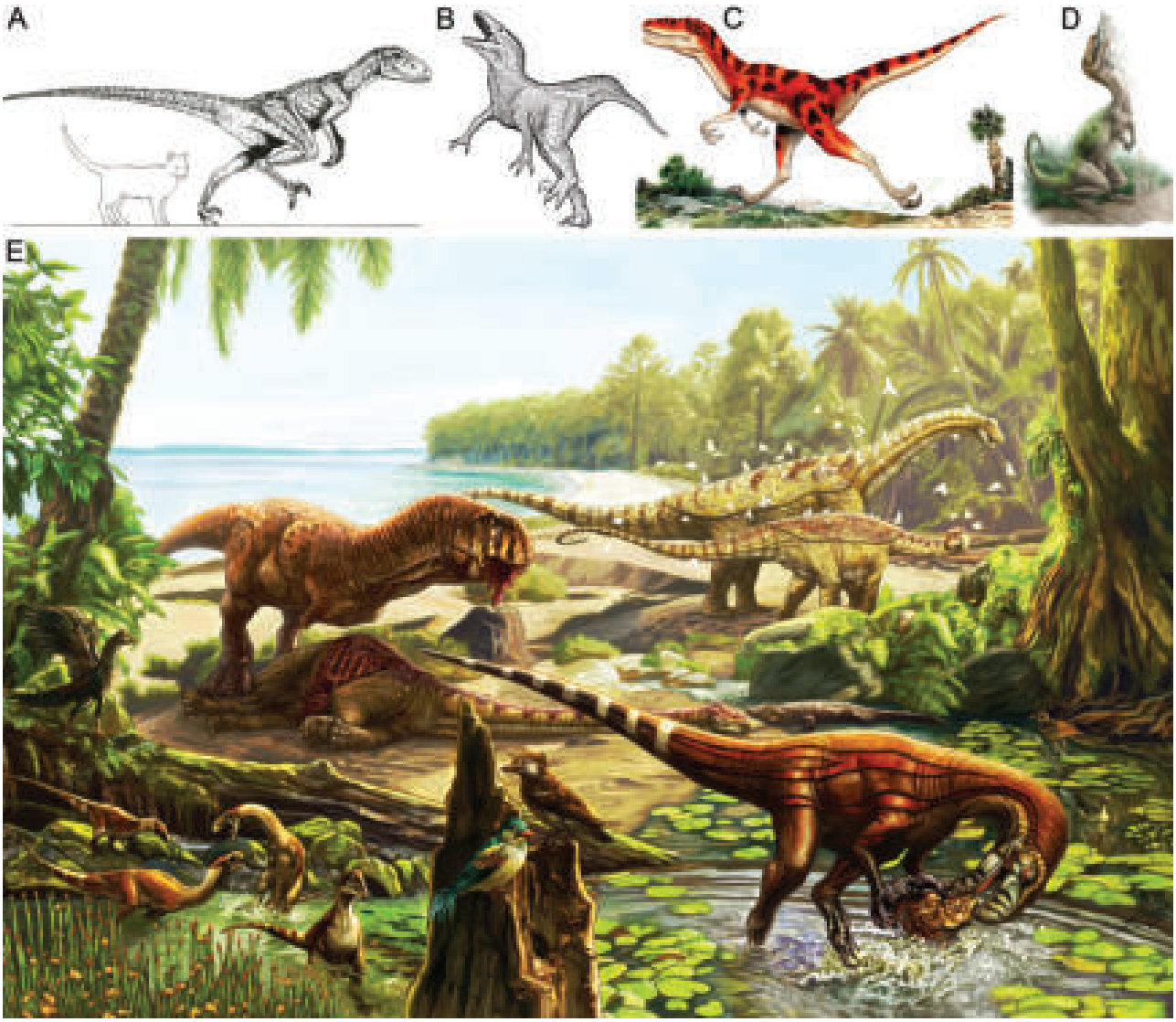

Figure 22. Artistic reconstructions of *Noasaurus* through time. Illustration in: A, Lambert (1990; unknown artist); B, Novas *et al.* (1992; artwork from Sebastián Cerruti); C, Orbis Publishing Ltd. (1994; artwork from Philip Hood); and D, Molina-Pérez and Larramendi (2019; artwork from Sante Mazzei; used with permission); E, a *Noasaurus* family in the coastal environment of what is now north-western Argentina around 70 Mya. Faunal assemblage (from left to right): the enantiornithes *Enantiornis* opening its wings, four juvenile *Noasaurus* playing in the stream of a river, an indeterminate abelisaurid theropod feeding on a carcass of the armoured titanosaurid sauropod *Saltasaurus*, the enantiornithes *Soroavisaurus* and *Martinavis* at the top of a dead trunk, an adult *Noasaurus* catching a fish with its strongly curved manual claws and procumbent mesial dentition, a *Saltasaurus* with its offspring surrounded by a flock of enantiornithes, as well as an indeterminate crocodylomorph and the enantiornithes *Lectavis* (top) and *Yungavolucris* (bottom) lurking in the river. Artwork from Bruno Salica.

is most similar to that of microraptorines, as well as basally branching theropods (*Dracoraptor* and *Eodromaeus*) and coelurosaurs (*Bicentenaria*, compsognathids, *Ornitholestes*; Fig. 17A). Direct evidence of the diet reveals an opportunistic nature in these theropods, which fed on a large array of typically small prey items (Fig. 17A). Gut contents preserved in *Microraptor*, *Scipionyx*, and *Compsognathus* show that these small-bodied theropods were eating a large variety of small to large vertebrates, such as lizards, birds, fish, mammals, and pterosaurs (e.g. Peyer 2006, Dal Sasso and Maganuco 2011, O'Connor *et al.* 2011, 2019, Xing *et al.* 2013, Conrad 2018; Fig. 17A). Based on the maxillary dentition made of minute teeth and large denticles, *Noasaurus* is, therefore, interpreted as an opportunistic carnivore [both a predator and a scavenger, as illustrated by Jorge A. González in Apesteguía *et al.* (2022): 121] feeding on a large variety of small prey items.

The phylogenetic and anatomical proximity with the noasaurid *Masiakasaurus*, the closest relative of *Noasaurus* for which the dentition is well known, may also provide information on the possible feeding ecology of *Noasaurus*. Carrano *et al.* (2002) interpreted *Masiakasaurus* as a possible insectivore or piscivore, using its strongly procumbent mesial dentition, clearly adapted for prehension, to grasp small, whole prey items, whereas the more conservative ziphodont lateral dentition was used for holding, cutting, and/or slicing flesh. These authors, nevertheless, note that the dentitions of *Masiakasaurus* and spinosaurids, well known to have a specialized skull and dentition adapted to hunting elusive prey of relatively small size

in general and fish in particular (e.g. Charig and Milner 1997, Dal Sasso *et al.* 2005, Rayfield *et al.* 2007, Ibrahim *et al.* 2014, Hendrickx *et al.* 2016, Hone and Holtz 2021, Schade *et al.* 2023), do not resemble each other, adding that spinosaurids do not display the same procumbency seen in *Masiakasaurus* (Carrano *et al.* 2002). We agree with Carrano *et al.* (2002) that the dental and cranial morphology of *Masiakasaurus* strongly departs from that of spinosaurids in the presence of folidont (i.e. spatulate) mesialmost dentary teeth, a lateral dentition made of non-fluted ziphodont lateral crowns with large denticles, a short rostrum with no terminal rosette, sigmoid alveolar margin, and retracted nares, as well as a downturned symphyseal region of the dentary. Folidont teeth and a downturned anterior portion of the dentary are, in fact, features typically present in omnivorous or herbivorous theropods such as therizinosaurs (Zanno and Makovicky 2011). We, nonetheless, argue that *Masiakasaurus* and some, if not all, spinosaurids shared many derived dental features relevant to a piscivorous diet: (i) procumbent mesial dentary teeth (present in some *Spinosaurus* specimens like NHMUK R16421); (ii) a laterally expanded anterior portion of the dentary with enlarged mesial dentary teeth (all spinosaurids); (iii) mesial dentary teeth with fluted lingual surfaces and minute denticles (Baryonychinae); and (iv) lateral dentition of the dentary made of relatively labiomesially thick (CBR > 0.6) ridged crowns (all spinosaurids; Carrano *et al.* 2002; C.H. pers. obs.). In addition, the mesial maxillary teeth of spinosaurids and mesialmost dentary teeth of the *Spinosaurus* specimen NHMUK R16421 display the same level of procumbency seen in *Masiakasaurus*. Likewise, the morphology of the poorly compressed and slightly procumbent rdt6 of *Masiakasaurus* (UA 8680), with minute denticles and two lingual ridges, reveals that not all lateral teeth of *Masiakasaurus* had the labiolingually compressed ziphodont morphology. Although we agree that *Masiakasaurus* does not show the numerous cranial and dental adaptations to ichthyophagy of spinosaurids, the combination of dental features present in *Masiakasaurus* (as well as a new noasaurid specimen from the Maastrichtian Lameta Formation of India; Mohabey *et al.* 2024) would suggest that fish was at least part of its diet. If future discoveries, therefore, reveal that *Noasaurus* and *Masiakasaurus* had similar mesial dentition and dentary morphology, we argue that the diet of *Noasaurus* probably included fish at least partially, as represented by Molina-Pérez and Larramendi (2019) (Fig. 22D).

The morphology of the manual unguals of *Noasaurus* would, in fact, support this hypothesis. The manual ungual of *Noasaurus* is unusual in being proximodistally short, dorsoventrally tall, extremely curved, and having a thick and robust apex but no flexor tubercle (Fig. 20A). Our analysis on manual ungual elongation and curvature reveals that the manual claw of *Noasaurus* is almost comparable to that of the basally branching alvarezsaur and coelurosaur *Tugulusaurus* and *Bicentenaria*, respectively, the allosaurid *Allosaurus*, and the megalosaurid *Torvosaurus* (Fig. 20J) [NB—this claw was referred to *Torvosaurus tanneri* by Galton and Jensen (1979) while Allain *et al.* (2012) suggested that it might belong to a spinosaurid, whose presence in Northern America has never been confirmed; given its size, proportion, and overall morphology, this large claw may instead pertain to the first digit a particularly large *Allosaurus* individual], and relatively similar to that of the baryonychine *Baryonyx* (Fig. 20L), the megalosaurid *Afrovenator* (Fig. 20I), the basally branching alvarezsaur *Haplocheirus* (Fig. 20V), the unenlagiine *Buitreraptor*, and the troodontid *Xixiasaurus* (Fig. 17B). With tall crowns (>5 cm), large skulls, massive manual unguals, and particularly large body-size (body length > 6 m), the carnosaurs *Afrovenator*, *Allosaurus*, *Baryonyx*, and *Torvosaurus* were carnivores at the top of the food chain, a position that the much smaller *Noasaurus* did not occupy (NB—the role of apex predators in the southern Hemisphere was instead played by abelisaurids during the latest part of the Cretaceous; Hendrickx *et al.* 2015b). Nevertheless, and although direct evidence shows that *Allosaurus* was feeding on large-bodied herbivorous dinosaurs such as *Stegosaurus* and sauropods (e.g. Chure 2000, Carpenter *et al.* 2005, Hone and Rauhut 2010), we note that the presence of scales and other fish remains in the gastric region of *Baryonyx* and the megalosaurid *Poekilopleuron* reveal that spinosaurids and megalosaurids were at least partially piscivorous theropods (Eudes-Deslongchamps 1837, Charig and Milner 1986, 1997, Allain 2005). Unlike carnosaurs, *Bicentenaria*, *Buitreraptor*, *Xixiasaurus*, *Tugulusaurus*, and *Noasaurus* were mesopredators (*sensu* Therrien *et al.* 2023) with strongly curved manual claws, small to minute ziphodont crowns, and small body-length (<3 m), suggesting close-feeding ecologies. If the diet of the alvarezsaur *Tugulusaurus* and the indeterminate coelurosaur *Bicentenaria* was never discussed, the unenlagiine *Buitreraptor* was interpreted to be a (non-strictly) piscivorous theropod (Gianechini *et al.* 2011, Brum *et al.* 2021) or a generalist preying on other small elusive animals, such as arthropods, lizards, and mammals (Gianechini *et al.* 2020, Brum *et al.* 2021), whereas the basal alvarezsaur *Haplocheirus* was suggested to be a nocturnal carnivore feeding on small prey items based on its weak bite force, rapid jaw closure ability, and the size of its sclerotic ring (Choiniere *et al.* 2014b, 2021). Conversely, an omnivorous or herbivorous feeding ecology was suggested by Lü *et al.* (2010) for *Xixiasaurus* based on an heterodont dentition made of a majority of unserrated folidont teeth. We, nonetheless, argue that a non-carnivorous diet was highly unlikely in a heterodont theropod whose largest teeth had strongly recurved and pointy ziphodont crowns. All these theropods with short but strongly curved manual unguals are, therefore, seen by most authors as opportunistic mesopredators feeding on small vertebrates such as fish, a hypothesis consistent with that proposed for *Noasaurus*.

Interestingly, the manual unguals of *Noasaurus* and spinosaurids [especially those illustrated by Russell (1996: fig. 24a, b) and tentatively referred to *Spinosaurus* by Ibrahim *et al.* (2014)], share a reduced/absent flexor tubercle (Fig. 20A, K, L), whereas the latter remains particularly well-developed in megalosaurids, allosaurids, and coelurosaurs with strongly curved claws (e.g. *Bicentenaria*, *Haplocheirus*, *Tugulusaurus*, and *Buitreraptor*; Fig. 17C). A well-developed flexor tubercle provides a larger muscle attachment surface and increased force efficiency in manual claws that would be utilized for producing large forces compared to those with a reduced (or fully absent) flexor tubercles (Chinzorig *et al.* 2018). The hypertrophied and strongly curved manual claw I characteristic of *Baryonyx* was interpreted by Charig and Milner (1986, 1997) as a tool to gaff and impale fishes [NB—Kitchener (1987) instead suggested

that it was used to open carcasses, an hypothesis contested by Reid (1987) and Charig and Milner (1997)]. Likewise, Ibrahim *et al.* (2014) argued that the elongated manual unguals probably referable to *Spinosaurus*, which show a particularly reduced flexor tubercle, were possibly used in gaffing and slicing aquatic prey. Given the poorly developed flexor tubercle in spinosaurids, this suggests that the whole arm instead of the ungual was used during the fast-moving gaffing motion, a hypothesis in accordance with the strong development of the pectoral girdle and robustness of the humerus in *Baryonyx*, interpreted by Charig and Milner (1997) as facilitating the movement of the forelimb as a whole. If the humerus of noasaurines is longer, much slender, and far less robust than that of spinosaurids, Carrano *et al.* (2011) argued that 'the morphology of the humeral head and the expanded muscles origination areas on the ventral pectoral girdle [of *Masiakasaurus*] suggest that forelimb mobility was significant and perhaps enhanced over the primitive theropod condition'. Although the manual ungual of *Noasaurus* has a much broader and less acute tip than that of spinosaurids, we hypothesize that it was used in the same functional way as in baryonychines, i.e. to gaff and impale fish using a rapid movement of the whole forelimb, a feeding behaviour in accordance with the gracile and swift nature of noasaurines with elongated neck, procumbent dentition, and fluted mesial teeth, which would facilitate the capture of fast-moving and slippery preys like fish (Fig. 22E). This hypothesis, however, requires further investigations using FEA applied to 3D models of the manual ungual of *Noasaurus* and a large sample of amniotes with different feeding ecologies [as recently done by Qin *et al.* (2023) for therizinosaurs and alvarezsaurs], as well as isotopic analyses on tooth enamel using oxygen isotope ratios (δ18Op) from biogenic apatite in a wide range of noasaurid remains [as done by Amiot *et al.* (2010) for spinosaurids].

Implications for the phylogeny, size evolution, and palaeogeographical history of noasaurids

Ceratosauria is a poorly resolved clade made of many unstable taxa in the phylogenetic analyses performed on the three independent datamatrices on theropod relationships (Supporting Information, S3). Excluding these wildcard taxa from the analyses yielded better-resolved topologies in which Noasauridae is either recovered as the sister-clade of Abelisauridae among Abelisauroidea (Figs 15, 16A), or Etrigansauria (Fig. 16B). Two distinct topologies were, nevertheless, recovered for Noasauridae. In the first, obtained with Baiano *et al.*'s (2023) and Rauhut and Pol's (2021) datasets, Noasauridae correspond to a worldwide radiation of Jurassic and Cretaceous ceratosaurs encompassing noasaurines, elaphrosaurines, and a few other taxa (Fig. 16), a topology recently recovered by Pol *et al.* (2024) using both parsimony and Bayesian analyses. Noasauridae are diagnosed by two synapomorphies related to the mid-cervical vertebrae in Baiano *et al.*'s (2023) dataset and four derived characters on the pneumatization in the cervical vertebra and the length of the cervical and dorsal centra in Rauhut and Pol's (2021) dataset (Supporting Information, S3.2.5, S3.3.5). The clade Noasaurinae recovered with the latter dataset is diagnosed by six synapomorphies related to the maxilla, cervical, metatarsal II, and pedal ungual morphology in some MPTs (Supporting Information, S3.3.5).

Conversely, Noasauridae form a more inclusive clade of strictly Late Cretaceous Gondwanan taxa in the second topology recovered by Agnolín *et al.*'s (2022) updated datamatrix (Fig. 15A). The noasaurid clade is here diagnosed by two synapomorphies related to the width of MtII when all trees are considered, and seven on the maxilla, postaxial cervical vertebra, cervical ribs, and metatarsals III and IV when some MPTs are considered (see Supporting Information, S3.1.5). In this configuration, Elaphrosaurinae (diagnosed by eight synapomorphies found in all MPTs; see Supporting Information, S3.1.5) are placed at the base of Ceratosauria, as the sister-clade of Neoceratosauria, whereas the taxa recovered as noasaurids in the first topology are either found at the base of a clade made of non-ceratosaurid neoceratosaurs (*Ligabueino*) or within the sister-clade of Abelisauroidea, here coined Berthasauridae clade nov. [see definition in Table 1; NB—*Berthasaura* was chosen as the name-bearing taxon of this new clade over the older genus names *Austrocheirus* and *Afromimus*, both retrieved among this clade, for stability reason, i.e. *Berthasaura* is known from an almost complete skeleton, while *Austrocheirus* and *Afromimus* are highly incomplete and considered as an indeterminate theropod and an ornithomimosaur by Rauhut (2012) and Sereno (2017), respectively; Fig. 15A]. Two synapomorphies related to the fibular crest and the astragalar facet of the tibia and found only in some MPTs diagnose Berthasauridae (see Supporting Information, S3.1.5), which is therefore a poorly supported clade. We note that *Noasaurus* is closely related to *Velocisaurus* from the Santonian of Patagonia, *Masiakasaurus* from the Maastrichtian of Madagascar, and *Laevisuchus* from the Maastrichtian of India in all three datasets (Figs 15A, 16), supporting a Gondwanan radiation of 'noasaurs' [i.e. Noasaurinae in the topology obtained with Rauhut and Pol's (2021) dataset and Noasauridae in the second using Agnolín *et al.*'s (2022) datamatrix] during the Late Cretaceous. This radiation is only comprised of small-bodied theropods (<2.5m; Figs 15A, 16B) and a miniaturization probably occurred during the evolution of this clade in the Early Cretaceous (Fig. 16B). Noasaurinae indeed appear to evolve from medium-sized ceratosaurs in the topology obtained with Rauhut and Pol's (2021) dataset, while non-noasaurine noasaurids include several taxa of more than 2.5 m, such as MNN TIG6 and *Elaphrosaurus* (Fig. 16). With more than 6 m in length, the possible elaphrosaurine *Deltadromeus agilis* from the Cenomanian Kem Kem Group of Morocco (Sereno *et al.* 1996, Seebacher 2001, Ibrahim *et al.* 2020), as well as an indeterminate theropod from the Cenomanian Bahariya oasis of Egypt referred to *Bahariasaurus ingens* by Stromer (1934) and possibly related to *Deltadromeus* [Ibrahim *et al.* (2020) but see Kellermann (2021) for a different opinion], would attest the presence of particularly large-bodied noasaurids (and the largest for this clade) in Northern Africa during the middle part of the Cretaceous if this classification is followed. Conversely, a diminution in size during the evolution of noasaurids does not seem to have occurred when Noasauridae represent a Gondwanan radiation of ceratosaurs restricted to the Late Cretaceous [as obtained with Agnolín *et al.*'s (2022) dataset; Fig. 15A]. In this scenario, noasaurids instead appear to have evolved from small-bodied ceratosaurs similar to *Ligabueino* and *Berthasaura* from the Early Cretaceous of South America and of less than 1.5 m in body length (Fig. 15A).

The palaeogeographic history of Noasauridae also changes dramatically with the placement of Elaphrosaurinae inside or outside this clade. A South American origin for Noasauridae during the Early Cretaceous seems probable when the clade is comprised of Late Cretaceous forms from the Southern Hemisphere (Fig. 15B). Conversely, Noasauridae could have originated from any continent of the Northern or Southern hemispheres during the Early and Middle Jurassic when elaphrosaurines are part of this clade (Fig. 16). Indeed, even though a South American origin appears to be the most plausible scenario based on the provenance of the earliest branching abelisaurids/etrigansaurs (all from Argentina or Brazil), the Pangea still existed in the Early and Middle Jurassic, which would have made dispersal from any part of the world much easier than during the Cretaceous. Conversely, noasaurids crossing Africa from South America and migrating to Madagascar and India during the Late Cretaceous appears to be the best supported scenario to explain the presence of *Masiakasaurus* and *Laevisuchus* in these countries during the Maastrichtian when Noasauridae are made of strictly Late Cretaceous Gondwanan forms (Fig. 15B). The inclusion of the Jurassic taxa *Elaphrosaurus* and MNN TIG6 among Noasauridae instead suggests that members of this clade may have originated in Africa and moved to South America, Madagascar, and India during the Cretaceous (Fig. 16). The palaeogeographic history of elaphrosaurines is also highly dependent of the general topologies of the ceratosaur phylogeny, with this clade probably originating in Africa and moving to Asia during the Middle and Late Jurassic when recovered as basal ceratosaurs and comprised of MNN TIG6 from the Middle Jurassic of Niger (Fig. 15B). Instead, Elaphrosaurinae may have originated in Asia and migrated to Africa [and South America if *Berthasaura* and *Vespersaurus* are also classified among this clade, as recovered with Rauhut and Pol's (2021) dataset; Fig. 16B] during the Late Jurassic as part of the noasaurid radiation. As noted by previous authors (e.g. Carrano *et al.* 2002, Rauhut and Carrano 2016), the size evolution and biogeographic history of noasaurids remain highly speculative and may change dramatically with the discovery of new taxa and a much better understanding of the ceratosaur phylogeny in the future.

CONCLUSION

Although known from a particularly incomplete skeleton, *Noasaurus leali* plays a pivotal role in our understanding of the anatomy, classification, palaeoecology, and biogeography of ceratosaur theropods. The discovery of this small theropod in Maastrichtian deposits of Southern Salta in 1975, the first and currently most complete non-avian theropod from northern Argentina, not only revealed the existence of a peculiar carnivorous dinosaur with specialized hand claws and, more importantly, a representative of a new clade of small and gracile ceratosaurs. The detailed description of this eponymous taxon has allowed its diagnosis to be fully revised. *Noasaurus leali* can be diagnosed by many apomorphies, such as a maxilla with a concave alveolar surface and a dorsal ridge crossing the maxillary fossa, a strongly arched quadrate with a short anterior margin of the pterygoid flange, a strongly curved manual ungual with a deep flexor fossa delimited by two ridges forming a V, as well as a cervical neural arch with anterior epipophyseal prongs. The tiny and relatively thick maxillary crowns with minute mesial denticles and comparatively large distal denticles, associated with the strongly curved manual unguals with a deep flexor fossa and no flexor tubercle, suggest that this agile theropod was an opportunist carnivore feeding on small prey items and a probable piscivore using its peculiar hand claws to catch fish. Results of the phylogenetic analyses reveal that *Noasaurus* belongs to a particularly inclusive clade of small-bodied (<2.5m) ceratosaurs with specialized morphologies that radiated in the Southern Hemisphere during the Late Cretaceous, and reached Madagascar and India by the end of the Cretaceous. This contribution finally invites the publication of exhaustive and well-illustrated osteological descriptions of dinosaurs lacking such a thorough treatment, especially those used as the type genus of important nominal clades such as Noasauridae.

SUPPLEMENTARY DATA

Supplementary data are available at *Zoological Journal of the Linnean Society* online.

ACKNOWLEDGEMENTS

First and foremost, we are honoured and incredibly indebted to Argentinian artist Bruno Salica, who kindly offered to provide an accurate reconstruction of *Noasaurus* in its environment. We are grateful to Oliver Rauhut (BSPG), Matthew Carrano (Smithsonian), Geovane A. de Souza (Federal University of Rio de Janeiro), Jonah Choiniere (Uni. Witwatersrand), Matthew C. Lamanna (Carnegie Museum), Philip J. Currie (Uni. of Alberta), Mark Loewen (Uni. of Utah), Julia B. McHugh (Museums of Western Colorado), Pablo Ortiz (PVL), Josef Stiegler (Stony Brook Uni.), Serjoscha Evers (Uni. of Fribourg), and Paul Sereno (Uni. of Chicago) for accepting to use their photos in the figures. Special thanks go to Juan I. Canale, Martín Ezcurra, Agustín Martinelli, Rodolfo Coria, and to the late Jorge O. Calvo (1961–2023), especially, for allowing access to specimens under their care, and to Josef Stiegler for permitting to use illustrations from his unpublished PhD thesis. We thank Eduardo Benedicto for allowing us to use a screenshot of the film of the El Brete excavation 'La Universidad Trabaja' in Figure 1, as well as Andrea Cau and Alejandro Otero for their feedback on Figure 22E. We also acknowledge Stephanie Abramowicz and Luis Chiappe from the Dinosaur Institute (Natural History Museum of Los Angeles County), as well as Anusuya Chinsamy-Turan (University of Cape Town), for sharing the map of Argentina used in Figure 2. Thank you to Scott Hartman and Jaime Headden for granting us permission to use and modify their reconstruction of *Noasaurus* in Figure 3, and Sante Mazzei and Asier Larramendi for allowing us to use the illustration of *Noasaurus* in Figure 22D. We are particularly thankful to Emanuele Martini (IFOM, FIRC Institute of Molecular Oncology, Milan, Italy) and Prof. Dr H. Glünder (Munich Center for Neuroscience and Technische Universität Darmstadt) for giving us the tools to measure the elongation and curvature of theropod manual unguals. We also thank Leonardo Ortiz David (Laboratorio y Museo de Dinosaurios, Univesidad Nacional de Cuyo) for his help in the identification of MACN-PV 622. We acknowledge the use of the Willi Hennig Society edition of TNT for the cladistic analysis and Phylopic for the theropod silhouettes, and thank Scott Hartman, Tasman Dixon, Jaime Headden, Alessio Ciaffi, Funkmonk, Geovane Alves de Souza, Iain Reid, Jagged Fang Designs, Julio Garza, and Ville-Veikko Sinkkonen for sharing their artworks on this website. Ronan Allain, Oliver Rauhut, and editor Jeff Streicher are thanked for their thorough reviews, which

considerably improved the quality of this study. This research was supported by the Consejo Nacional de Investigaciones Científicas y Técnicas (CONICET) and Agencia Nacional de Promoción Científica y Tecnológica, Argentina to C.H. (Beca Pos-doctoral CONICET Legajo 181417). RD was supported by the Fundação de Amparo à Pesquisa do Estado de São Paulo (FAPESP—2021/12231-3 and 2022/14375-5). C.H. dedicates this work to Prof. Fernando Abdala, who flirted with death, and to the memory of Jacqueline Ernst Lambert and Dr. Jaime Powell.

CONFLICT OF INTEREST

The authors declare not conflicts of interest.

DATA AVAILABILITY

The data used in this study are available in the online supporting material.

REFERENCES

Abdala F, Martinelli AG, González FR. La paleoherpetología en el Instituto Miguel Lillo de la Universidad Nacional de Tucumán, Argentina. *Publicación Electrónica de la Asociación Paleontológica Argentina* 2022;**22**:67–87.

Agnolín FL, Chiarelli P. The position of the claws in Noasauridae (Dinosauria: Abelisauroidea) and its implications for abelisauroid manus evolution. *Paläontologische Zeitschrift* 2010;**84**:293–300. https://doi.org/10.1007/s12542-009-0044-2

Agnolín FL, Martinelli AG. Did oviraptorosaurs (Dinosauria; Theropoda) inhabit Argentina? *Cretaceous Research* 2007;**28**:785–90.

Agnolín F, Apesteguia S, Chiarelli P. The end of a myth: the mysterious ungual claw of *Noasaurus leali*. *Journal of Vertebrate Paleontology* 2004;**24**:3–3A.

Agnolín FL, Cerroni MA, Scanferla A *et al.* First definitive abelisaurid theropod from the Late Cretaceous of Northwestern Argentina. *Journal of Vertebrate Paleontology* 2022;**41**:e2002348.

Allain R. Discovery of megalosaur (Dinosauria, Theropoda) in the middle Bathonian of Normandy (France) and its implications for the phylogeny of basal Tetanurae. *Journal of Vertebrate Paleontology* 2002;**22**:548–63. https://doi.org/10.1671/0272-4634(2002)022[0548:domdti]2.0.co;2

Allain R. The postcranial anatomy of the megalosaur *Dubreuillosaurus valesdunensis* (Dinosauria Theropoda) from the Middle Jurassic of Normandy, France. *Journal of Vertebrate Paleontology* 2005;**25**:850–8. https://doi.org/10.1671/0272-4634(2005)025[0850:tpaotm]2.0.co;2

Allain R, Xaisanavong T, Richir P *et al.* The first definitive Asian spinosaurid (Dinosauria: Theropoda) from the early cretaceous of Laos. *Naturwissenschaften* 2012;**99**:369–77. https://doi.org/10.1007/s00114-012-0911-7

Allain R, Vullo R, Le Loeuff J *et al.* European ornithomimosaurs (Dinosauria, Theropoda): an undetected record. *Geologica Acta: an International Earth Science Journal* 2014;**12**:127–35.

Amiot R, Buffetaut E, Lécuyer C *et al.* Oxygen isotope evidence for semi-aquatic habits among spinosaurid theropods. *Geology* 2010;**38**:139–42. https://doi.org/10.1130/g30402.1

Apesteguía S, Alvarez S, Giacchino A. Bonaparte, el amo de los dinosaurios. Buenos Aires: Fundación de Historia Natural Félix de Azara, 2022.

Apesteguía S, Smith ND, Valieri RJ *et al.* An unusual new theropod with a didactyl manus from the Upper Cretaceous of Patagonia, Argentina. *PLoS One* 2016;**11**:e0157793.

Aranciaga Rolando M, Cerroni MA, Garcia Marsà JA *et al.* A new medium-sized abelisaurid (Theropoda, Dinosauria) from the late cretaceous (Maastrichtian) Allen Formation of Northern Patagonia, Argentina. *Journal of South American Earth Sciences* 2021;**105**:102915. https://doi.org/10.1016/j.jsames.2020.102915

Averianov AO, Skutschas PP, Atuchin AA *et al.* The last ceratosaur of Asia: a new noasaurid from the Early Cretaceous Great Siberian Refugium. *Proceedings of the Royal Society B* 2024;**291**:20240537. https://doi.org/10.1098/rspb.2024.0537

Baiano MA, Coria RA. Revisiting *Velocisaurus unicus* Bonaparte, 1991 (Theropoda, Ceratosauria, Noasauridae): inferences on the Noasauridae/Abelisauridae systematic. In: *Second Jornadas de Paleovertebrados de la Cuenca Neuquina: libro de resúmenes*. Neuquén: Asociación Paleontológica Argentina, 2019, R5.

Baiano MA, Coria RA, Cau A. A new abelisauroid (Dinosauria: Theropoda) from the Huincul Formation (lower Upper Cretaceous, Neuquén Basin) of Patagonia, Argentina. *Cretaceous Research* 2020;**110**:104408. https://doi.org/10.1016/j.cretres.2020.104408

Baiano MA, Coria RA, Canale JI *et al.* New abelisaurid material from the Anacleto Formation (Campanian, Upper Cretaceous) of Patagonia, Argentina, shed light on the diagnosis of the Abelisauridae (Theropoda, Ceratosauria). *Journal of South American Earth Sciences* 2021;**110**:103402. https://doi.org/10.1016/j.jsames.2021.103402

Baiano MA, Coria R, Chiappe LM *et al.* Osteology of the axial skeleton of *Aucasaurus garridoi*: phylogenetic and paleobiological inferences. *PeerJ* 2023;**11**:e16236. https://doi.org/10.7717/peerj.16236

Barta DE, Nesbitt SJ, Norell MA. The evolution of the manus of early theropod dinosaurs is characterized by high inter- and intraspecific variation. *Journal of Anatomy* 2018;**232**:80–104. https://doi.org/10.1111/joa.12719

Benson RBJ, Xing X. The anatomy and systematic position of the theropod dinosaur *Chilantaisaurus tashuikouensis* Hu, 1964 from the Early Cretaceous of Alanshan, People's Republic of China. *Geological Magazine* 2008;**145**:778–89. https://doi.org/10.1017/s0016756808005475

Benson RBJ, Campione NE, Carrano MT *et al.* Rates of dinosaur body mass evolution indicate 170 million years of sustained ecological innovation on the avian stem lineage. *PLoS Biology* 2014;**12**:e1001853. https://doi.org/10.1371/journal.pbio.1001853

Benton M. *The Dinosaur Encyclopedia*. New York: Simon Pulse, 1984.

Bonaparte JF. The Gondwanian theropod families Abelisauridae and Noasauridae. *Historical Biology* 1991;**5**:1–25. https://doi.org/10.1080/10292389109380385

Bonaparte JF. Cretaceous tetrapods of Argentina. *Münchener Geowissenschaftliche Abhandlungen, A* 1996a;**30**:73–130.

Bonaparte JF. *Dinosaurios de America del Sur*. Ed. Sagitario, Buenos Aires, 1996b.

Bonaparte JF. *Dinosaurios y Pterosaurios de América del Sur*. Ed. Albatros, Buenos Aires, 2007.

Bonaparte JF, Novas FE. *Abelisaurus comahuensis*, n.g., Carnosauria del Crétacico Tardio de Patagonia. *Ameghiniana* 1985;**21**:259–65.

Bonaparte JF, Powell JE. A continental assemblage of tetrapods from the Upper Cretaceous beds of El Brete, northwestern Argentina (Sauropoda-Coelurosauria-Carnosauria-Aves). *Mémoires de la Société Géologique de France, Nouvelle Série* 1980;**139**:19–28.

Bonaparte JF, Salfity JA, Bossi G *et al.* Hallazgo de dinosaurios y aves cretácicas en la Formación Lecho de El Brete (Salta), próximo al límite con Tucumán. *Acta Geológica Lilloana* 1977;**14**:5–17.

Bonaparte JF, Novas FE, Coria RA. *Carnotaurus sastrei* Bonaparte, the horned, lightly built carnosaur from the Middle Cretaceous of Patagonia. *Contributions in science* 1990;**416**:1–41. https://doi.org/10.5962/p.226819

Brissón Egli F, Agnolín FL, Novas F. A new specimen of *Velocisaurus unicus* (Theropoda, Abelisauroidea) from the Paso Córdoba locality (Santonian), Río Negro, Argentina. *Journal of Vertebrate Paleontology* 2016;**36**:e1119156. https://doi.org/10.1080/02724634.2016.1119156

Brougham T, Smith ET, Bell PR. Noasaurids are a component of the Australian 'mid'-Cretaceous theropod fauna. *Scientific Reports* 2020;**10**:1428.

Brum AS, Machado EB, de Almeida Campos D *et al.* Description of uncommon pneumatic structures of a noasaurid (Theropoda, Dinosauria) cervical vertebra from the Bauru Group (Upper

Cretaceous), Brazil. *Cretaceous Research* 2018;**85**:193–206. https://doi.org/10.1016/j.cretres.2017.10.012
Brum AS, Pêgas RV, Bandeira KLN *et al.* A new unenlagiine (Theropoda, Dromaeosauridae) from the Upper Cretaceous of Brazil. *Papers in Palaeontology* 2021;**7**:2075–99. https://doi.org/10.1002/spp2.1375
Brusatte SL, Benson RBJ, Currie PJ *et al.* The skull of *Monolophosaurus jiangi* (Dinosauria: Theropoda) and its implications for early theropod phylogeny and evolution. *Zoological Journal of the Linnean Society* 2010;**158**:573–607. https://doi.org/10.1111/j.1096-3642.2009.00563.x
Buchmann R, Rodrigues T. The evolution of pneumatic foramina in pterosaur vertebrae. *Anais da Academia Brasileira de Ciências* 2019;**91**:e20180782.
Buchmann R, Rodrigues T. Arthrological reconstructions of the pterosaur neck and their implications for the cervical position at rest. *PeerJ* 2024;**12**:e16884. https://doi.org/10.7717/peerj.16884
Buchmann R, Avilla L dos S, Rodrigues T. Comparative analysis of the vertebral pneumatization in pterosaurs (Reptilia: Pterosauria) and extant birds (Avialae: Neornithes). *PLoS One* 2019;**14**:e0224165.
Burch SH, Carrano MT. An articulated pectoral girdle and forelimb of the abelisaurid theropod *Majungasaurus crenatissimus* from the Late Cretaceous of Madagascar. *Journal of Vertebrate Paleontology* 2012;**32**:1–16. https://doi.org/10.1080/02724634.2012.622027
Campione NE, Evans DC. The accuracy and precision of body mass estimation in non-avian dinosaurs. *Biological Reviews of the Cambridge Philosophical Society* 2020;**95**:1759–97. https://doi.org/10.1111/brv.12638
Campione NE, Evans DC, Brown CM *et al.* Body mass estimation in non-avian bipeds using a theoretical conversion to quadruped stylopodial proportions. *Methods in Ecology and Evolution* 2014;**5**:913–23. https://doi.org/10.1111/2041-210x.12226
Canale JI, Scanferla CA, Agnolín FL *et al.* New carnivorous dinosaur from the Late Cretaceous of NW Patagonia and the evolution of abelisaurid theropods. *Naturwissenschaften* 2009;**96**:409–14. https://doi.org/10.1007/s00114-008-0487-4
Candeiro CRA. Padrões morfológicos dos dentes de Abelisauroidea y Carcharodontosauridae (Theropoda, Dinosauria) do Cretáceo da América do Sul. Unpublished Ph.D. Thesis, Universidade Federal do Rio de Janeiro, Departamento de Geología, 2007.
Carpenter K, Sanders F, McWhinney LA *et al.* Evidence for predator-prey relationships. In: Carpenter K (ed.), *The Carnivorous Dinosaurs.* Bloomington, IN, 2005, 325–50.
Carrano MT. The appendicular skeleton of *Majungasaurus crenatissimus* (Theropoda: Abelisauridae) from the Late Cretaceous of Madagascar. *Journal of Vertebrate Paleontology* 2007;**27**:163–79. https://doi.org/10.1671/0272-4634(2007)27[163:tasomc]2.0.co;2
Carrano MT, Choiniere J. New information on the forearm and manus of *Ceratosaurus nasicornis* Marsh, 1884 (Dinosauria, Theropoda), with implications for theropod forelimb evolution. *Journal of Vertebrate Paleontology* 2016;**36**:e1054497. https://doi.org/10.1080/02724634.2015.1054497
Carrano MT, Hutchinson JR. Pelvic and hindlimb musculature of *Tyrannosaurus rex* (Dinosauria: Theropoda). *Journal of Morphology* 2002;**253**:207–28. https://doi.org/10.1002/jmor.10018
Carrano MT, Sampson SD. The phylogeny of Ceratosauria (Dinosauria: Theropoda). *Journal of Systematic Palaeontology* 2008;**6**:183–236. https://doi.org/10.1017/s1477201907002246
Carrano MT, Sampson SD, Forster CA. The osteology of *Masiakasaurus knopfleri*, a small abelisauroid (Dinosauria: Theropoda) from the Late Cretaceous of Madagascar. *Journal of Vertebrate Paleontology* 2002;**22**:510–34. https://doi.org/10.1671/0272-4634(2002)022[0510:toomka]2.0.co;2
Carrano M, Sampson SD, Loewen M. New discoveries of *Masiakasaurus knopfleri* and the morphology of the Noasauridae (Dinosauria: Theropoda). *Journal of Vertebrate Paleontology* 2004;**24**:4–4A.
Carrano MT, Loewen MA, Sertich JJW. New materials of *Masiakasaurus knopfleri* Sampson, Carrano, and Forster, 2001, and implications for the morphology of the Noasauridae (Theropoda: Ceratosauria). *Smithsonian Contributions to Paleobiology* 2011;**95**:1–53. https://doi.org/10.5479/si.00810266.95.1
Cerda IA, Powell JE. Dermal armor histology of *Saltasaurus loricatus*, an Upper Cretaceous sauropod dinosaur from Northwest Argentina. *Acta Palaeontologica Polonica* 2010;**55**:389–98. https://doi.org/10.4202/app.2009.1101
Cerroni MA, Agnolín FL, Brissón Egli F *et al.* The phylogenetic position of *Afromimus tenerensis* Sereno, 2017 and its paleobiogeographical implications. *Journal of African Earth Sciences* 2019;**159**:103572. https://doi.org/10.1016/j.jafrearsci.2019.103572
Cerroni MA, Canale JI, Novas FE. The skull of *Carnotaurus sastrei* Bonaparte 1985 revisited: insights from craniofacial bones, palate and lower jaw. *Historical Biology* 2020a;**33**:2444–85. https://doi.org/10.1080/08912963.2020.1802445
Cerroni MA, Motta MJ, Agnolín FL *et al.* A new abelisaurid from the Huincul Formation (Cenomanian-Turonian; Upper Cretaceous) of Río Negro province, Argentina. *Journal of South American Earth Sciences* 2020b;**98**:102445. https://doi.org/10.1016/j.jsames.2019.102445
Cerroni MA, Baiano MA, Canale JI *et al.* Appendicular osteology of *Skorpiovenator bustingorryi* (Theropoda, Abelisauridae) with comments on phylogenetic features of abelisaurids. *Journal of Systematic Palaeontology* 2022;**20**:1–32. https://doi.org/10.1080/14772019.2022.2093661
Charig AJ, Milner AC. *Baryonyx*, a remarkable new theropod dinosaur. *Nature* 1986;**324**:359–61. https://doi.org/10.1038/324359a0
Charig AJ, Milner AC. *Baryonyx walkeri*, a fish-eating dinosaur from the Wealden of Surrey. *Bulletin of the Natural History Museum* 1997;**53**:11–70.
Chiappe LM. Enantiornithine (Aves) tarsometatarsi from the Cretaceous Lecho formation of northwestern Argentina. *American Museum Novitates* 1993;**3083**:1–27.
Chinzorig T, Kobayashi Y, Tsogtbaatar K *et al.* Ornithomimosaurs from the Nemegt Formation of Mongolia: manus morphological variation and diversity. *Palaeogeography, Palaeoclimatology, Palaeoecology* 2018;**494**:91–100. https://doi.org/10.1016/j.palaeo.2017.10.031
Choiniere JN, Clark JM, Forster CA *et al.* A juvenile specimen of a new coelurosaur (Dinosauria: Theropoda) from the Middle–Late Jurassic Shishugou Formation of Xinjiang, People's Republic of China. *Journal of Systematic Palaeontology* 2014a;**12**:177–215. https://doi.org/10.1080/14772019.2013.781067
Choiniere JN, Clark JM, Norell M *et al.* Cranial osteology of *Haplocheirus sollers* Choiniere *et al.*, 2010 (Theropoda, Alvarezsauroidea). *American Museum Novitates* 2014b;**3816**:1–44.
Choiniere JN, Neenan JM, Schmitz L *et al.* Evolution of vision and hearing modalities in theropod dinosaurs. *Science* 2021;**372**:610–3. https://doi.org/10.1126/science.abe7941
Chure DJ. A new species of *Allosaurus* from the Morrison Formation of Dinosaur National Monument (Utah-Colorado) and a revision of the theropod family Allosauridae. Unpublished Ph.D. Thesis, Columbia University, 2000.
Conrad JL. A new lizard (Squamata) was the last meal of *Compsognathus* (Theropoda: Dinosauria) and is a holotype in a holotype. *Zoological Journal of the Linnean Society* 2018;**183**:584–634. https://doi.org/10.1093/zoolinnean/zlx055
Coria RA, Salgado L. A basal Abelisauria Novas, 1992 (Theropoda-Ceratosauria) from the Cretaceous of Patagonia, Argentina. *Gaia* 1998;**15**:89–102.
Coria RA, Chiappe LM, Dingus L. A new close relative of *Carnotaurus sastrei* Bonaparte 1985 (Theropoda: Abelisauridae) from the Late Cretaceous of Patagonia. *Journal of Vertebrate Paleontology* 2002;**22**:460–5. https://doi.org/10.1671/0272-4634(2002)022[0460:ancroc]2.0.co;2
Currie PJ. Cranial anatomy of tyrannosaurid dinosaurs from the Late Cretaceous of Alberta, Canada. *Acta Palaeontologica Polonica* 2003;**48**:191–226.
Currie PJ, Zhao XJ. A new carnosaur (Dinosauria, Theropoda) from the Jurassic of Xinjiang, People's Republic of China. *Canadian Journal of Earth Sciences* 1993;**30**:2037–81. https://doi.org/10.1139/e93-179

Currie PJ, Rigby JK Jr, Sloan RE. Theropod teeth from the Judith River Formation of southern Alberta, Canada. In: Carpenter K, Currie PJ (eds), *Dinosaur Systematics: Approaches and Perspectives*. New York, NY: Cambridge University Press, 1990, 107–25.

D'Amore DC. A functional explanation for denticulation in theropod dinosaur teeth. *The Anatomical Record* 2009;**292**:1297–314. https://doi.org/10.1002/ar.20977

D'Amore DC, Blumenschine RJ. Komodo monitor (*Varanus komodoensis*) feeding behavior and dental function reflected through tooth marks on bone surfaces, and the application to ziphodont paleobiology. *Paleobiology* 2009;**35**:525–52.

Dal Sasso C, Maganuco S. *Scipionyx samniticus* (Theropoda: Compsognathidae) from the Lower Cretaceous of Italy: osteology, ontogenetic assessment, phylogeny, soft tissue anatomy, taphonomy and palaeobiology. *Memorie della Società Italiana di Scienze Naturali e del Museo Civico di Storia Naturale di Milano* 2011;**37**:1–281.

Dal Sasso C, Maganuco S, Buffetaut E *et al*. New information on the skull of the enigmatic theropod *Spinosaurus*, with remarks on its size and affinities. *Journal of Vertebrate Paleontology* 2005;**25**:888–96.

Dal Sasso C, Maganuco S, Cau A. The oldest ceratosaurian (Dinosauria: Theropoda), from the Lower Jurassic of Italy, sheds light on the evolution of the three-fingered hand of birds. *PeerJ* 2018;**6**:e5976. https://doi.org/10.7717/peerj.5976

Danieli C, Fabre V, Quartino B. Restos óseos uraníferos de la zona de El Brete, Dpto. Candelaria, Prov. de Salta. *Acta Geológica Lilloana* 1960;**3**:5–14.

Delcourt R. Ceratosaur palaeobiology: new insights on evolution and ecology of the southern rulers. *Scientific Reports* 2018;**8**:1–12.

Deschamps R, Rohais S, Hamon Y *et al*. Dynamic of a lacustrine sedimentary system during late rifting at the Cretaceous–Palaeocene transition: example of the Yacoraite Formation, Salta Basin, Argentina. *The Depositional Record* 2020;**6**:490–523. https://doi.org/10.1002/dep2.116

Eudes-Deslongchamps JA. *Mémoire sur le Poekilopleuron bucklandii, grand saurien fossile, intermédiaire entre les crocodiles et les lézards, découvert dans les carrières de la Maladrerie, près Caen, au mois de juillet 1835*. impr. A. Hardel, Caen, 1837.

Evans DC, Barrett PM, Brink KS *et al*. Osteology and bone microstructure of new, small theropod dinosaur material from the early Late Cretaceous of Morocco. *Gondwana Research* 2015;**27**:1034–41. https://doi.org/10.1016/j.gr.2014.03.016

Ezcurra MD, Novas FE. Theropod dinosaurs from Argentina. *Contribuciones del Museo Argentino de Ciencias Naturales* 2016;**6**:139–56.

Feduccia A. Evidence from claw geometry indicating arboreal habits of *Archaeopteryx*. *Science* 1993;**259**:790–3. https://doi.org/10.1126/science.259.5096.790

Fernández DS, Lutz MA, Pereyra FX *et al*. Programa Nacional de Cartas Geológicas de la República Argentina 1:250.000. Carta de Línea de Base Ambiental 2766-II Tucumán. Provincias de Tucumán, Salta,Catamarca y Santiago del Estero. Dirección de Geología Ambiental y Aplicada. Boletín N° 374, Buenos Aires, 2008.

Filippi LS, Méndez AH, Juárez Valieri RD *et al*. A new brachyrostran with hypertrophied axial structures reveals an unexpected radiation of latest Cretaceous abelisaurids. *Cretaceous Research* 2016;**61**:209–19. https://doi.org/10.1016/j.cretres.2015.12.018

Fowler DW, Freedman EA, Scannella JB *et al*. The predatory ecology of *Deinonychus* and the origin of flapping in birds. *PLoS One* 2011;**6**:e28964. https://doi.org/10.1371/journal.pone.0028964

Frankfurt NG, Chiappe LM. A possible oviraptorosaur from the Late Cretaceous of northwestern Argentina. *Journal of Vertebrate Paleontology* 1999;**19**:101–5. https://doi.org/10.1080/02724634.1999.10011126

Galton PM. *Elaphrosaurus*, an ornithomimid dinosaur from the Upper Jurassic of North America and Africa. *Paläontologische Zeitschrift* 1982;**56**:265–75. https://doi.org/10.1007/bf02988803

Galton PM, Jensen JA. A new large theropod dinosaur from the Upper Jurassic of Colorado. *Brigham Young University Geology Studies* 1979;**26**:1–12.

Giacchino A, Agnolín F. Obituario: José Fernando Bonaparte (14/06/1928-18/02/2020). *Historia Natural* 2020;**10**:175–80.

Gianechini FA, Makovicky PJ, Apesteguía S. The teeth of the unenlagiine theropod *Buitreraptor* from the Cretaceous of Patagonia, Argentina, and the unusual dentition of the Gondwanan dromaeosaurids. *Acta Palaeontologica Polonica* 2011;**56**:279–90. https://doi.org/10.4202/app.2009.0127

Gianechini FA, Ercoli MD, Díaz-Martínez I. Differential locomotor and predatory strategies of Gondwanan and derived Laurasian dromaeosaurids (Dinosauria, Theropoda, Paraves): inferences from morphometric and comparative anatomical studies. *Journal of Anatomy* 2020;**236**:772–97. https://doi.org/10.1111/joa.13153

Gianechini FA, Méndez AH, Filippi LS *et al*. A new furileusaurian abelisaurid from La Invernada (Upper Cretaceous, Santonian, Bajo de la Carpa Formation), northern Patagonia, Argentina. *Journal of Vertebrate Paleontology* 2021;**40**:e1877151. https://doi.org/10.1080/02724634.2020.1877151

Gilmore CW. Osteology of the carnivorous Dinosauria in the United State National museum: with special reference to the genera *Antrodemus* (*Allosaurus*) and *Ceratosaurus*. *Bulletin of the United States National Museum* 1920;**110**:i–159. https://doi.org/10.5479/si.03629236.110.i

Goloboff PA, Catalano SA. TNT version 1.5, including a full implementation of phylogenetic morphometrics. *Cladistics* 2016;**32**:221–38. https://doi.org/10.1111/cla.12160

Goloboff PA, Morales ME. TNT version 1.6, with a graphical interface for MacOS and Linux, including new routines in parallel. *Cladistics* 2023;**39**:144–53. https://doi.org/10.1111/cla.12524

Gómez Omil RJ, Boll A, Hernández RM. Cuenca Cretácico-Terciaria del Noroeste Argentino (Grupo Salta). *Cuencas Sedimentarias Argentinas. Universidad Nacional de Tucumán, Serie de Correlación Geológica* 1989;**6**:43–64.

Harris JD. Confusing dinosaurs with mammals: tetrapod phylogenetics and anatomical terminology in the world of homology. *The Anatomical Record Part A: Discoveries in Molecular, Cellular, and Evolutionary Biology* 2004;**281A**:1240–6. https://doi.org/10.1002/ar.a.20078

Hedrick BP, Zanno LE, Wolfe DG *et al*. The slothful claw: osteology and taphonomy of *Nothronychus mckinleyi* and *N. graffami* (Dinosauria: Theropoda) and anatomical considerations for derived therizinosaurids. *PLoS One* 2015;**10**:e0129449. https://doi.org/10.1371/journal.pone.0129449

Hendrickx C. Evolution of teeth and quadrate in non-avian Theropoda (Dinosauria: Saurischia), with the description of *Torvosaurus* remains from Portugal. Unpublished Ph.D. Thesis, Universidade Nova de Lisboa, 2015.

Hendrickx C, Mateus O. Abelisauridae (Dinosauria: Theropoda) from the Late Jurassic of Portugal and dentition-based phylogeny as a contribution for the identification of isolated theropod teeth. *Zootaxa* 2014a;**3759**:1–74. https://doi.org/10.11646/zootaxa.3759.1.1

Hendrickx C, Mateus O. *Torvosaurus gurneyi* n. sp., the largest terrestrial predator from Europe, and a proposed terminology of the maxilla anatomy in nonavian theropods. *PLoS One* 2014b;**9**:e88905. https://doi.org/10.1371/journal.pone.0088905

Hendrickx C, Araújo R, Mateus O. The non-avian theropod quadrate I: standardized terminology with an overview of the anatomy and function. *PeerJ* 2015a;**3**:e1245. https://doi.org/10.7717/peerj.1245

Hendrickx C, Hartman SA, Mateus O. An overview of non-avian theropod discoveries and classification. *PalArch's Journal of Vertebrate Palaeontology* 2015b;**12**:1–73.

Hendrickx C, Mateus O, Araújo R. The dentition of megalosaurid theropods. *Acta Palaeontologica Polonica* 2015c;**60**:627–42.

Hendrickx C, Mateus O, Araújo R. A proposed terminology of theropod teeth (Dinosauria, Saurischia). *Journal of Vertebrate Paleontology* 2015d;**35**:e982797. https://doi.org/10.1080/02724634.2015.982797

Hendrickx C, Mateus O, Buffetaut E. Morphofunctional analysis of the quadrate of Spinosauridae (Dinosauria: Theropoda) and the presence of *Spinosaurus* and a second spinosaurine taxon in the Cenomanian of North Africa. *PLoS One* 2016;**11**:e0144695. https://doi.org/10.1371/journal.pone.0144695

Hendrickx C, Mateus O, Araújo R *et al*. The distribution of dental features in non-avian theropod dinosaurs: taxonomic potential, degree of homoplasy, and major evolutionary trends. *Palaeontologia Electronica* 2019;**22**:1–110.

Hendrickx C, Stiegler J, Currie PJ *et al*. Dental anatomy of the apex predator *Sinraptor dongi* (Theropoda: Allosauroidea) from the Late Jurassic of China. *Canadian Journal of Earth Sciences* 2020a;**57**:1127–47. https://doi.org/10.1139/cjes-2019-0231

Hendrickx C, Tschopp E, Ezcurra MD. Taxonomic identification of isolated theropod teeth: the case of the shed tooth crown associated with *Aerosteon* (Theropoda: Megaraptora) and the dentition of Abelisauridae. *Cretaceous Research* 2020b;**108**:104312.

Hendrickx C, Trapman TH, Wills S *et al*. A combined approach to identify isolated theropod teeth from the Cenomanian Kem Kem Group of Morocco: cladistic, discriminant, and machine learning analyses. *Journal of Vertebrate Paleontology* 2023;**43**:e2311791.

Holtz TRJ. *Dinosaurs: The Most Complete, Up-to-Date Encyclopedia for Dinosaur Lovers of All Ages*. New York: Random House Books for Young Readers, 2007.

Holtz TR. The phylogenetic position of the Tyrannosauridae: implications for theropod systematics. *Journal of Paleontology* 1994;**68**:1100–17. https://doi.org/10.1017/s0022336000026706

Holtz TRJ, Padian K. Definition and diagnosis of Theropoda and related taxa. *Journal of Vertebrate Paleontology* 1995;**15**:35A.

Hone DWE, Holtz TRJ. Evaluating the ecology of *Spinosaurus*: shoreline generalist or aquatic pursuit specialist? *Palaeontologia Electronica* 2021;**24**:a03.

Hone DWE, Rauhut OWM. Feeding behaviour and bone utilization by theropod dinosaurs. *Lethaia* 2010;**43**:232–44. https://doi.org/10.1111/j.1502-3931.2009.00187.x

Ibiricu LM, Baiano MA, Martínez RD *et al*. A detailed osteological description of *Xenotarsosaurus bonapartei* (Theropoda: Abelisauridae): implications for abelisauroid phylogeny. *Cretaceous Research* 2021;**124**:104829. https://doi.org/10.1016/j.cretres.2021.104829

Ibrahim N, Sereno PC, Sasso CD *et al*. Semiaquatic adaptations in a giant predatory dinosaur. *Science* 2014;**345**:1613–6.

Ibrahim N, Sereno PC, Varricchio DJ *et al*. Geology and paleontology of the Upper Cretaceous Kem Kem Group of eastern Morocco. *ZooKeys* 2020;**928**:1–216. https://doi.org/10.3897/zookeys.928.47517

Iori FV, Araújo-Júnior HIde, Tavares SAS *et al*. New theropod dinosaur from the Late Cretaceous of Brazil improves abelisaurid diversity. *Journal of South American Earth Sciences* 2021;**112**:103551.

Janensch W. Die Coelurosaurier und Theropoden der Tendaguruschichten Deutsch-Ostafrikas. *Palaeontographica-Supplementbände* 1925;**7**:1–100.

Kellermann M. New data on dinosaur diversity in the 'middle' Cretaceous (Albian, Cenomanian) of North Africa. Unpublished M.Sc. Thesis, Ludwig-Maximilians-Universität Munich, 2021.

Kellner AW, Weinschütz LC, Holgado B *et al*. A new toothless pterosaur (Pterodactyloidea) from Southern Brazil with insights into the paleoecology of a Cretaceous desert. *Anais da Academia Brasileira de Ciências* 2019;**91**:e20190768.

Kitchener A. Function of Claws' claws. *Nature* 1987;**325**:114–114. https://doi.org/10.1038/325114a0

Kortyna C, DeCelles PG, Carrapa B. Chapter 15—Structural and thermochronologic constraints on kinematics and timing of inversion of the Salta rift in the Tonco-Amblayo sector of the Andean retroarc fold-thrust belt, northwestern Argentina. In: Horton BK, Folguera A (eds), *Andean Tectonics*. Elsevier, Amsterdam, Netherlands, 2019, 429–64.

Kubota K, Kobayashi Y, Ikeda T. Early Cretaceous troodontine troodontid (Dinosauria: Theropoda) from the Ohyamashimo Formation of Japan reveals the early evolution of Troodontinae. *Scientific Reports* 2024;**14**:16392. https://doi.org/10.1038/s41598-024-66815-2

La Universidad Trabaja. San Miguel de Tucumán. Argentina: Instituto Cinefotográfico Universidad Nacional de Tucumán y Canal, 1976, 10.

Lambert D. *A Field Guide to Dinosaurs: The First Complete Guide to Every Dinosaur Now Known*. New York: Avon Books, 1983.

Lambert D. *Dinosaur Data Book: The Definitive, Fully Illustrated Encyclopedia of Dinosaurs*. New York: Avon Books, 1990.

Lambert D. *The Ultimate Dinosaur Book*. London; NY: DK ADULT, 1993.

Langer MC, Martins Nde O, Manzig PC *et al*. A new desert-dwelling dinosaur (Theropoda, Noasaurinae) from the Cretaceous of south Brazil. *Scientific Reports* 2019;**9**:1–31.

Lautenschlager S. Morphological and functional diversity in therizinosaur claws and the implications for theropod claw evolution. *Proceedings Biological Sciences* 2014;**281**:20140497. https://doi.org/10.1098/rspb.2014.0497

Longrich NR, Saitta ET. Taxonomic status of *Nanotyrannus lancensis* (Dinosauria: Tyrannosauroidea)—a distinct taxon of small-bodied Tyrannosaur. *Fossil Studies* 2024;**2**:1–65. https://doi.org/10.3390/fossils2010001

Lü J, Xu L, Liu Y *et al*. A new troodontid theropod from the Late Cretaceous of central China, and the radiation of Asian troodontids. *Acta Palaeontologica Polonica* 2010;**55**:381–8. https://doi.org/10.4202/app.2009.0047

Maddison WP, Maddison DR. *Mesquite: A Modular System for Evolutionary Analysis, v.3.2*. http://www.mesquiteproject.org. Accessed 20 September 2017, 2017.

Madsen JH. *Allosaurus fragilis*: a revised osteology. *Utah Geological Survey Bulletin* 1976;**109**:1–177.

Madsen JH, Welles SP. *Ceratosaurus* (Dinosauria, Theropoda): a revised osteology. *Utah Geological Survey, Miscellaneous Publication* 2000;**00–2**:1–89.

Marquillas RA, Del Papa C, Sabino IF. Sedimentary aspects and paleoenvironmental evolution of a rift basin: Salta Group (Cretaceous–Paleogene), northwestern Argentina. *International Journal of Earth Sciences* 2005;**94**:94–113. https://doi.org/10.1007/s00531-004-0443-2

Marsh OC. Principal characters of American Jurassic dinosaurs. Part V. *American Journal of Science (Series 3)* 1881;**21**:417–23.

Marsh OC. Principal characters of the American Jurassic dinosaurs. Part VIII. The order Theropoda. *American Journal of Science, Series 3* 1884;**27**:329–40.

Marsh AD, Rowe TB. A comprehensive anatomical and phylogenetic evaluation of *Dilophosaurus wetherilli* (Dinosauria, Theropoda) with descriptions of new specimens from the Kayenta Formation of northern Arizona. *Journal of Paleontology* 2020;**94**:1–103. https://doi.org/10.1017/jpa.2020.14

Mohabey DM, Samant B, Vélez-Rosado KI *et al*. A review of small-bodied theropod dinosaurs from the Upper Cretaceous of India, with description of new cranial remains of a noasaurid (Theropoda: Abelisauria). *Journal of Vertebrate Paleontology* 2024;**43**:e2288088.

Molina-Pérez R, Larramendi A. *Dinosaur Facts and Figures: The Theropods and Other Dinosauriformes*. Princeton and Oxford: Princeton University Press, 2019.

Montano D, Gasparrini M, Rohais S *et al*. Depositional age models in lacustrine systems from zircon and carbonate U-Pb geochronology. *Sedimentology* 2022;**69**:2507–34. https://doi.org/10.1111/sed.13000

Narváez PL, Volkheimer W. Palynostratigraphy and paleoclimatic inferences of the Balbuena and Santa Bárbara subgroups (Salta Group Basin, Cretaceous–Paleogene): Correlation with Patagonian basins. *Cenozoic geology of the Central Andes of Argentina* 2011:283–300.

Nesbitt SJ, Denton RK, Loewen MA *et al*. A mid-Cretaceous tyrannosauroid and the origin of North American end-Cretaceous dinosaur assemblages. *Nature Ecology & Evolution* 2019;**3**:892–9. https://doi.org/10.1038/s41559-019-0888-0

Nopcsa BF. The genera of reptiles. *Palaeobiologica* 1928;**1**:163–88.

Norell MA, Clark JM, Turner AH *et al*. A new dromaeosaurid theropod from Ukhaa Tolgod (Ömnögov, Mongolia). *American Museum Novitates* 2006;**3545**:1–51. https://doi.org/10.1206/0003-0082(2006)3545[1:andtfu]2.0.co;2

Norell MA, Makovicky PJ, Bever GS *et al*. A review of the Mongolian Cretaceous dinosaur *Saurornithoides* (Troodontidae: Theropoda). *American Museum Novitates* 2009;**3654**:1–63. https://doi.org/10.1206/648.1

Norman D. *The Illustrated Encyclopedia of Dinosaurs*. New York: Crescent, 1985.
Norman DB. Problematic Theropoda: 'Coelurosaurs'. In: Weishampel DB, Dodson P, Osmólska H (eds), *The Dinosauria*. University of California Press, Berkeley, California, 1990, 280–305.
Novas FE. Los dinosaurios carnívoros de la Argentina. Unpublished Ph.D. Thesis, Universidad Nacional de La Plata, 1989.
Novas FE. La evolución de los dinosaurios carnivoros. In: Sanz JL, Buscalioni AD (eds), *Los Dinosaurios y Su Entorno Biotico: Actas del Segundo Curso de Paleontología en Cuenca*. Cuenca, Spain: Instituto 'Juan Valdez', 1992, 126–63.
Novas FE. Abelisauridae. In: Currie PJ, Padian K (eds), *Encyclopedia of Dinosaurs*. San Diego, CA: Academic Press, 1997, 1–2.
Novas FE. *Megaraptor namunhuaiquii*, gen. et sp. nov., a large-clawed, Late Cretaceous theropod from Patagonia. *Journal of Vertebrate Paleontology* 1998;**18**:4–9. https://doi.org/10.1080/02724634.1998.10011030
Novas FE. *The Age of Dinosaurs in South America*. Bloomington: Indiana University Press, 2009.
Novas FE, Bandyopadhyay S. Abelisaurid pedal unguals from the Late Cretaceous of India. *Publicación Electrónica de la Asociación Paleontológica Argentina* 2001;**7**:145–49.
Novas FE, Labaronnie UG, Cerruti S. *Guía De Los Dinosaurios Argentinos*. Buenos Aires, Argentina, 1992.
Novas FE, Agnolín FL, Bandyopadhyay S. Cretaceous theropods from India: a review of specimens described by Huene and Matley (1933). *Revista del Museo Argentino de Ciencias Naturales, ns* 2004;**6**:67–103. https://doi.org/10.22179/revmacn.6.74
Novas FE, Dalla Vecchia F, Pais DF. Theropod pedal unguals from the Late Cretaceous (Cenomanian) of Morocco, Africa. *Revista del Museo Argentino de Ciencias Naturales* 2005;**7**:167–75.
Novas FE, Rolando AMA, Agnolin FL. Phylogenetic relationships of the Cretaceous Gondwanan theropods *Megaraptor* and *Australovenator*: the evidence afforded by their manual anatomy. *Memoirs of Museum Victoria* 2016;**74**:49–61. https://doi.org/10.24199/j.mmv.2016.74.05
O'Connor PM. The postcranial axial skeleton of *Majungasaurus crenatissimus* (Theropoda: Abelisauridae) from the Late Cretaceous of Madagascar. *Journal of Vertebrate Paleontology* 2007;**27**:127–63.
O'Connor J, Zhou Z, Xu X. Additional specimen of *Microraptor* provides unique evidence of dinosaurs preying on birds. *Proceedings of the National Academy of Sciences of the United States of America* 2011;**108**:19662–5. https://doi.org/10.1073/pnas.1117727108
O'Connor J, Zheng X, Dong L *et al*. *Microraptor* with ingested lizard suggests non-specialized digestive function. *Current Biology: CB* 2019;**29**:2423–9.e2. https://doi.org/10.1016/j.cub.2019.06.020
Orbis Publishing. *Dinosaurs!*, Orbis Publishing Ltd, London, UK, 1994, 1609–11.
Ortiz David LD, González Riga BJ, Kellner AWA. *Thanatosdrakon amaru*, gen. et sp. nov., a giant azhdarchid pterosaur from the Upper Cretaceous of Argentina. *Cretaceous Research* 2022;**137**:105228.
Owen R. Report on British fossil reptiles. *Report of the British Association for the Advancement of Science* 1842;**11**:60–294.
Paul GS. *Predatory Dinosaurs of the World: A Complete Illustrated Guide*. Simon & Schuster, New York, Toronto, Sydney, Tokyo, 1988.
Paul GS. *The Princeton Field Guide to Dinosaurs*, 1st edn. Princeton University Press, Princeton, New Jersey, 2010.
Paul GS. *The Princeton Field Guide to Dinosaurs*, 2nd edn. Princeton University Press, Princeton, New Jersey, 2016.
Paul GS. *The Princeton Field Guide to Dinosaurs*, 3rd edn. Princeton University Press, Princeton, New Jersey, 2024.
Pei R, Li Q, Meng Q *et al*. A new specimen of *Microraptor* (Theropoda: Dromaeosauridae) from the Lower Cretaceous of western Liaoning, China. *American Museum Novitates* 2014;**3821**:1–28. https://doi.org/10.1206/3821.1
Peyer K. A reconsideration of *Compsognathus* from the upper Tithonian of Canjuers, southeastern France. *Journal of Vertebrate Paleontology* 2006;**26**:879–96. https://doi.org/10.1671/0272-4634(2006)26[879:arocft]2.0.co;2
Pol D, Rauhut OWM. A Middle Jurassic abelisaurid from Patagonia and the early diversification of theropod dinosaurs. *Proceedings Biological Sciences* 2012;**279**:3170–5. https://doi.org/10.1098/rspb.2012.0660
Pol D, Baiano MA, Černý D *et al*. A new abelisaurid dinosaur from the end Cretaceous of Patagonia and evolutionary rates among the Ceratosauria. *Cladistics* 2024;**40**:307–56. https://doi.org/10.1111/cla.12583
Poropat SF, Pentland AH, Duncan RJ *et al*. First elaphrosaurine theropod dinosaur (Ceratosauria: Noasauridae) from Australia—a cervical vertebra from the Early Cretaceous of Victoria. *Gondwana Research* 2020;**84**:284–95. https://doi.org/10.1016/j.gr.2020.03.009
Powell JE. Osteologia de *Saltasaurus loricatus* (Sauropoda-Titanosauridae) del Cretácico Superior del noroeste Argentino. In: Sanz JL, Buscalioni AD (eds), *Los Dinosaurios y Su Entorno Biotico: Actas del Segundo Curso de Paleontologia in Cuenca*. Cuenca, Argentina: Institutio 'Juan de Valdes', 1992, 165–230.
Powell JE. *Revision of South American Titanosaurid Dinosaurs: Palaeobiological, Palaeobiogeographical and Phylogenetic Aspects*. Queen Victoria Museum and Art Gallery, Launceston, Tasmania, Australia, 2003.
Powell JE, Ortiz PE. Los vertebrados fósiles de la provincia de Tucumán. In: Moyano S, Puchulu ME, Fernández DS, Vides ME, Nieva S, Aceñolaza GF (eds), *Geología de Tucumán*. San Miguel de Tucumán, Argentina: Publicación Especial del Colegio de Graduados en Ciencias Geológicas de Tucumán, 2014, 208–27.
Qin Z, Liao CC, Benton MJ *et al*. Functional space analyses reveal the function and evolution of the most bizarre theropod manual unguals. *Communications Biology* 2023;**6**:1–13.
Quattrocchio ME, Volkheimer W, Marquillas RA *et al*. Palynostratigraphy, palaeobiogeography and evolutionary significance of the Late Senonian and Early Palaeogene palynofloras of the Salta Group, northern Argentina. *Revista Española de Micropaleontología* 2005;**37**:259–72.
Rauhut OWM. Provenance and anatomy of *Genyodectes serus*, a large-toothed ceratosaur (Dinosauria: Theropoda) from Patagonia. *Journal of Vertebrate Paleontology* 2004;**24**:894–902. https://doi.org/10.1671/0272-4634(2004)024[0894:paaogs]2.0.co;2
Rauhut OWM. A reappraisal of a putative record of abelisauroid theropod dinosaur from the Middle Jurassic of England. *Proceedings of the Geologists' Association* 2012;**123**:779–86.
Rauhut OWM, Carrano MT. The theropod dinosaur *Elaphrosaurus bambergi* Janensch, 1920, from the Late Jurassic of Tendaguru, Tanzania. *Zoological Journal of the Linnean Society* 2016;**178**:546–610. https://doi.org/10.1111/zoj.12425
Rauhut OWM, Pol D. Probable basal allosauroid from the early Middle Jurassic Cañadón Asfalto Formation of Argentina highlights phylogenetic uncertainty in tetanuran theropod dinosaurs. *Scientific Reports* 2019;**9**:1–9.
Rauhut OWM, Pol D. New theropod remains from the Late Jurassic Cañadón Calcáreo formation of Chubut, Argentina. *Journal of South American Earth Sciences* 2021;**111**:103434.
Rauhut OWM, Milner AC, Moore-Fay S. Cranial osteology and phylogenetic position of the theropod dinosaur *Proceratosaurus bradleyi* (Woodward, 1910) from the Middle Jurassic of England. *Zoological Journal of the Linnean Society* 2010;**158**:155–95. https://doi.org/10.1111/j.1096-3642.2009.00591.x
Rauhut OW, Hübner T, Lanser KP. A new megalosaurid theropod dinosaur from the late Middle Jurassic (Callovian) of north-western Germany: Implications for theropod evolution and faunal turnover in the Jurassic. *Palaeontologia Electronica* 2016;**19**:1–65.
Rayfield EJ, Milner AC, Xuan VB *et al*. Functional morphology of spinosaur 'crocodile-mimic' dinosaurs. *Journal of Vertebrate Paleontology* 2007;**27**:892–901. https://doi.org/10.1671/0272-4634(2007)27[892:fmoscd]2.0.co;2
Reid REH. Claws' claws. *Nature* 1987;**325**:487–487. https://doi.org/10.1038/325487b0
Rohais S, Hamon Y, Deschamps R *et al*. Patterns of organic carbon enrichment in a lacustrine system across the K–T boundary: Insight from a multi-proxy analysis of the Yacoraite Formation, Salta rift basin,

Argentina. *International Journal of Coal Geology* 2019;**210**:103208. https://doi.org/10.1016/j.coal.2019.05.015
Rowe T, Gauthier J. Ceratosauria. In: Weishampel D, Dodson P, Osmólska H (eds), *The Dinosauria*, 1st edn. Berkeley, CA: University of California Press, 1990, 151–68.
Rueden CT, Schindelin J, Hiner MC *et al.* ImageJ2: ImageJ for the next generation of scientific image data. *BMC Bioinformatics* 2017;**18**:529. https://doi.org/10.1186/s12859-017-1934-z
Ruiz J, Torices A, Serrano H *et al.* The hand structure of *Carnotaurus sastrei* (Theropoda, Abelisauridae): implications for hand diversity and evolution in abelisaurids. *Palaeontology* 2011;**54**:1271–7. https://doi.org/10.1111/j.1475-4983.2011.01091.x
Russell DA. Isolated dinosaur bones from the Middle Cretaceous of the Tafilalt, Morocco. *Bulletin du Muséum National d'Histoire Naturelle* 1996;**4**:349–402.
Samathi A, Sander PM, Chanthasit P. A spinosaurid from Thailand (Sao Khua Formation, Early Cretaceous) and a reassessment of *Camarillasaurus cirugedae* from the Early Cretaceous of Spain. *Historical Biology* 2021;**33**:3480–94. https://doi.org/10.1080/08912963.2021.1874372
Sampson SD, Witmer LM. Craniofacial anatomy of *Majungasaurus crenatissimus* (Theropoda: Abelisauridae) from the Late Cretaceous of Madagascar. *Journal of Vertebrate Paleontology* 2007;**27**:32–104. https://doi.org/10.1671/0272-4634(2007)27[32:caomct]2.0.co;2
Sampson SD, Witmer LM, Forster CA *et al.* Predatory dinosaur remains from Madagascar: implications for the Cretaceous biogeography of Gondwana. *Science* 1998;**280**:1048–51. https://doi.org/10.1126/science.280.5366.1048
Sampson SD, Carrano MT, Forster CA. A bizarre predatory dinosaur from the Late Cretaceous of Madagascar. *Nature* 2001;**409**:504–6. https://doi.org/10.1038/35054046
Sánchez-Hernández B, Benton MJ. Filling the ceratosaur gap: a new ceratosaurian theropod from the Early Cretaceous of Spain. *Acta Palaeontologica Polonica* 2014;**59**:581–600.
Schade M, Rauhut OW, Foth C *et al.* A reappraisal of the cranial and mandibular osteology of the spinosaurid *Irritator challengeri* (Dinosauria: Theropoda). *Palaeontologia Electronica* 2023;**26**:1–116.
Schindelin J, Arganda-Carreras I, Frise E *et al.* Fiji: an open-source platform for biological-image analysis. *Nature Methods* 2012;**9**:676–82. https://doi.org/10.1038/nmeth.2019
Seebacher F. A new method to calculate allometric length–mass relationships of dinosaurs. *Journal of Vertebrate Paleontology* 2001;**21**:51–60. https://doi.org/10.1671/0272-4634(2001)021[0051:anmtca]2.0.co;2
Sereno PC. The pectoral girdle and forelimb of the basal theropod *Herrerasaurus ischigualastensis*. *Journal of Vertebrate Paleontology* 1994;**13**:425–50. https://doi.org/10.1080/02724634.1994.10011524
Sereno PC. A rationale for phylogenetic definitions, with application to the higher-level taxonomy of Dinosauria. *Neues Jahrbuch fur Geologie und Palaontologie Abhandlungen* 1998;**210**:41–83.
Sereno PC. Stem Archosauria—TaxonSearch. *TaxonSearch Database for Suprageneric Taxa & Phylogenetic Definitions* 2005.
Sereno PC. Early Cretaceous ornithomimosaurs (Dinosauria: Coelurosauria) from Africa. *Ameghiniana* 2017;**54**:576–616. https://doi.org/10.5710/amgh.23.10.2017.3155
Sereno PC, Brusatte SL. Basal abelisaurid and carcharodontosaurid theropods from the Lower Cretaceous Elrhaz Formation of Niger. *Acta Palaeontologica Polonica* 2008;**53**:15–46. https://doi.org/10.4202/app.2008.0102
Sereno PC, Dutheil DB, Larochene M *et al.* Predatory dinosaurs from the Sahara and Late Cretaceous faunal differentiation. *Science* 1996;**272**:986–91.
Sereno PC, Wilson JA, Conrad JL. New dinosaurs link southern landmasses in the Mid–Cretaceous. *Proceedings of the Royal Society of London. Series B: Biological Sciences* 2004;**271**:1325–30. https://doi.org/10.1098/rspb.2004.2692
Sereno PC, Tan L, Brusatte SL *et al.* Tyrannosaurid skeletal design first evolved at small body size. *Science* 2009;**326**:418–22. https://doi.org/10.1126/science.1177428
Smith JB, Dodson P. A proposal for a standard terminology of anatomical notation and orientation in fossil vertebrate dentitions. *Journal of Vertebrate Paleontology* 2003;**23**:1–12. https://doi.org/10.1671/0272-4634(2003)23[1:apfast]2.0.co;2
Smyth RSH, Ibrahim N, Kao A *et al.* Abelisauroid cervical vertebrae from the Cretaceous Kem Kem beds of Southern Morocco and a review of Kem Kem abelisauroids. *Cretaceous Research* 2020;**108**:104330.
Snively E, Russell AP. Functional variation of neck muscles and their relation to feeding style in Tyrannosauridae and other large theropod dinosaurs. *The Anatomical Record* 2007;**290**:934–57. https://doi.org/10.1002/ar.20563
de Souza GA, Soares MB, Brum AS *et al.* Osteohistology and growth dynamics of the Brazilian noasaurid *Vespersaurus paranaensis* Langer *et al.*, 2019 (Theropoda: Abelisauroidea). *PeerJ* 2020;**8**:e9771. https://doi.org/10.7717/peerj.9771
de Souza GA, Soares MB, Weinschütz LC *et al.* The first edentulous ceratosaur from South America. *Scientific Reports* 2021;**11**:22281. https://doi.org/10.1038/s41598-021-01312-4
Stiegler JB. Anatomy, systematics, and paleobiology of noasaurid ceratosaurs from the Late Jurassic of China. Unpublished Ph.D. Thesis, The George Washington University, 2019.
Stromer E. Ergebnisse der Forschungsreisen Prof. E. Stromers in den Wüsten Ägyptens. II. Wirbeltier-Reste der Baharîje-Stufe (unterstes Cenoman). 13. Dinosauria. *Abhandlungen der Bayerischen Akademie der Wissenschaften, Mathematisch-naturwissenschaftliche Abteilung, Neue Folge* 1934;**22**:1–79.
Therrien F, Zelenitsky DK, Tanaka K *et al.* Exceptionally preserved stomach contents of a young tyrannosaurid reveal an ontogenetic dietary shift in an iconic extinct predator. *Science Advances* 2023;**9**:eadi0505. https://doi.org/10.1126/sciadv.adi0505
Thomas O. XXVIII.—The method of taking the incisive index in rodents. *Annals and Magazine of Natural History* 1919;**4**:289–90. https://doi.org/10.1080/00222931908673892
Tortosa T, Buffetaut E, Vialle N *et al.* A new abelisaurid dinosaur from the Late Cretaceous of southern France: Palaeobiogeographical implications. *Annales de Paléontologie* 2014;**100**:63–86. https://doi.org/10.1016/j.annpal.2013.10.003
Tykoski RS, Rowe T. Ceratosauria. In: Weishampel D, Dodson P, Osmólska H (eds), *The Dinosauria*, 2nd edn. Berkeley, CA: University of California Press, 2004, 47–70.
Veldmeijer AJ. Toothed pterosaurs from the Santana Formation (Cretaceous; Aptian-Albian) of northeastern Brazil. A reappraisal on the basis of newly described material. Unpublished Ph.D. Thesis, Utrecht University, 2006.
Villafañe PG, Cónsole-Gonella C, Citton P *et al.* Three-dimensional stromatolites from Maastrichtian–Danian Yacoraite Formation, Argentina: modelling and assessing hydrodynamic controls on growth patterns. *Geological Magazine* 2021;**158**:1756–72.
Waibl H, Gasse H, Constantinescu GM *et al.* In: Gasse H, Van Den Broek W, Hashimoto Y, Constantinescu GM, Budras KD, Saber AS, Simoens P, Bragulla H, Sótonyi P, Salazar I, Augsburger H (eds), *Nomina Anatomica Veterinaria*. Hannover; Columbia, MO: Ghent: Editorial Committee, 2012.
Walker CA. New subclass of birds from the Cretaceous of South America. *Nature* 1981;**292**:51–3. https://doi.org/10.1038/292051a0
Walker CA, Dyke GJ. Euenantiornithine birds from the late Cretaceous of El Brete (Argentina). *Irish Journal of Earth Sciences* 2009;**27**:15–62. https://doi.org/10.1353/ijes.2009.a810006
Walker CA, Buffetaut E, Dyke GJ. Large euenantiornithine birds from the Cretaceous of southern France, North America and Argentina. *Geological Magazine* 2007;**144**:977–86. https://doi.org/10.1017/s0016756807003871
Wang S, Stiegler J, Amiot R *et al.* Extreme ontogenetic changes in a ceratosaurian theropod. *Current Biology: CB* 2017a;**27**:144–8. https://doi.org/10.1016/j.cub.2016.10.043
Wang S, Stiegler J, Wu P *et al.* Heterochronic truncation of odontogenesis in theropod dinosaurs provides insight into the macroevolution of avian beaks. *Proceedings of the National Academy of Sciences of the United*

States of America 2017b;**114**:10930–5. https://doi.org/10.1073/pnas.1708023114

Wilson JA. A nomenclature for vertebral laminae in sauropods and other saurischian dinosaurs. *Journal of Vertebrate Paleontology* 1999;**19**:639–53. https://doi.org/10.1080/02724634.1999.10011178

Wilson JA. Anatomical nomenclature of fossil vertebrates: standardized terms or 'lingua franca?'. *Journal of Vertebrate Paleontology* 2006;**26**:511–8. https://doi.org/10.1671/0272-4634(2006)26[511:anofvs]2.0.co;2

Wilson JA, Sereno PC, Srivastava S *et al*. A new abelisaurid (Dinosauria, Theropoda) from the Lameta Formation (Cretaceous, Maastrichtian) of India. *Contributions from the Museum of Paleontology University of Michigan* 2003;**31**:1–42.

Wilson JA, D'Emic MD, Ikejiri T *et al*. A nomenclature for vertebral fossae in sauropods and other saurischian dinosaurs. *PLoS One* 2011;**6**:e17114. https://doi.org/10.1371/journal.pone.0017114

Witmer LM. The evolution of the antorbital cavity of archosaurs: a study in soft-tissue reconstruction in the fossil record with an analysis of the function of pneumaticity. *Journal of Vertebrate Paleontology* 1997;**3**:1–76. https://doi.org/10.2307/3889342

Wu XC, Shi JR, Dong LY *et al*. A new tyrannosauroid from the Upper Cretaceous of Shanxi, China. *Cretaceous Research* 2020;**108**:104357. https://doi.org/10.1016/j.cretres.2019.104357

Xing L, Persons WS, Bell PR *et al*. Piscivory in the feathered dinosaur *Microraptor*. *Evolution* 2013;**67**:2441–5. https://doi.org/10.1111/evo.12119

Xu X, Clark JM, Mo J *et al*. A Jurassic ceratosaur from China helps clarify avian digital homologies. *Nature* 2009;**459**:940–4. https://doi.org/10.1038/nature08124

Xu X, Zheng X, Sullivan C *et al*. A bizarre Jurassic maniraptoran theropod with preserved evidence of membranous wings. *Nature* 2015;**521**:70–3. https://doi.org/10.1038/nature14423

Xu X, Currie P, Pittman M *et al*. Mosaic evolution in an asymmetrically feathered troodontid dinosaur with transitional features. *Nature Communications* 2017;**8**:ncomms14972.

Zaher H, Pol D, Navarro BA *et al*. An Early Cretaceous theropod dinosaur from Brazil sheds light on the cranial evolution of the Abelisauridae. *Comptes Rendus Palevol* 2020;**19**:101.

Zanno LE. The pectoral girdle and forelimb of the primitive therizinosauroid *Falcarius utahensis* (Theropoda, Maniraptora): analyzing evolutionary trends within Therizinosauroidea. *Journal of Vertebrate Paleontology* 2006;**26**:636–50. https://doi.org/10.1671/0272-4634(2006)26[636:tpgafo]2.0.co;2

Zanno LE, Makovicky PJ. Herbivorous ecomorphology and specialization patterns in theropod dinosaur evolution. *Proceedings of the National Academy of Sciences of the United States of America* 2011;**108**:232–7. https://doi.org/10.1073/pnas.1011924108

Zurriaguz V, Powell J. New contributions to the presacral osteology of *Saltasaurus loricatus* (Sauropoda, Titanosauria) from the Upper Cretaceous of northern Argentina. *Cretaceous Research* 2015;**54**:283–300. https://doi.org/10.1016/j.cretres.2014.12.012